PEOPLE'S DEMOCRATIC REPUBLIC OF ALGERIA

MINISTRY OF HIGHER EDUCATION AND SCIENTIFIC RESEARCH

UNIVERSITY OF MSILA

FACULTY OF SCIENCES

DEPARTMENT OF CHEMISTRY

N°:……..…/……/……

DOMAIN: SCIENCE OF MATTER

STREAM: CHEMISTRY

OPTION: ORGANIC

Phytochemical investigation of the *n*-BuOH extract of *Scilla lingulata* using LC-ESI/MS technique, enriched with molecular docking studies

Dissertation submitted to the department of chemistry for the fulfillment of Master degree in Organic chemistry

Submitted by

Ms BENRAMDANE Zeyneb

Supervised by

Dr CHERIET Thamere

Publically defended before the following jury

M[m] MERATATE Faiza	MCB–University of Msila	Chairperson
M[r] CHERIET Thamere	MCA–University of Msila	Supervisor
M[m] MOHAMADI Sabrina	MCB–University of Msila	Examiner

2019-2020

Acknowledgments

All praises and glory belong to the almighty **Allah**, who gave me health, courage, strength, and heart-felt enthusiasm to carry out this work, and who has placed his righteous servants at my service.

May **Allah** will give me strength and increase me in the knowledge that I need to continue…

At the outset, I would like to express my deepest gratitude to the head of the Department of Chemistry and his staff for their kindness, help, and for being always on duty. Special thanks go to all of my teachers, for whom I hold endless respect, for their knowledgeable lectures, guidance, unflinching encouragements, pieces of advice, patience, and for their precious time that I spent with them.

Thank you a bunch for the tiny things that cost a lot

I want to give my sincere appreciation to my supervisor for his faith in my scientific capacities, by allowing me to work on this project under his supervision. I am really grateful for your constant guidance, valuable feedback and for responding to my questions and queries so promptly.

I would also like to thank the jury members for reading the manuscript and for accepting to discuss honestly the work. Thank you for enriching this one with your knowledgeable remarks.

Finally, no words of the world can convey my profound gratitude and thankfulness to whole my family for their boundless support and motivation; in particular, my

Acknowledgments

beloved parents. I send all my lovely words to the strong and gentle soul who taught me how to trust in **Allah**, believe in myself, and in the hard work, my wonderful mum♥ I love you from the bottom of my heart, this phrase is less than your sacrificing and love. Dear dad, I would like to thank you for giving me the push up to be tough and self-made. I am deeply grateful to my sweetheart sister, for being always by my side. You are one of the greatest gifts that I have.

I can never thank my family as much as I should like

So, simply thank you all

To be fair with all of my friends and people, who know me from near or far, I would like to tell you, I am so grateful for your support and encouragement.

''Every challenging work needs to self-efforts as well as guidance and support''

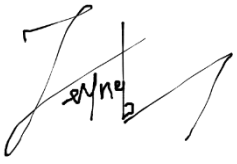

Table of Contents

Chapter I

Literature survey

Chapter II

Experimental part

About S. lingulata

Phytochemical study

Molecular docking simulation studies

Chapter III

Results and discussions

Phytochemical study

Molecular docking studies

List of Abbreviations

Unities

°C	Degree Celsius
Da	Dalton
GHz	Gega Hertez
h	Hours
Kcal	Kilcalorie
M	Mole per litre
mm	Millimetre
mg	Milligram
mL	Millilitre
mM	Millimole per litre
min	Minute
nm	Nanometre
µL	Microlitre
µm	Micromitre
µg	Microgram
V	Volt

Other abbreviations

APG	Angiosperm phylogeny group
AGS	Human gastric adenocarcinoma cell line
AChE	Acetylcholinoesterase
ATP-ase	Adenosine triphosphatase (enzyme)
Ara	Arabinose
Ac	Acetyl
AD	Alzheimer's disease
n-BuOH	Normal-Butanol
BFL	2-(1, 1'-Biphenyl-4-yl) propanoic acid
BChE	Butyrylcholinoesterase
COX-1/ COX-2	Cyclooxygenase 1 / 2
CDX	ChemDraw exchange format
$CHCl_3$	Chlorform
CH_3CN	Acetonitrile
Cp	Compound
C	Carbon

DCM	Dichloromethan
EtOH	Ethanol
EtOAc	Ethyl Acetate
EC_{50}	Half maximal effective concentration
ESI	Electrospray ionisation
ESI/MS	Electrospray ionisation source used in mass spectrometry
Gal	Galactose
Glc	Glucose
GNT	Galantamine
H	Hydrogen
H_2O	Water
H_2O_2	Hydrogen peroxyde
HUVECs	Human umbilical vein endothelial cells
HRECs	Human retinal microvascular endothelial cells
IC_{50}	Half maximal inhibitory concentration
I.D	Inner diameter
K (or K^+)	Potassium (ion form)
LC	Liquid chromatography
LC-MS	Liquid chromatography coupled with mass spectrometry
M	Molecular weight
Me	Methyl
MeOH	Methanol
m/z	Mass to charge ratio
Na (or Na^+)	Sodium (ion form)
NMR	Nuclear magnetic resonance
NPX	Naproxen
O	Oxygen
OH	Hydroxyl
PDA	Photodiode array detector
PDB	Protein data bank
PDBQT	Protein data bank, partial charge (Q) and atom type (T)
R	Radical
Rha	Rhamnose
Ref.	Reference
Rotavap.	Rotary evaporator
S.	*Scilla*
Syn.	Synonym
SDF	Stands for structure-data file
THA	Tacrine
tR	Retention time
UV-Vis	Ultraviolet – visible
UV-DAD	Ultraviolet – Diode array detector
VDW	Van der waals
WEHI-164	Mouse fibrosarcoma cell line
Y	Yield
$X^\bullet$	Radical element
2D	Two dimension
3D	Three dimension

List of Tables

Chapter II

Chapter III

List of Figures

Chapter I

Chapter II

Chapter III

Phytochemical study

Molecular docking simulation studies

List of Schemes

Chapter III

General

Introduction

From plants to medicine

Over the years, people from virtually all cultures used to treat their sickness through traditional herbal remedies, which have been prescribed by folk healers. Their knowledge in curing human sufferance has resulted from the daily practicing medication using directly or indirectly medicinal plants as a miracle source of healing. Hence, this sort of treating the human set was as old as humankind itself. After centuries of empirical uses of herbal preparations, the first isolation of active principles alkaloids such as morphine, strychnine, quinine…, etc. in the early 19th century marked a new era in the use of medicinal plants and the beginning of modern medicinal plant research **[1]**.

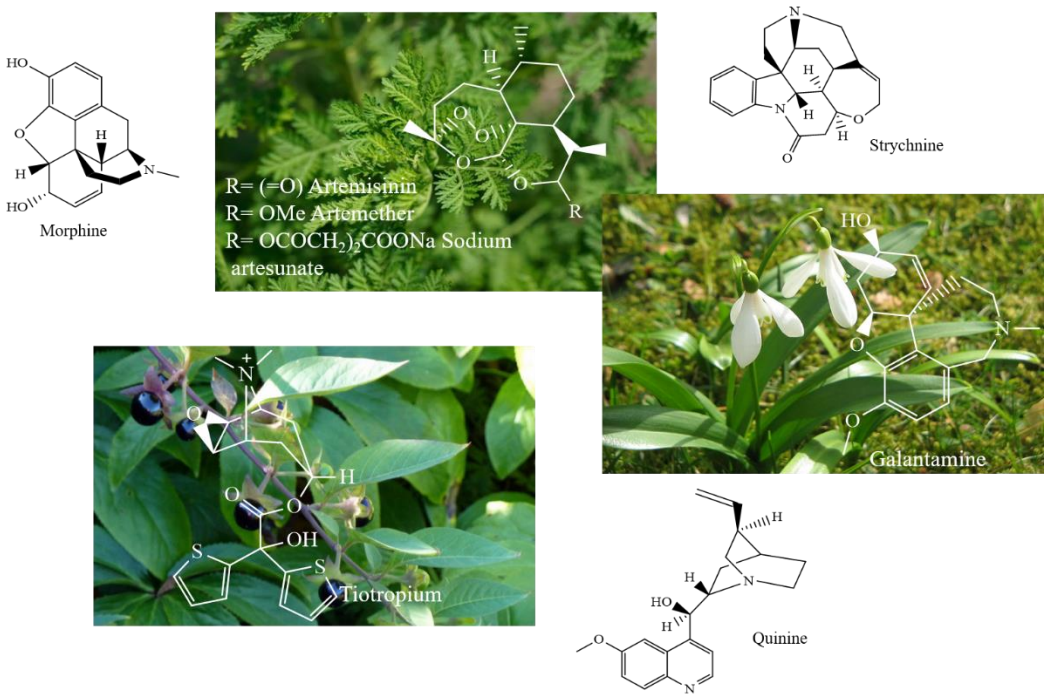

Until now, huge varieties of medicinal plants continue to retain their historical significance as important sources of novel compounds useful directly as medicinal agents, model compounds for synthetic or semisynthetic structure modifications and optimizations, and as sources of inspiration for new generation of synthetic drugs with potent effects. Some relevant examples are artemisinin, from *Artemisia annua* (L.), which used for the treatment of malaria **[2]**. Structural modification of the natural product artemisinin has resulted in a series of ether and ester analogues including artemether and sodium artesunate respectively **[3, 4]**, where the first one was clinically as effective as quinine in the treatment of cerebral malaria **[5]**. Galantamine (trade name Reminyl®) is a natural product isolated from *Galanthus woronowii* (Losinsk.), which was approved for the treatment of

Alzheimer's disease **[6]**. Barton and Kirby **[7]** were perfected the laboratory synthesis of this valuable compound in the 1960s. Atropine, the chief alkaloid in *Atropa belladonna* (L.) roots **[8]**, has a derivative compound named Tiotropium (trade name Spiriva®) which was reported as a treatment of chronic obstructive pulmonary disease **[9, 10]**.

Broadly speaking, natural products and related structures are essential sources of new pharmaceuticals, because of the immense variety of functionality relevant secondary metabolites of plant species. The developments of powerful analytical tools in the 21st century such as high-liquid chromatography, nuclear magnetic resonance spectroscopy, mass spectrometry and the availability of advanced *in vitro* screening methods greatly expedite identification and characterization of these natural products, in particular, those of medicinal plants **[11]**.

In the same context, hayacinthaceae family is one of the largest groups of bulbous plants, where the species belonging to this family are traditionally used either for the prevention or for the curative treatment of several diseases **[12]**. In Algeria, the traditional healers recommend a decoction of *Scilla* (L.) against liver diseases, where the most widely used species is *Scilla maritima* (syn. *Drimia maritima*, *Urginea maritima*) **[13, 14]**. More researches on *Scilla* species have been revealed the presence of numerous classes of secondary metabolites including homoisoflavonoids, alkaloids, terpenoids, and cardiac glycosides (bufadienolides), which are involved in the pharmacological properties of this species in treating diverse illnesses **[15]**. In 2014, a potent homoisoflavonoid named **cremastranone**, isolated from *Scilla natalensis*, was synthesized by Lee et *al* **[16]**. The anti-proliferation activities on the ocular disease relevant endothelial cells such as HUVECs and HRECs were demonstrated, that the synthetic **cremastranone** showed a potent inhibitor activity against those cell models. Thus, this result indicated that synthetic homoisoflavonoid could be used as an anti-angiogenic in treating eye diseases **[16]**.

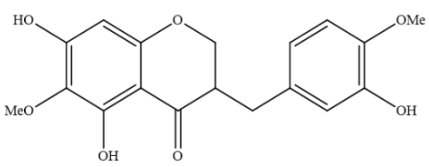

Cremastranone

From this perspective, our research work is focused on the phytochemical investigations of the *n*-butanolic extract of the endemic Algerian plant **[17]** *Scilla lingulata* using LC-ESI/MS technique. Besides, the identified compounds are enriched with molecular docking studies. This study was planned to include the following chapters:

Chapter I Highlights

- The botanical taxonomy of both Hayacinthaceae and Asparagaceae families according to the APG classification. The taxonomical identification of *Scilla* genus within those families
- The traditional uses of *Scilla* species in treating several diseases
- The main secondary metabolites that have been formerly identified in this genus with their biological activities

Chapter II Shows

- The experimental technique that used to investigate phytochemically the *n*-butanolic extract of *scilla lingulata*
- The molecular docking protocols that operated to recognize *in silico* enzymatic activities of the identified compounds

Chapter III Reveals

- The subtle interpretations of the obtained ESI/MS and UV-Vis spectra which were concluded by sketching the chemical structures of the identified molecules
- The discussions of *in silico* inhibition mode of the tested compounds and it displays an approach to the glycosylated flavonoids class in inhibiting target proteins.

References

[1]. Hamburger M, Hostettmann K. Bioactivity in plants: the link between phytochemistry and medicine. *Phytochemistry* **1991**, 30(12): 3864–3874

[2]. Klayman DL. *Artemisia annua*, from weed to respectable antimalarial plant. In: Human Medicinal Agents from Plants, ed. by Kinghorn AD, Balandrin MF. *Am. Chem. Soc.*, Washington. **1993**, pp. 242–255

[3]. Haynes, RK, Vonwiller SC. Extraction of artemisinin and artemisinic acid: preparation of artemether and new analogues. *Trans. R. Soc. Trop. Med. Hyg*. **1994**, 88:23–26

[4]. Chaturvedi D, Goswami A, Pratim Saikia P, Barua NC, Rao PG. Artemisinin and its derivatives: a novel class of anti-malarial and anti-cancer agents. *Chem. Soc. Rev*.**2010**, 39(2): 435–454

[5]. Van Hensbroek MB, Onyiorah E, Jaffar S, Schneider G, Palmer A, Frenkel J, et al. A trial of artemether or quinine in children with cerebral malaria. *N. Engl. J. Med*. **1996**, 335(2):69–75

[6]. Heinrich M, Lee Teoh H. Galanthamine from snowdrop—the development of a modern drug against Alzheimer's disease from local Caucasian knowledge. *J. Ethnopharmacol*. **2004**, 92(2-3):147–162

[7]. Barton DHR, Kirby GW.153. Phenol oxidation and biosynthesis. Part V. The synthesis of galanthamine. *J. Chem. Soc* (Resumed). **1962**, 806–817

[8]. Dimitrov K, Metcheva D, Boyadzhiev L. Integrated processes of extraction and liquid membrane isolation of atropine from Atropa belladonna roots. *Sep. Purif. Technol*. **2005**, 46(1-2): 41–45.

[9]. Disse B, Witek Jr TJ. Anticholinergics: Tiotropium. ed. by Hansel TT, Barnes PJ: New Drugs for Asthma, Allergy and COPD. *Prog. Respir. Res.* **2001**, 31: 72–76

[10]. Disse B, Speck GA, Rominger KL, Witek TJ, Hammer R.Tiotropium (SPIRIVA™): Mechanistical considerations and clinical profile in obstructive lung disease. *Life Sci.* **1999**, 64(6-7):457–464

[11]. Thomford N, Senthebane D, Rowe A, Munro D, Seele P, Maroyi A, Dzobo K. Natural products for drug discovery in the 21st century: Innovations for novel drug discovery. *Int. J. Mol. Sci.* **2018**, 19(6):1578

[12]. Azizi N, Amirouche R, Amirouche N. Cytotaxonomic diversity of some medicinal species of Hyacinthaceae from Algeria. *Pharmacogn. Commn*. **2016**, 6(1):34–38

[13]. Tahri D, Elhouiti F, Ouinten M, Yousfi M. Historical perspective of Algerian pharmacological knowledge. *Orient. Pharm. Exp. Med.* **2019**

[14]. Mahboubi M, Mohammad Taghizadeh Kashani L, Mahboubi M. Squill (*Drimia maritima* L.) and its novel biological activity. *Orient. Pharm. Exp. Med*. **2018**

[15]. Mulholland DA, Schwikkard SL, Crouch NR. The chemistry and biological activity of the Hyacinthaceae. *Nat. Prod. Rep*. **2013**, 30(9):1165– 1210

[16]. Lee B, Basavarajappa HD, Sulaiman RS, Fei X, Seo S-Y, Corson TW. The first synthesis of the antiangiogenic homoisoflavonoid, cremastrone. *Org. Biomol. Chem*. **2014**, 12:7673–7677

[17]. Hamouche Y. Etude biosystématique du genre *Scilla* (Hyacinthaceae) : Analyses de populations polyploïdes de *S.autumnalis* L. et *S.lingulata* Poiret du littoral algérois. Thèse doctorat. **2004**, USTHB, Alger, p17

Chapter I

Literature Survey

Botanical taxonomy of Hyacinthaceae family and Scilla genus

Chemical compositions of Scilla species

Traditional medicinal uses

Biological activities

I.1 | Hyacinthaceae and Asparagaceae families

In 1981, Cronquist used to include most of the monocots (Angiosperm[1]) bearing showy flowers with six tepals[2], six stamens and trilocular superior ovary in Liliaceae. Since the studies of Dahlgren et *al.* in 1985, the genera formerly classified under Liliaceae have been distributed among many smaller families organized in two main orders: *Asparagales* and *Liliales* (in APG I, II and III) **[1, 2]**. Although Cronquist classification still in frequent use, it has become outdated classification **[3]** compared to APG one. Thus, the two new families Hyacinthaceae and Asparagaceae are recently highlighted by the APG classification where the first one was described to comprise about 46 genera with 700–900 species **[4]** of bulbous plants **[5]** which are mainly distributed through Europe, but most richly represented in Southern Africa and in a region from Mediterranean sea to the South-west Asia, with a single genus in South America. This family is best adapted to a fluctuating moist-arid climate **[6–8] (**Figure I.1**)**.

In the first phylogenetic classification named APG I in 1998, the Hyacinthaceae family was listed as separate family within the order *Asparagales* **[3]**, but it can be treated currently as subfamily *Scilloideae* of Asparagaceae (in APG III) **[7]**. Moreover, the Asparagaceae family of the flowering monocot plant within the largest order *Asparagales* (in APG III) **[9]**, consists of about 114 genera and about 2900 species **[10]**, which is widely distributed through the world **[11]**.

The plants of Asparagaceae family are perennial, bulbous or rhizomatous[3] herbs as well as subshrubs, shrubs and sparingly branched trees, with leaves basally aggregated when stemless or along stems, simple, alternate sometimes scale-like. The Inflorescences are borne terminally or laterally and they are often scapose or bracteates (racemes, panicles, spikes, solitary flowers or umbel-like), where flowers are bisexual or rarely unisexual, actinomorphic[4] or zygomorphic[5] with free or fused perianth. Stamens filaments usually free or basally fused, sometimes attached to perianth. Ovary superior or inferior; carpels fused, usually septal nectaries, the plants have a capsule, berry, drupe or nut fruit where seeds are usually black or pale brown **[11]**.

[1] A plant that have flowers and produce seeds enclosed within a carpel, including herbaceous plants, shrubs, grasses, and most trees.
[2] The outer parts of flower (perianth). The term tepal is used when these parts cannot be classified either sepal or petal
[3] Producing or proliferating by rhizome (a root like subterranean stem, commonly horizontal in position that usually produces roots below and sends up shoots progressively from the upper surface).
[4] An actinomorphic flower is a type of flower that possesses radial symmetry. Any type of cut through the center will divide the flower into two equal parts.
[5] When flowers are zygomorphic, they are only bilaterally symmetrical, meaning they can bisected into two halves, forming mirror images only by a medial cut through the central axis.

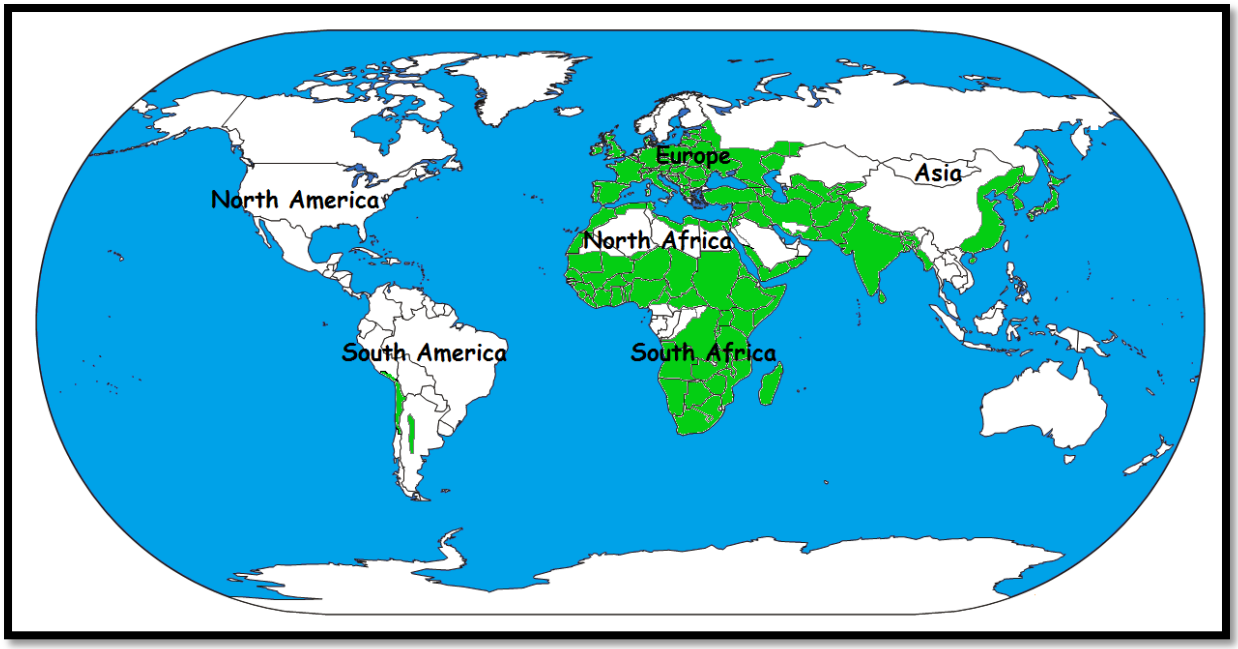

Figure I.1. Geographic distribution map of Hyacinthaceae family (the native one, in green).

I.2 | Presentation of the genus *Scilla*

The genus *Scilla*, comprises approximately 81 taxa (or species) **[12]** of bulb forming perennial herbs belonging either to the Liliaceae family in the order *Liliales* according to Cronquist classification or to the Asparagaceae family, subfamily *Scilloideae* in the order *Asparagales* according to the APG III (2009). The main distribution areas are Europe (29%), Southern Africa (42%), and Southwest Asia (24%) as native plant **[13]**, and are scarce in North America (5%) as cultivated plant **[13, 14]**.

This genus is monocotyledonous herbaceous plants; the strap shaped leaves are produced from oval or spherical bulbs (as storage organs) in the spring and are followed by the terminal racemes (inflorescence) of pink, violet, blue, or white flowers with six petals, where tepals are single-veined and are borne in two whorls with three tepals in each. Six stamens and three chambered pistils with septal nectaries are located in the flowers; the fruit with seeds are in capsule **[15, 16] (**Figure I.2**)**.

Figure I.2. Different parts of *Scilla* plant.

Generally, the *Scilla* species live on limestone rocks, in grassland, open wood, grassy slopes under shrubs, subalpine meadows, by streams, on rocky steppes and screes near permanent snows **[17]**. In Algeria, this genus is represented by five native species, which are *S. anthericoides* **[18]**, *S. autumnalis*, *S. obtusifolia*, *S. numidica* and *S. lingulata* **[19]**.

I.3 | Traditional medicinal uses of *Scilla*

Traditional or folk medicine is an ancient method of healing that practiced by more than 80% of the world's population to treat various diseases using plants as sources of conventional medicaments **[20]**. *Scilla* species is one of oldest medicinal plants used by Romains (Southern Europe) and Egyptians as heart stimulant and regulator of heartbeat **[21]**. Many herbal remedies, which contain some Scilla species, are used to treat various lung diseases such as asthma, chronic bronchitis and whooping cough. Chronic pain stemming from overstressed muscles ailments (as fibromyalgia[6]) can be treated by *Scilla* extracts **[22]**.

[6] Is a chronic rheumatic disorder .It is associated with widespread pain in the muscles and bones with general fatigue. https://www.mayoclinic.org/diseases-conditions/fibromyalgia/symptoms-causes/syc-20354780

According to vastly distribution of Hyacinthaceae family of bulbous plants in South Africa, *Scilla* species have been widely used in African folk medicine by **Zulu**, **Sotho** and **Tswana** people to treat different health problems **[23]**. From previous published studies on *Scilla* species **(**Figure I.3**)**, some of traditional medicine uses has been documented where we can listed some of their uses here:

- ***S. scilloides* (Lind.) Druce**: A perennial herb native to far Eastern Asia including Korea, Japan and China. The bulb part has been historically used in traditional Chinese medicine as an antidote, blood circulatory activator and as a treatment of dermal inflammation such as abscess and dermatitis combustions **[24]**.
- ***S. nervosa* (Burch.) Jessop** [Syn. ***S. rigidifolia* Kunth**, ***Schizocarphus nervosus* (Burch.) Van der Merwe**], is the only most widespread plant of the genus *Scilla* in Botswana (Southern Africa). It is an important medicinal plant to local people where the bulbs have been used to treat nervous condition in children, dysentery and gastro-intestinal ailments **[25]**.They have also been used as analgesics against rheumatic fever pains and as laxative for condition associated with infection and inflammation **[26–28]**
- ***S. maritima* L.** [Syn. ***Uriginea maritima* (L.) Baker**, ***Drimia maritima* (L.) Stearn**], is a native plant to the Mediterranean region, Africa and India. The bulbs have been used traditionally to relieve joint pain when combined with oil **[29, 30]**. They are also applied fresh (or dried) for the treatment of tumors and to heal neurological pains (such as sciatica[7]), skin diseases (wound, edema and dermal fungus infection), heart diseases (heart failure and fluid retention, cardio-tonic), chest ailments (bronchial asthma, allergic cough …), constipation, diabetes, renal diseases and rheumatic diseases **[31, 32]**.
- ***S. natalensis* (Planch.)** [Syn. ***S. Kraussii* Bak.**] **[33]**: This plant is widely distributed in South Africa occurring in Lesotho, Kwazulu-Natal **[34]**, Swaziland, Eastern Free State and Gauteng. It is one of the top ten most popular medicinal plants that have used to treat various ailments including gastro-intestinal diseases (such as stomachache, constipation and diarrhea), rheumatism, paralysis, sprains and fractures **[35]** and skin diseases (eczema) **[36]**.
- ***S. maderensis* Menezes**: A vulnerable plant has purple bulbs, large green leaves with brown-reddish spots, many very small flowers with blue-lilac perinath. It is endemic to

[7] Common type of pain affecting the sciatic nerve. Sciatica usually affects only one side of the lower body. Often, the pain extends from the lower back all the way through the back of the thigh and down through the leg.

the Portuguese Archipelago of Madeira. From the ethno-pharmacological[8] point of view, this herb was originally used in Madeira to treat people suffering from erysipelas[9] **[36, 37]**.

- ***S. bifolia* (L.)**: A perennial plant herb native to Southern Europe and Asia Minor **[38]**. The bulbs have a medicinal uses to treat skin problems like healing wound or herniated disc disease **[39]**.

As we have already mentioned, several medicinal uses of *Scilla* species in traditional medicine were reported since ancient time by various people in different part of the world to treat many diseases. Nevertheless, *Scilla* has been reported to display negative effects such as diarrhea, abdominal pain **[16]**, emphysema[10] and increased pulse rat which can be fetal **[36]** for human while it is considered as toxic herb to sheep **[16]**.

The presence of curative and poisoning side in the genus *Scilla* make the traditional knowledge of healers become limited in folklore uses. So recently, many researchers posed the question of how such medicinal or toxic effects can be explained. For that, several studies have focused on various aspect related to the isolation, characterization and biological activities of different pure compounds present in the genus *Scilla* or even its species where we will treat them in next section.

[8] The study of the action and properties of medicinal agents, often derived from plants indigenous to population or ethnic groups.
[9] It is a bacterial skin infection involving the super dermis.
[10] It is a lung condition that causes shortness of breath.

Figure I.3. Photos of some *Scilla* species**.**

I.4 | Previous phytochemical investigation on *Scilla* species

Because of the therapeutic value of the bulbs, more researches on the phytochemistry of *Scilla* species have been demonstrated the presence of different secondary metabolites such as alkaloids, terpenoids, cardiac glycosides (bufadienolides) and homoisoflavonoids in this genus.

Extensive phytochemical investigations into the MeOH extract of fresh bulbs of *S. scilloides* resulted in the isolation of nine homoisoflavones **1–9** specific to this plant, norlanostane-type triterpenoids **10–15**, lanostane-type triterpenoids **16, 17**, xanthones **18–21**, two homostilbenes **22, 23**, a lignan **24**, tow alkaloids **25, 26 (**Figure I.4**)**, lanostane-type triterpenoids glycoside **27–29**, norlanostane-type triterpenoids glycosides **30–39** and phenylpropanoid glycoside **40 [40–49] (**Figure I.5.A/B**).**

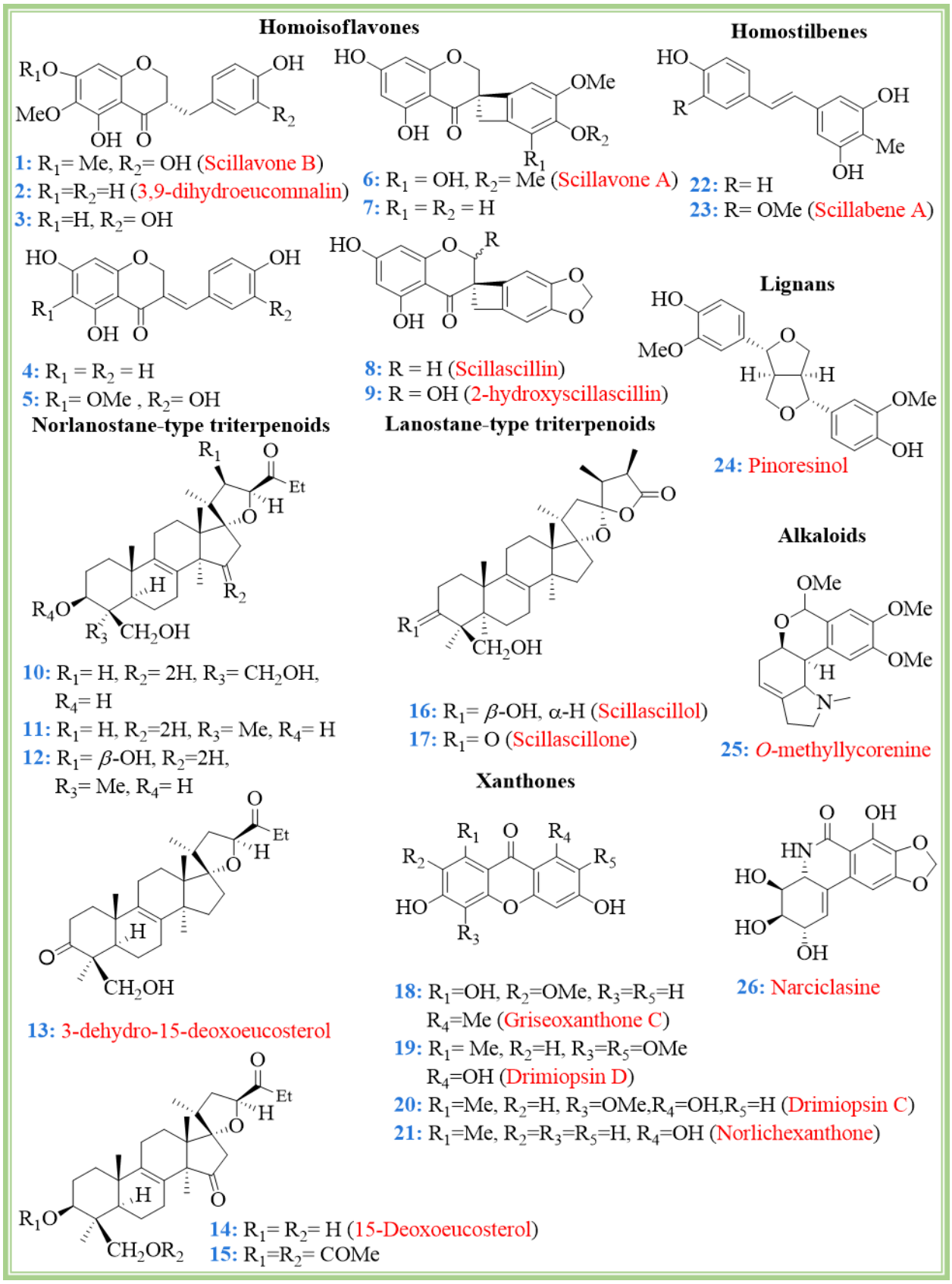

Figure I.4. Chemical structures of different compounds isolated from the bulbs of *S. scilloides* (Lind.) Druce.

A

Oligoglycosides

Lanostane-type triterpenoids glycosides

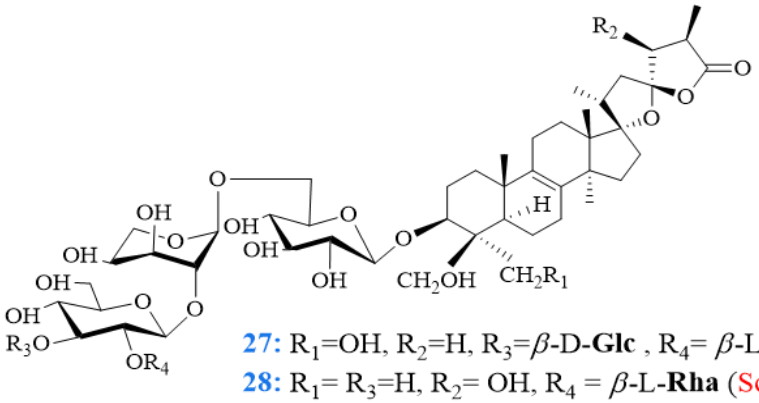

27: R_1=OH, R_2=H, R_3=β-D-**Glc** , R_4= β-L-**Rha** (Scillasaponin B)
28: R_1= R_3=H, R_2= OH, R_4 = β-L-**Rha** (Scillasaponin D)
29: R_1=H, R_2= OH, R_3= Sug-1, R_4=β-L-**Rha** (Scillanostaside E)

Norlanostane-type triterpenoids glycosides

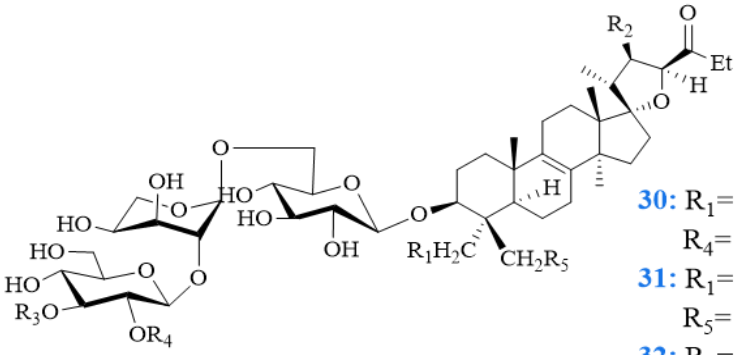

30: R_1= R_2= R_5= H, R_3 = β-D-**Glc**,
R_4= α-L-**Rha** (Scillascilloside E-1)
31: R_1= R_2=H , R_3 = β-D-**Glc**, R_4= α-L-**Ara**
R_5= OH (Scillascilloside E-2)
32: R_1= R_2= H, R_3= β-D-**Glc**, R_4= α-L-**Rha**,
R_5= OAc (Scillascilloside E-3)

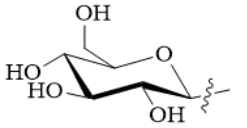

β-D-**Glc**

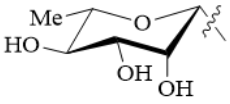

α-L-**Rha**

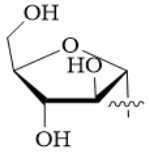

α-L-**Ara**

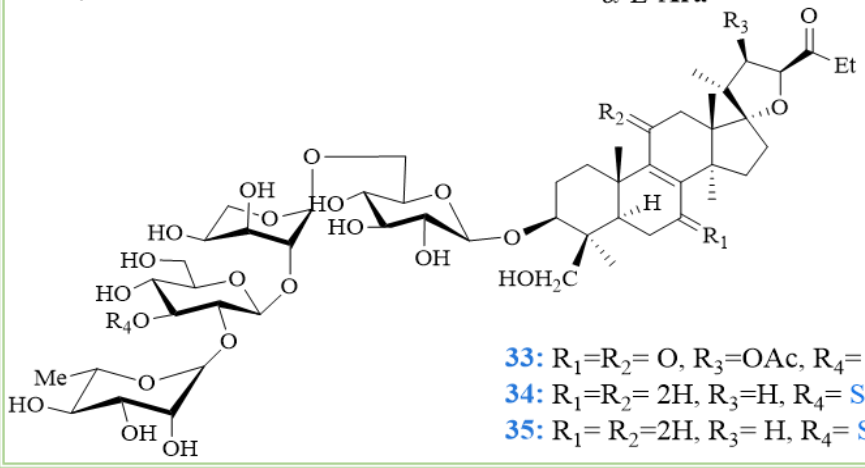

33: R_1=R_2= O, R_3=OAc, R_4= β-D-**Glc** (Scillanostaside A)
34: R_1=R_2= 2H, R_3=H, R_4= Sug-1 (Scillascilloside G-1)
35: R_1= R_2=2H, R_3= H, R_4= Sug-2 (Scillanostaside C)

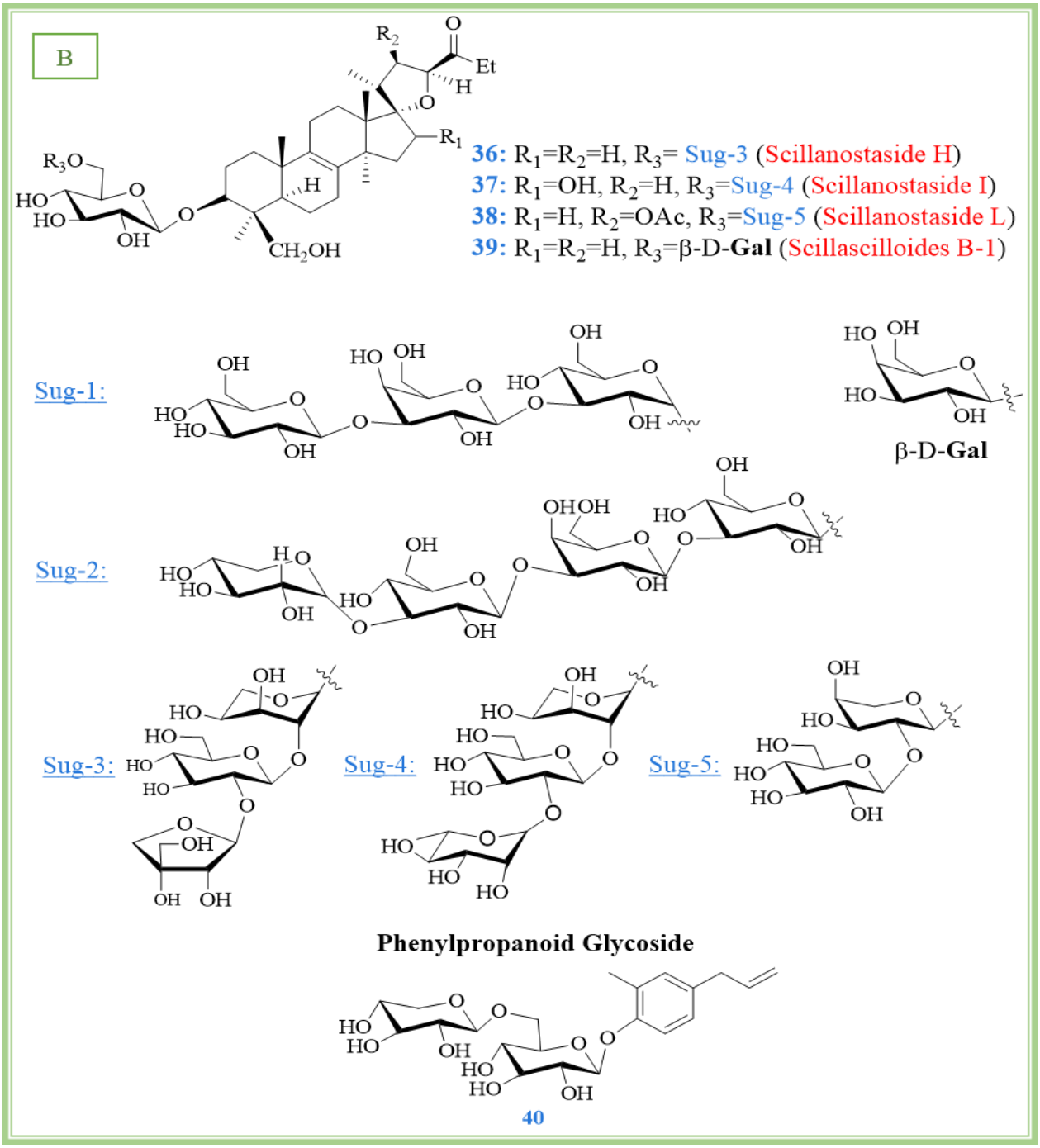

Figure I.5 (A/B). Different oligoglycosides isolated from the bulbs of *S. scilloides* (Lind.) Druce.

S. nervosa is a rich source of homoisoflavonoids which have been reported to display multiple biological effects. An HPLC analysis on the MeOH extract of both yellow inter-bulb surface and whole bulb of *S. nervosa* yielded twenty-one homoisoflavonoids **41–61** and three stilbenoids **62–64** **[26–38, 50, 51] (**Figure I.5**)**.

Homoisoflavonoids

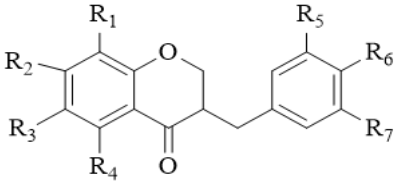

41: R_1=R_5=R_7=H, R_2=R_3=OH, R_4=R_6=OMe
42: R_1=R_3=R_6=OMe, R_2=OH, R_4=R_5=R_7=H
43: R_1=R_3=R_6=OMe, R_2= R_4=R_5=R_7=H
44: R_1=R_3=R_5=OH, R_2=R_4=R_7=H, R_6=OMe
45: R_1=R_7=H, R_2=R_4=R_6=OH, R_3=OMe
46: R_1=R_3=R_5=R_7=H, R_2=R_4=R_6=OMe
47: R_1=R_3=R_5=H, R_2=R_6=OMe, R_4=R_7=OH
48: R_1=R_3=R_5=R_7=H, R_2=R_4=OMe, R_6=OH
49: R_1=R_3=R_4=R_5=R_7=H, R_2=R_6=OMe

50: R_1=R_3=R_5=H, R_2=R_7=OMe, R_4=R_6=OH
51: R_1=R_5=H, R_2=R_3=R_7=OMe, R_4=R_6=OH
52: R_1=R_3=R_5=H, R_2=R_4=OH, R_6=R_7=OMe
53: R_1=R_5=R_7=H, R_2=R_3=R_4=OMe, R_6=OH
54: R_1=OH, R_2=R_4=R_6=OMe, R_3=R_5=R_7=H
55: R_1=R_5=R_7=H, R_2=R_4=R_6=OMe, R_3=OH
56: R_1=R_2=R_3=R_6= OMe, R4=R_5=R_7=H
57: R_1=R_2=R_6=OMe, R_3=OH, R_4=R_5=R_7=H

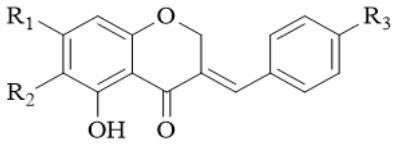

58: R_1=R_3=OH, R_2=OMe
59: R_1=OH, R_2=R_3=OMe
60: R_1=R_3=OH, R_2=H
61: R_1=OMe, R_2=H, R_3=OH

Stilbenoids

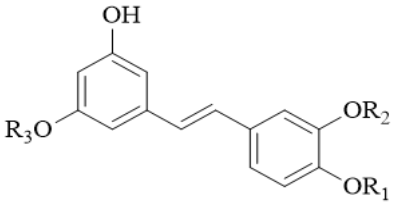

62: R_1=H, R_2=R_3=Me
63: R_1=Me, R_2=R_3=H
64: R_1=R_3=H, R_2=Me

Figure I.6. Chemical structures of compounds isolated from the bulbs of *S. nervosa* (Burch.) Jessop.

Extensive work on different extracts of *S. maritima* (L.) bulbs lead to the isolation of numerous bufadienolides **65–73** as main components of this plant, with various chemical structures **[52, 53, 31]**, Some of them are illustrated in **(**Figure I.7.A**)**. Other biochemicals such as flavonoids **74–78** **[54, 55]**, anthocyanins **79–81** **[56]**, fatty acids **82–84** and sterols **85–87** have been also identified **[57–59] (**Figure I.7.B**)**.

Bufadienolides

A

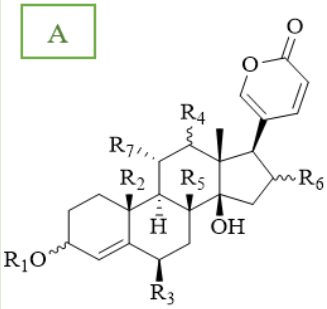

65: R_1= α-L-**Rha**, R_2=Me, R_3-R_7=H (Proscillaridin A)
66: R_1= Sug-6 R_2=Me, R_3-R_7=H (Scillaren A)
67: R_1= β-D-**Glc**, R_2=Me, R_3=OAc, R_4=R_6=R_7=H, R_5=OH (Scilliroside)
68: R_1= α-L-**Rha**, R_2=Me,R_4= β-OH, R_3=R_5-R_7=H (Scillapheoside A)
69: R_1= Sug-6, R_2=Me, R_4= β-OH, R_3=R_5-R_7=H (Glucoscillipheoside)
70: R_1= Sug-7, R_2=Me, R_3-R_7=H (GlucoScillaren A)

Sug-6:

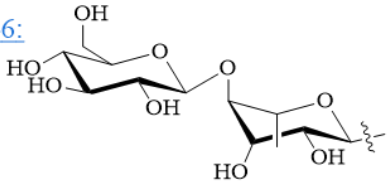

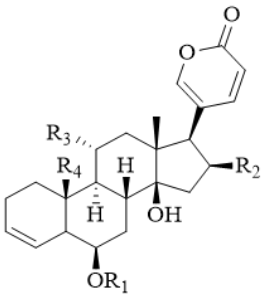

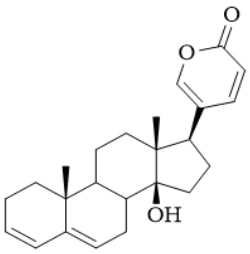

Sug-7:

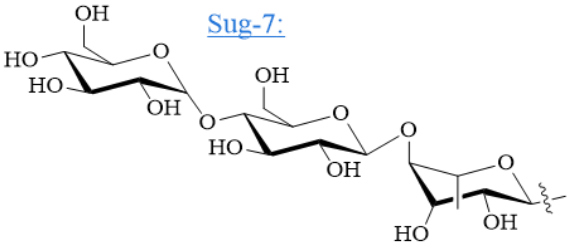

71: R_1= β-D-**Glc**, R_2=R_3=H, R_4= CHO (Scillaren F)
72: R_1= β-D-**Glc**, R_2= OAc, R_3=H, R_4= CHO (Scillicyanoside)

73: Scillaridin A

Flavonoids

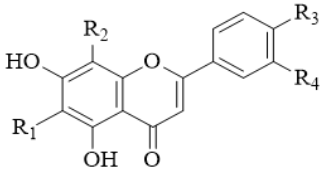

74: R_1=H , R_2=β-D-**Glc**, R_3=OH, R_4=OMe (Scoparin)
75: R_1=R_4= H,R_3=OH, R_2= β-D-**Glc** (Vitexin)
76: R_1= H, R_4= R_3=OH, R_2= β-D-**Glc** (Orientin)

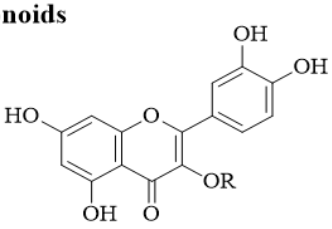

77: R=β-D-**Glc** (Quercetin-3-*O*-glucoside)

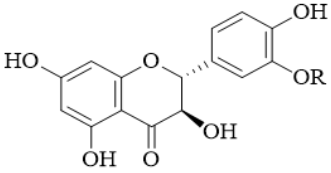

78: R=β-D-**Glc** (Taxifolin-3-*O*-glucoside)

Anthocyanins

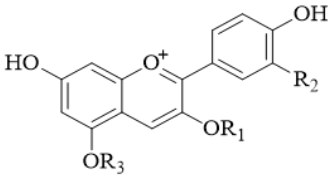

79: R_1= β-D-**Glc,** R_2=OH,R_3=H (Cyanidin 3-*O*-glucoside)
80: R_1=R_3= β-D-**Glc,** R_2=OH (Cyanidin 3,5-*O*-diglucoside)
81: R_1= β-D-**Glc**, R_2=R_3= H (Pelargonidin 3-*O*-glucoside)

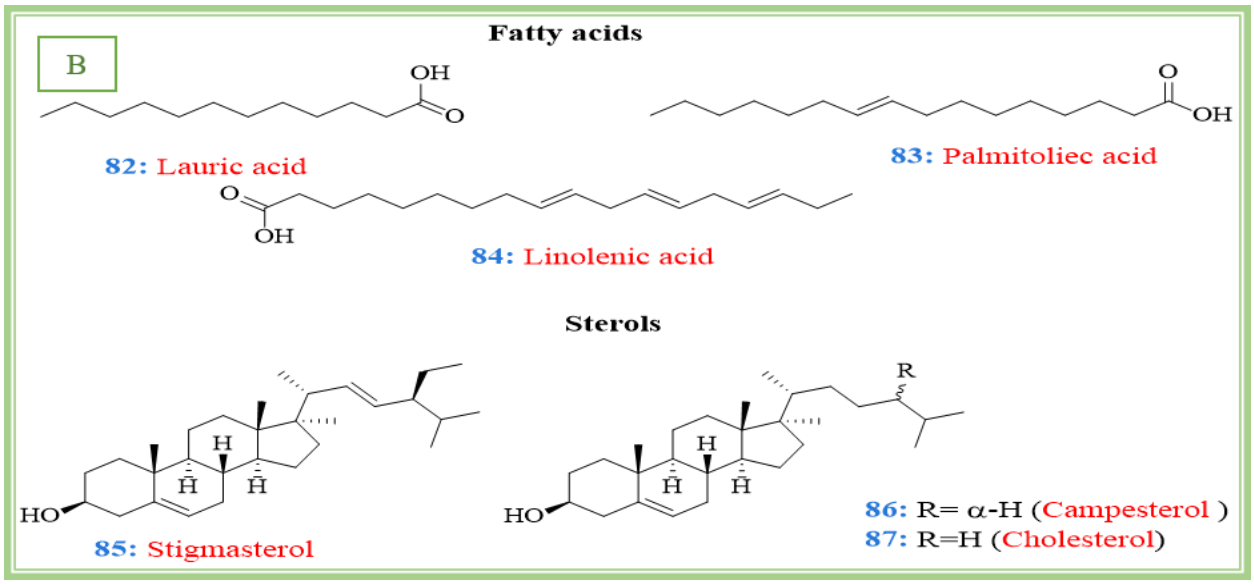

Figure I.7 (A/B). Chemical composition of *S. maritima* L. bulbs

In addition to the homoisoflavones, the NMR examination of the hydro-ethanolic extract obtained from the bulbs of *S. socialis* (Baker) has resulted in the isolation of hyacinthacines **88–98** where the genus *Scilla* is an especially rich source of these compounds, pyrrolidines **99, 100** and piperidines **101–103** **[60]**. The DCM and MeOH extracts of the bulb have yielded other constituents such as polyhydroxylated difuran derivative **104**, a sterol (stigmasterol) **85** and an alcohol diterpenoid **105** **[61]** **(**Figure I.8.A/B**)**.

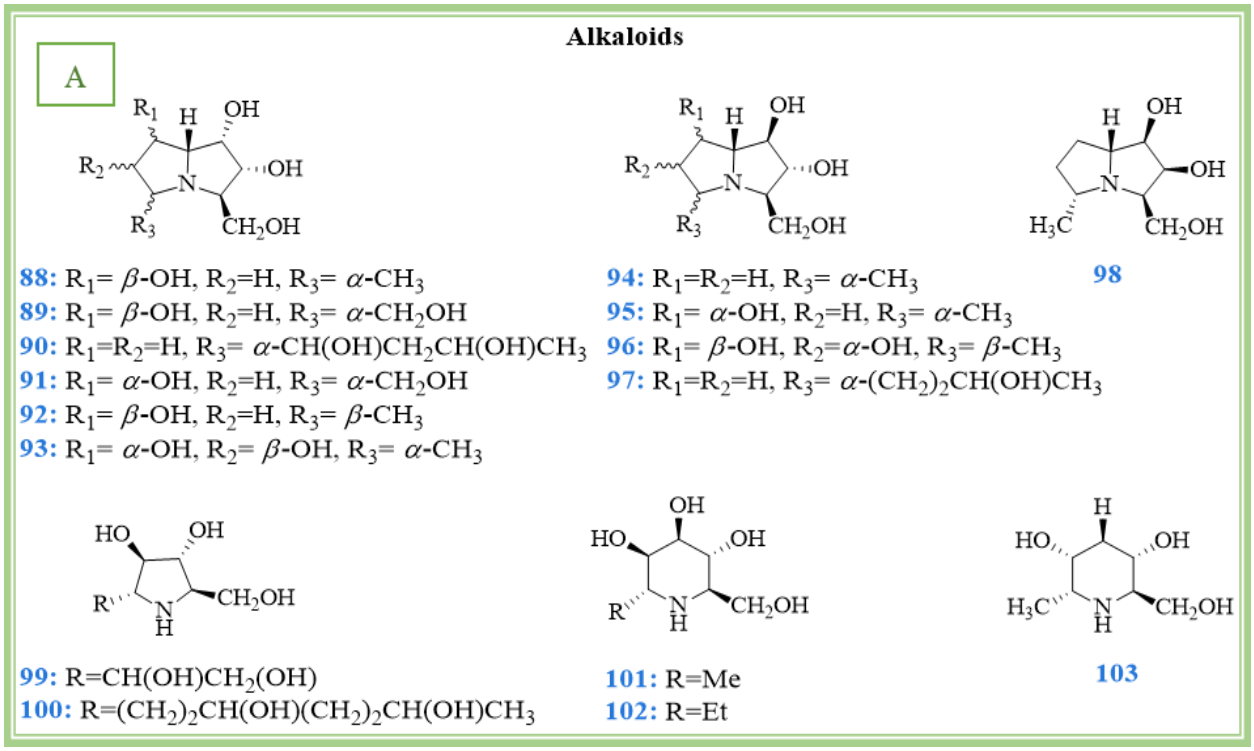

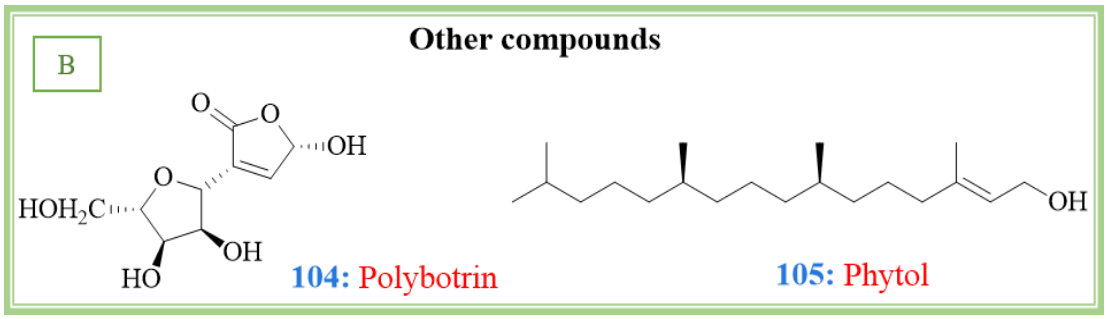

Figure I.8 (A/B). Alkaloids and other biochemicals isolated from the bulbs of *S. socialis* Bak.

HPLC and MS examination of extracts obtained from bulbs and aerial parts of *S. bifolia* (L.) have yielded some of polyphenolic compounds **106–114 [62] (**Figure I.9**)**.

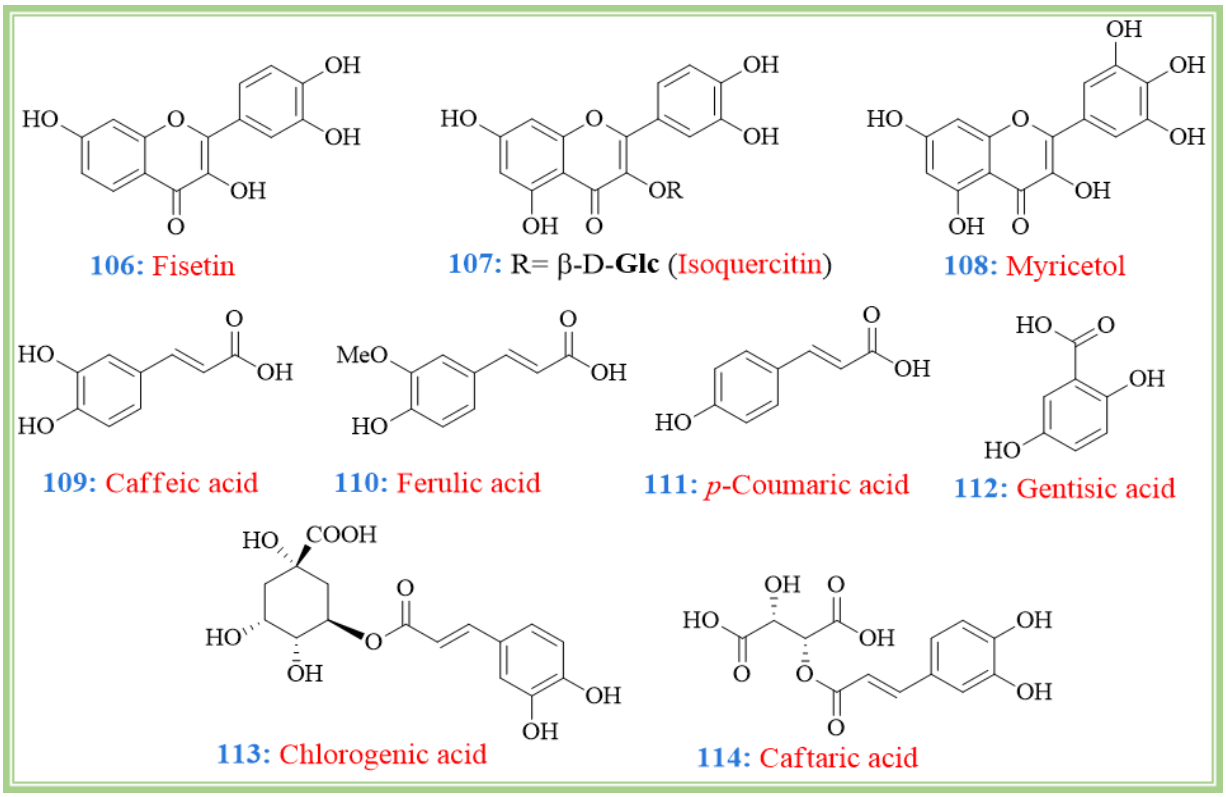

Figure I.9. Polyphenols isolated from the bulbs and aerial part of *S. bifolia* L.

I.5 | Biological activities review of *Scilla* species

Phytochemical studies on *Scilla* species revealed the presence of main biochemicals including homoisoflavonoids, bufadienolides and some types of alkaloids. Herein, many investigations of the biological activities are associated to these compounds.

I.5.1 | Homoisoflavonoids

Homoisoflavonoids have been reported to show a wide range of biological properties including antimicrobial, antimutagenic, antioxidant, immunomodulatory, anti-diabetic, cytotoxic, antiangiogenic, vasorelaxant and anti-inflammatory effects. In addition, homoisoflavonoids were reported to inhibit protein tyrosine kinase and showed estrogenic and anti-estrogenic activities **[63]** some examples will be discussed here:

A homoisoflavonoid named Scillapersicone **(**Figure I.10**)** was isolated from *S. persica* HAUSSKN, showed significant *in vitro* **cytotoxic** activity with IC_{50} values of 25 and 28 µM against AGS and WEHI-164 cells **[64]**. **Antimicrobial** activity of $CHCl_3$ and EtOAc extracts of the plant bulb exhibited an efficient *in vitro* action on *Escherichia coli*, *Staphylococcus aureus* and *Bacillus cereus* **[65]** which lead the research team to think that the presence of this class of flavonoids is probably responsible of this activity **[66]**.

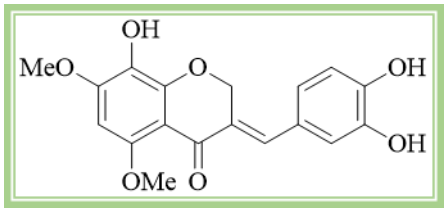

Figure I.10. Structure of Scillapersicone.

Significantly, high **anti-inflammatory** activity (inhibition of prostaglandin synthesis ≥70% in microsomal cell fractions) and selective inhibitory activity on COX-1 enzyme **[67]** were observed for homoisoflavonoids isolated from *S. natalensis* **[68]**, *S. scilloides* and *S. nervosa***.**

Antioxidant examination of nine homoisoflavonoids isolated from *S. scilloides* resulted in showing higher activities of compounds **1–3, 5** and **7** in DPPH test while EC_{50} values indicate that compound **3** displayed a potent antioxidant activity with EC_{50} value of 8.1µM .In H_2O_2 scavenging assay, compounds **1–3, 5–7** showed 85.4-99.3% of high activity **[69]**.

I.5.2 | Bufadienolides

Bufadienolides have been reported to be functioned as cardiotonic, blood pressure stimulant and also to have antineoplastic activity **[70]**. Scillaren A **66** and proscillaridin A **65** are the major glycosides found in the bulbs of *S. maritima*, *S. indica* Baker **[71]** and *S. maderensis* **[37]**.

In vitro study on isolated pulmonary artery of rabbit, showed that the extract of *S. maritima* has a quite clear positive **inotropic effect**[11] resulted from blocking Na^+/K^+-ATPase by glycoside constituents (bufadienolide especially proscillaridin A **65**) **[72]**.

In vivo studies on the renal function of rabbit by intravenous injection of aqueous extract of *S. martima* produced significant increases in urine flow, urinary Na^+ excretion rate and reduction in urinary K^+ excretion rate (diuretic and natriuretic effects) which mean that the isolated bufadienolides has an **aldosterone antagonist activity** on Na^+/K^+ pump (inhibitory effect). In the same conditions, subcutaneous injection on rat showed decreases in both blood pressure and heart rate, for that the plant extract display the **hypotensive effect** and **vasoconstrictor activity**[12] **[72]**.

The major toxic bufadienolide named scilliroside **67** from *S. maritima* has been reported to have cardiovascular activity and rodenticide property (causing convulsion and death to rats) **[73]**.

I.5.3 | Alkaloids

In 2007, three alkaloids classes were isolated from *S. socialis* Baker where four hyacinthacines were found to be **glycosidase inhibitors**. Compound **89** was found to be a good inhibitor of *β*-glucosidase extracted from the named bacteria *Caldocellum sacchrolyticim* (IC_{50} 13 µM), while compound **96** showed a moderate inhibition effect (IC_{50} 48 µM). Compound **91** was demonstrated to be a potent inhibitor of *β*-galactosidase isolated from bovine liver. Compound **93** was shown to have an inhibitory potential toward rat intestinal maltase *α*-glucosidase (IC_{50} 45 µM) **[60]**.

Pyrrolidine type alkaloid isolated from *S. sibirica* (How.) was found to be a potent inhibitor of *Caldocellum sacchrolyticim* *β*-glucosidase (IC_{50} 3.2 $\mu g.ml^{-1}$) and bovine liver *β*-galactosidase (IC_{50} 4.4 $\mu g.ml^{-1}$) **[74]**.

In 2017, a study on the extract of *S. maritima* bulbs showed a significant inhibitory effect on **acetylcholinesterase activity**, where this enzyme was extracted from rice weevils (*Sitophilus oryzae*). This effect is due to the interaction between a complex (polyphenols and alkaloids) and insect tissues **[75]**.

[11] Is the contraction of the heart muscle.
[12] Vasoconstriction is the narrowing of the blood vessels resulting from contraction of the muscular wall of the vessels.

References

[1]. Peruzzi L. A new infrafamilial taxonomic setting for Liliaceae, with a key to genera and tribes. *Plant Biosyst*. **2016**, 150**(**6):1341–1347

[2]. Thorne RF. Classification and geography of the flowering plants. *Bot. Rev*. **1992**, 58(3):225–327

[3]. [APG] Angiosperm Phylogeny Group.An Ordinal Classification for the Families of Flowering plants. *Ann. Missouri Bot. Gard*.**1998**, 85(4):531–553

[4]. Taye T, Akinyele BO, Odiyi AC, Arotupin DJ. Phytochemicals of Some Members of the Family Hyacinthaceae and their Significance in plant Protection. *Proceeding of the WCE*. **2013**

[5]. Martínez-Azorín M, Crespo MB, Juan A, Fay MF. Molecular phylogenetics of subfamily Ornithogaloideae (Hyacinthaceae) based on nuclear and plastid DNA regions, including a new taxonomic arrangement. *Ann. Bot*. **2010**, 107(1):1–37

[6]. Dahlgren RMT, Clifford HT, Yeo PF. The Families of the Monocotyledons: Structure, Evolution, and Taxonomy. 1st Edition. Berlin Heidelberg New York Tokyo: *Springer-Verlag*; (January 22, **1985**). p.188, p.191

[7]. [APG] Angiosperm Phylogeny Group. An update of the Angiosperm Phylogeny Group classification for the orders and families of flowering plants: APG III. *Bot. J. Linn. Soc*.**2009**, 161:105–121

[8]. [APG] Angiosperm Phylogeny Group. An update of the Angiosperm Phylogeny Group classification for the orders and families of flowering plants: APG II. *Bot. J. Linn. Soc*. **2003**, 141:399 – 436

[9]. Chase MW, Reveal JL, Fay MF. A sub familial classification for the expanded Asparagalean families Amaryllidaceae, Asparagaceae and Xanthorrhoeaceae *Bot. J. Linn. Soc*. **2009**, 161(2): 132–136

[10]. Maarten JM, Christenhusz & James W.BYNG. The number of known plants species in the world and its annual increase. *Phytotaxa*. **2016**, 261(3): 201–217

[11]. Byng JW. The Flowering Plants Handbook: A practical guide to families and genera of the world. Hertford, UK: *Plant Gateway Ltd*.; **2014**. p.88

[12]. Ghoran SH, Saeidnia S, Babaei E, Kiuchi F, Hussain H**.** Scillapersicene: a new homoisoflavonoid with cytotoxic activity from the bulbs of *Scilla persica* HAUSSKN. *Nat. Prod. Res*. **2015**, 30(11): 1309–1314

[13]. Almeida da silva R, Rocha J, Silva A, García-Cabral I, Amich F,Crespí AL. The Iberian Species of *Scilla* (Subfamily Scilloideae, Family Asparagaceae) Under Climatic Change Scenarios in Southwestern Europe. *Syst. Bot*. **2014**, 39 (4):1083–1098

[14]. Gentry HS, Verbiscar AJ, Banigan TF. Red squill (*Urginea maritima*, Liliaceae). *Econ. Bot.* **1987**, 41(2):267–282

[15]. Żuraw B. Flowering biology of three taxa of the genus *Scilla* L. (Hyacinthaceae) and Flower Visitation by Pollinating insects. *Acta Agrobot.* **2010**, 64 (1): 11–18

[16]. Anthony P.Knight. A Guide to poisonous House and Garden Plants. 1st Edition. New York: *Teton New Media*; **2007**.p.249

[17]. Erek I, Akan H.Last Two Hundred Individuals: Rediscovery of *Scilla Mesopotamica* Speta (Hyacinthaceae) A Three Tened Endemic species In Turky. *Acta soc. Bota. Pol*. **2010**, 79 (1):31–36

[18]. Vela E, De Bélair G, Rosato M, Rosselló J. Taxonomic remarks on *Scilla anthericoides* Poir. (Asparagaceae, Scilloideae), a neglected species from Algeria. *Phytotaxa*. **2016**, 288(2):154

[19]. Hamouche Y, Amirouche N, Misset MT, Amirouche R. Cytotaxonomy of autumnal flowering species of Hyacinthaceae from Algeria. *Plant Syst. Evol*. **2010**, 285(3-4):177–187

[20]. Taylor JLS, Elgorashi EE, Maes A, Van Gorp U, De Kimpe N, Van Staden J, Verschaeve L. Investigating the safety of plants used in South African traditional medicine : Testing for genotoxicity in the micronucleus and alkaline comet assays. *Environ. Mol. Mutagen*. **2003**, 42(3):144–154

[21]. Deb DB, Dasgupta S. Studies on Indian Squill – *Urginea indica* (Roxb.) Kunth. *Q. J. Crude Drug Res*. **1976**, 14(2):49 – 60

[22]. Chittoor MS, Roger Binny AJ, Yadlapalli SK, Cheruku A, Dandu C, Nimmanapalli Y.Anthelmintic and antimicrobial studies of *Drimia indica* (Roxb.) Jessop.bulb aqueous extracts.*J. Pharm. Res*. **2012**, 5(5): 3677–3686

[23]. Williams VL, Raimondo D and Cunningham AB. Trade, bulb age and impacts on *Merwilla plumbea*. *South Africa. J. Bot*. **2007**, 73:321–322

[24]. Namba T. The Encyclopedia of Wakan-Yaku .Osaka, Japan: *Hoikusha*; **1993**

[25]. Mcartan SA, Van Staden J. Micropropagation of members of the Hyacinthaceae with medicinal and ornamental potential. A review *S. Afr. J. Bot*. **1999**, 65(5-6): 361–369

[26]. Samson OF, Aku NN, Andrae-Marobela K, Samuel OY. A new homoisoflavonoid and the bioactivities of some selected homoisoflavonoids from the inter-bulb surfaces of *Scilla nervosa* subsp. rigidifolia. *S. Afr. J. Bot*. **2013**, 88: 17–22

[27]. Silayoa A, Ngadjui BT, Abegaz BM. Homoisofavonoids and stilbenes from the bulbs of *Scilla nervosa* subsp.rigidifolia. *Phytochemistry* **1999**, 52:947– 955

[28]. Bangani V, Crouch NR, Mulholland DA. Homoisoavanones and stilbenoids from Scilla nervosa. *Phytochemistry* **1999**, 51:947– 951

[29]. Al-rhazes. Al havi. 1st Edition. Afsharipour S, Ed. Tehran: *Academy of medical sciences publication*; **2005**

[30]. Avicenna. The Canon of medicine. 2nd Edition .Sharafkandi A, Ed. Tehran: *Soroush press*; **1997**

[31]. IUCN Centre for Mediterranean cooperation. A guide to medicinal plants in North Africa. Malaga, Spain: *IUCN*; **2005**.p.251–253

[32]. Bozorgi M, Amin G, Shekarchi M, Rahimi R. Traditional medical uses of *Drimia* species in terms of phytochemistry, pharmacology and toxicology. *J. Tradit. Chin. Med*. **2017**, 37(1):124–139

[33]. Verschaeve L, VanStadenc J. Mutagenic and antimutagenic properties of extracts from South Africa traditional medicinal plants. *J. Ethnopharmacol*. **2008**, 119:575 –587

[34]. Du Plessis N, Duncan G. Bulbous Plants of Southern Africa-A guide to thier cultivation and propagation. Cape Town: *Tafelberg Publishers Ltd*; **1988**

[35]. Huntchings A. A survey and analysis of traditional medicinal plants as used by the Zulu, Xhosa and Sotho. *Bothalia*. **1989**, 19:111–123

[36]. Louw CAM, Regnier TJC, Korsten L. Medicinal bulbous plants of South Africa and their traditional relevance in the control of infectious diseases. *J. Ethnopharmacol*. **2002**, 82:147–154

[37]. Dias C, Graça JAB, Gonçalves ML. Scilla maderensis, TLC screening and positive inotropic effect of bulb extracts. *J. Ethnopharmacol*. **2000**, 71(3):487– 492

[38]. Pacificbulbsociety.org. (2019). *Pacific Bulbs society | Scilla species one*. [Online] Available at: https://www.pacificbulbsociety.org/pbswiki/index.php/ScillaSpeciesOne# bifolia [Accessed 4 Aug. 2019]

[39]. Kayiran SD, Özkan EE. The ethnobotanical uses of Hyacinthaceae species growing in Turkey and a review of pharmacological activities .*Indian J. Trad. Know.* **2017**, 16:243-250

[40]. NishidaY, Eto M, Ikeda T. A new homostilbene and two new homoisoflavones from the bulbs of *Scilla scilloides*. *Chem. Pharm. Bull*. **2008**, 56:1022–5

[41]. Kouno I, Noda N, Ida Y, Sholichin M, Miyahara K, Komori T, Kawasaki T. Zur Struktur eines neuen Nortriterpens aus den Bulbi von *Scilla scilloides* Druce. *Liebig Ann. Chem*. **1982**, (2):306–314 [In German]

[42]. Lee S-M, Chun H-K, Lee C-H, Min B-S, Lee E-S, Kho Y-H. Eucosterol oligoglycosides isolated from *Scilla scilloides* and their anti-tumor activity. *Chem. Pharm. Bull*. **2002**, 50(9):1245–1249

[43]. Sholichin M, Miyahara K, Kawasaki T. Oligoglycosides of spirocyclic nortriterpenoids related to eucosterol. *Chem. Pharm. Bull*. **1985**, 33(4):1756–1759

[44]. Lee S-M, Lee H-J ,Chun H-K, Lee C-H, Kang S-J, Maeng H-Y, Kho Y-H. Cytotoxicity and Quantitative Analysis of Nortriterpenoid glycoside from *Scilla scilloides*. *Korean J. Pharmacognosy*. **2001**, 32(3):189–192

[45]. Ono M, Toyohisa D, Morishita T, Horita H, Yasuda S, Nishida Y, Tanaka T, Okawa M, Kinjo J, Yoshimitsu H, Nohara T. Three New Nortriterpene Glycosides and Two New Triterpene Glycosides from the Bulbs of *Scilla scilloides*. *Chem. Pharm. Bull*. **2011**, 59(11):1348–1354

[46]. Ono M, Ochiai T, Yasuda S, Nishida Y, Tanaka T, Okawa M, Kinjo J, Yoshimitsu H, Nohara T. Five new nortriterpenoids glycosides from the bulbs of *Scilla scilloides*. *Chem. Pharm. Bull*. **2013**, 61(5) :592–598

[47]. Lee H-B, Lee S-M. Antimicrobial Activity of Eucosterol Oligosaccharides Isolated from Bulb of Squill (*Scilla Scilloides*). *Pharmacol. Pharm*. **2013**, 4 (1):110-114

[48]. Ono M, Takatsu Y, Ochiai T, Yasuda S, Nishida Y, Tanaka T , Okawa M , Kinjo J , Yoshimitsu H, Nohara T. Two New Nortriterpenoid Glycosides and a New Phenylpropanoid Glycoside from the Bulbs of Scilla scilloides. *Chem. Pharm. Bull*. **2012**, 60(10):1314–1319

[49]. Ren F-C, Wang L-X, Yu Q, Jiang X-J, Wang F. Lanostane-type triterpenoids from *Scilla scilloides* and structure revision of Drimiopsin D. *Nat. Prod. Bioprospect*. **2015**, 5:263–270

[50]. Du Toit K, E.Drewes S, Bodenstein J. The chemical structures, plans origins, ethnobotany and biological activities of homoisoflavanones. *Nat. Prod. Res*. **2010**, 24 (5):457–490

[51]. Bezabih M, Famuyiwa SO, Abegaz BM. HPLC analysis and NMR identification of homoisoflavanoids and stilbenoids from the inter-bulb surface of *scilla nervosa*. *Nat. Prod. Commun*. **2009**, 4 (10):1367–1370

[52]. Krenn L, Kopp B, Steurer S, Schubert-Zsilavecz M. 9-Hydroxyscilliphaeoside, a new bufadienolide from *Urginea maritima*. *J. Nat. Prod*. **1996**, 59:612–613

[53]. Stoll A. Sur les substances cardiotoniques de la scille maritime (*Scilla maritima L*). *Experientia*. **1954**, 10(7) : 282–297

[54]. Fernandez M, Renedo J, Arrupe T, Vega FA. C-Glycosylflavones in the bulbs of squill. *Phytochemistry* **1975**, 14(2):586

[55]. Vega FA, Garcia-Jalon I, Fernandez M, Renedo J. Anthocyanins of red squill, *Urginea maritima*. *Phytochemistry* **1972**, 11(9):2896

[56]. Fernandez M, Vega FA, Arrupe T, Renedo J. Flavonoids of squill, *Urginea maritima*. *Phytochemistry* **1972**, 11(4):1534

[57]. Couladi M and Loukis A. *Fitoterapia* **1987**, 58:57–58

[58]. Aliaga A, Fernandez M, Vega FA, Dios C. *Acta. Pol. Pharm*. **1987**, 44:560–562

[59]. Fernandez M, Oses M, Dios C. *An. Real Acad. Farm*. **1987**, 53:292–295

[60]. Kato A, Kato N, Adachi I, Hollinshead J, W.J.Fleet G, Kuriyama C, Ikeda I, Asano N, J.Nash R . Isolation of glycosidase-inhibiting Hyacinthaceae and related alkaloids *Scilla socialis*. *J. Nat. Prod*. **2007**, 70 (6):993–997

[61]. Waller CP. PhD Thesis, University of Surrey, Guildford, UK, **2012**

[62]. Bălăşoiu ML, Călina D, Vlase L, Bubulică MV. Qualitative and quantitive determination of polyphenol content of *Scilla bifolia*. *J. Med. Plants Res*. **2012**, 6 (20): 3664–3671

[63]. Lin L-G, Liu Q-Y, Ye Y. Naturally occurring homoisoflavonoids and their pharmacological activities. *Planta Med*. **2014**, 80:1053–1066

[64]. Ghoran SH, Saeidnia S,Babaei E, Kiuchi F, Dusek M, Eigner V, Khalaji AD, Soltani A. Biochemical and biophysical properties of a novel homoisoflavonoid extracted from *Scilla persica* HAUSSKN. *Bioorg. Chem*. **2014**, 57:51–56

[65]. Ghoran SH, Mighani H, Ebrahimi P. In vitro antibacterial activity of chloroform, ethyl acetate and hydroalcoholicextracts of *Scilla persica* HAUSSKN. *J. Gorgan Univ. Med. Sci*. **2014**, 16(1) :106–113

[66]. Ghorban SH, Ebrahimi P, Mighani M, Saeidnia S. Isolation and characterization of homoisoflavonoids from *Scilla persica* HAUSSKN. *BJPS*. **2015**, 51 (4):949–955

[67]. DuToit K, Elgorashi EE, Malan SF, Drewes SE, VanStaden J, Crouch NR, Mulholland DA. Anti-inflammatory activity and QSAR studies of compounds isolated from Hyacinthaceae species and Tachiadenus longiflorus Griseb (Gentianaceae). *Bioorg. Med. Chem*.**2005**, 13:2561–2568

[68]. Crouch NR, Bangani V, Mulholland DA. Homoisoflavanones from three South African *Scilla* species. *Phytochemistry* **1999**, 51(7):943–946

[69]. Nishida, Y, Wada K, Toyohisa D,Tanaka T, Ono M, Yasuda S. Homoisoflavones as the antioxidants responsible from bulbs of *Scilla scilloides*. *Nat. Prod. Res*. **2013**, 27(24):2360–2362

[70]. Ramawat KG, Merillon J-M. Bulbous plants biothecnology. 1st Edition. Boca Raton: *CRC press*; **2014**.p.350, p.351

[71]. Khare CP. Indien medicinal plants: An illustrated dictionary. 1st Edition. New Delhi, India: *Springer*; (april22, **2008**).p.590

[72]. Dizaye K, K.Hamad B-A. Cardiovascular studies of white squill (*Urginea maritima*) extract. *Zanco J. Med. Sci*. **2010**, 14

[73]. Verbiscar AJ, Patel J, Banigan TF, Schatz RA. Scilliroside and other *scilla* compounds in red squill. *J. Agric. Food Chem*. **1986**, 34:973–979

[74]. Yamashita T, Yasuda K, Kizu H, Kameda Y, Watson A, Nash RJ, Fleeta GWJ, Asano N. New Polyhydroxylated Pyrrolidine, Piperidine, and Pyrrolizidine Alkaloids from *Scilla sibirica*. *J. Nat. Prod*. **2002**, 65:1875–1881

[75]. Mani Maazoun A, Ben Hlel T, Hamdi SH, Belhadj F, Ben Jemaa JM, Marzouki MN. Screening for insecticidal potential and acetylcholinesterase activity inhibition of *Urginea maritima* bulbs extract for the control of *Sitophilus oryze* (L.). *J. Asia-Pac. Entomol*. **2017**, 20:752–760

Chapter II

Experimental part

Scilla lingulata

Phytochemical study

Molecular docking simulation

About *S. lingulata*

II.1 Description of the investigated plant

Scilla lingulata is characterized by a white, small and oval bulb, where the aerial parts are developed from this one. From 3 to 10 leaves with lanceolate shape, are joined in rosette form, which appear before flowering. Short and green inflorescence stem grows in the center of leaves' rosette, in which the end of the growing point produces a group of blue flowers well developed. This plant was described as an endemic species in North Africa **[1] (**Figure II.1**)**.

Figure II.1. *Scilla lingulata* Poir. (**a.** *Flower*, **b.** *Inflorescence*, **c.** *Bulb*)

II.2 Taxonomical identification of *Scilla lingulata* in plant kingdom

The botanical taxonomy of *S. lingulata* according to the APG III classification is outlined as below **[2-4]**:

Table II.1. Botanical systematic taxonomy

Major taxonomic ranks	**Taxon**
Kingdom	Plantae
Division	Angiospermae
Class	Monocotyledonae
Order	Asparagales
Family	Asparagaceae
Subfamily	Scilloideae / Hayacinthaceae
Genus	*Scilla*
Species	*Scilla lingulata* Poir.
Synonym	*Hyacinthoides lingulata* (Poir.)Rothm.

II.3 | Why *Scilla lingulata*?

The choice of this plant as a subject for phytochemical and biological investigations was motivated by:

- The lack of previous studies, regarding structural elucidation and biological activities on *S. lingulata*, make our work an original research.
- The wide uses of *Scilla* species in folk medicine to treat different illnesses (see Chapter I I.3).
- Previous phytochemical studies on *Scilla* species have demonstrated the presence of various secondary metabolites with potent biological effects (see Chapter I I.4 and5) that gave us the scientific curiosity to investigate the endemic *S. lingulata*, looking for important results.

II.4 | Extraction procedure of *Scilla lingulata*

In 2017, a Master's student at the University of Msila carried out the extraction of the whole plant using Soxhlet extraction method **[5]**. The work was summarized as below:

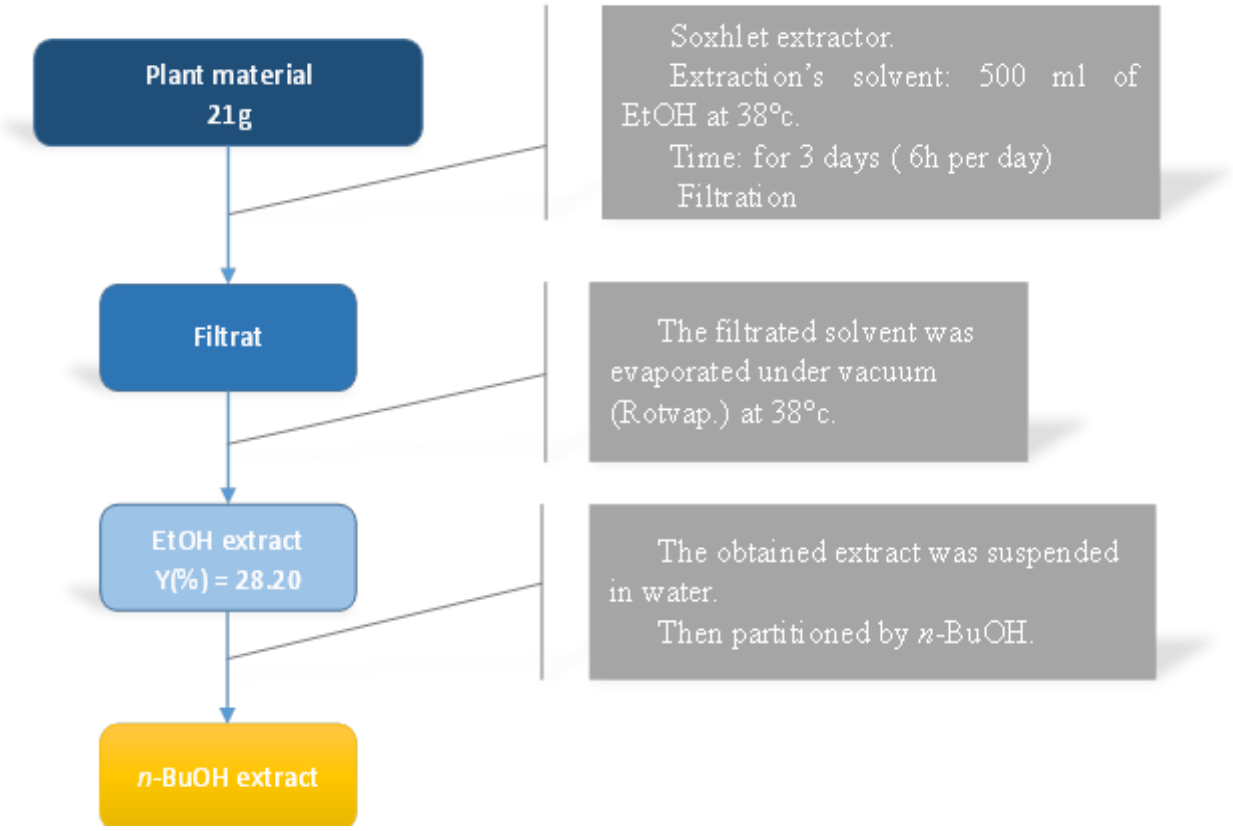

Figure II.2. Extraction procedure of *S. lingulata* to obtain the *n*-BuOH extract

Phytochemical study

II.5 | Phytochemical study

II.5.1 | Plant material

In the aim of determining the chemical composition of *S. lingulata*, in particular, the polar constituents, the study was oriented to investigate the *n*-butanolic extract (6 g).

II.5.2 | Apparatus and chromatographic conditions for LC-ESI/MS

All analyses were performed on a Hewlett–Packard (Palo Alto, CA, USA) Model 1100 Series, liquid chromatograph coupled to both PDA detector (Agilent, Palo Alto, CA, USA) 1100 Series and Esquire LC–ion trap mass spectrometer (BrukerDaltonics, Billerica, MA, USA) equipped with an electrospray ionization (ESI) interface. UV-DAD 200-700 nm; UV chain: 204, 234, 254, 470 and 665 nm.

ESI source: positive and negative mode; injection: 5µL. The elution system is 80:20 (H_2O + 1 mL ammonium acetate (10 mM): CH_3CN + 1 mL ammonium acetate (10 mM)) for 30 min and then it changes to 0:100 up to 56 min, the fractionation of the column effluent was performed with a flow rate of 1 mL/min flowing into the mass spectrometer.

The LC-MS spectrum was performed on a Nucleosil® C18 Macherey-Nagel column (250 mm × 4.6 mm I.D.; 5 µm particale size, end-capp). High-purity nitrogen was used as the nebulizer and as the drying gas at 300°C, at a constant flow rate of 6 L/min. The full spectra were acquired in negative ion mode in the *m/z* 100-1000 region, adopting the following parameters: trap drive units, 55.1; capillary output voltage, –120.4 V; skimmer 1 voltage, –43.3 V.

II.5.3 | Method

The *n*-butanolic sample of 400 µL (10 mg/mL) was sent to the Laboratory of Bioorganic Chemistry at the University of Trento-Italy for recording of the LC-ESI/MS profiles.

Molecular docking simulation studies

II.6 | Molecular docking

II.6.1 | Materials

- **Microcomputer**

Memory (RAM): 4.00 GB
Processor: i5_2520M CPU 2.50 GHz
System type: 64- bits Operating system
Windows edition: 10 Pro 2015 version

- **Software packages**

ChemDraw Pro 12.0.2 **OpenBabel** 3.0.0 **AutoDockTools** 1.5.6

BIOVIA Discovery Studio 2020 **Avogadro** 1.2.0 **AutoDockVina** 1.1.2

UCSF Chimera-alpha 1.15

II.6.2 | Method

II.6.2.1 | Data preparation

- **Ligand modeling**

The structures of the identified compounds were sketched and saved as CDX files format using ChemDraw. These files were converted to SDF format using OpenBabel then the 3D structures of those ligands were obtained and saved as PDB format by Avogadro software (Figure II.3– 5).

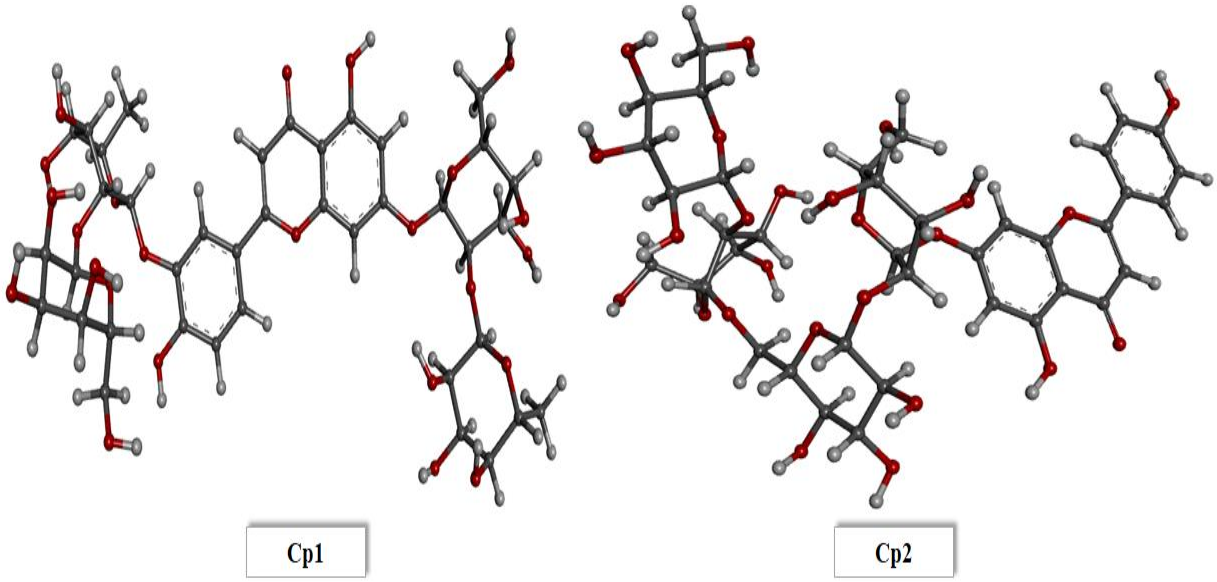

Figure II.3. 3D structure of the compounds Cp1 and Cp2 represented in ball and stick

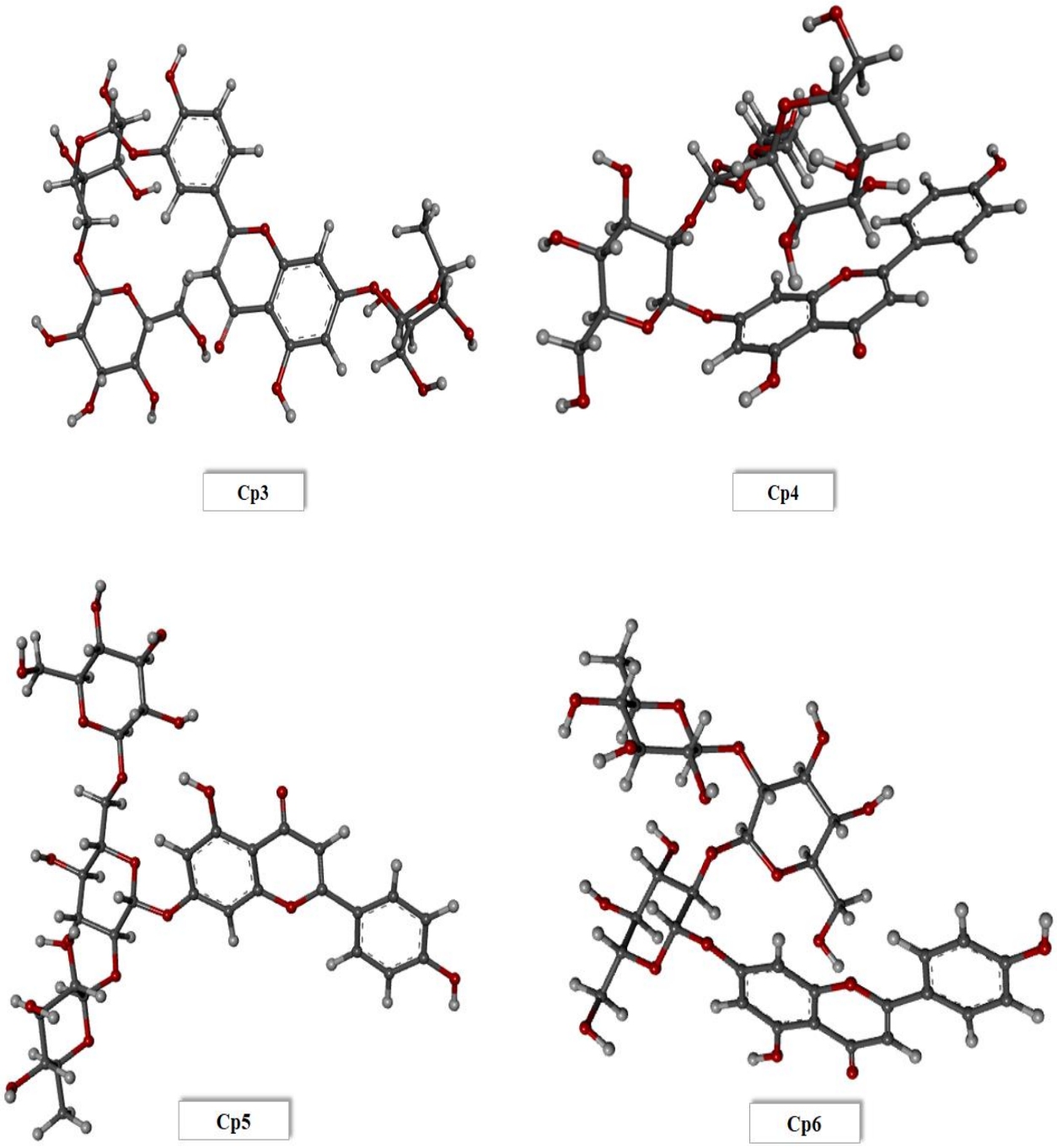

Figure II.4. 3D structure of the compounds Cp3–Cp6 represented in ball and stick

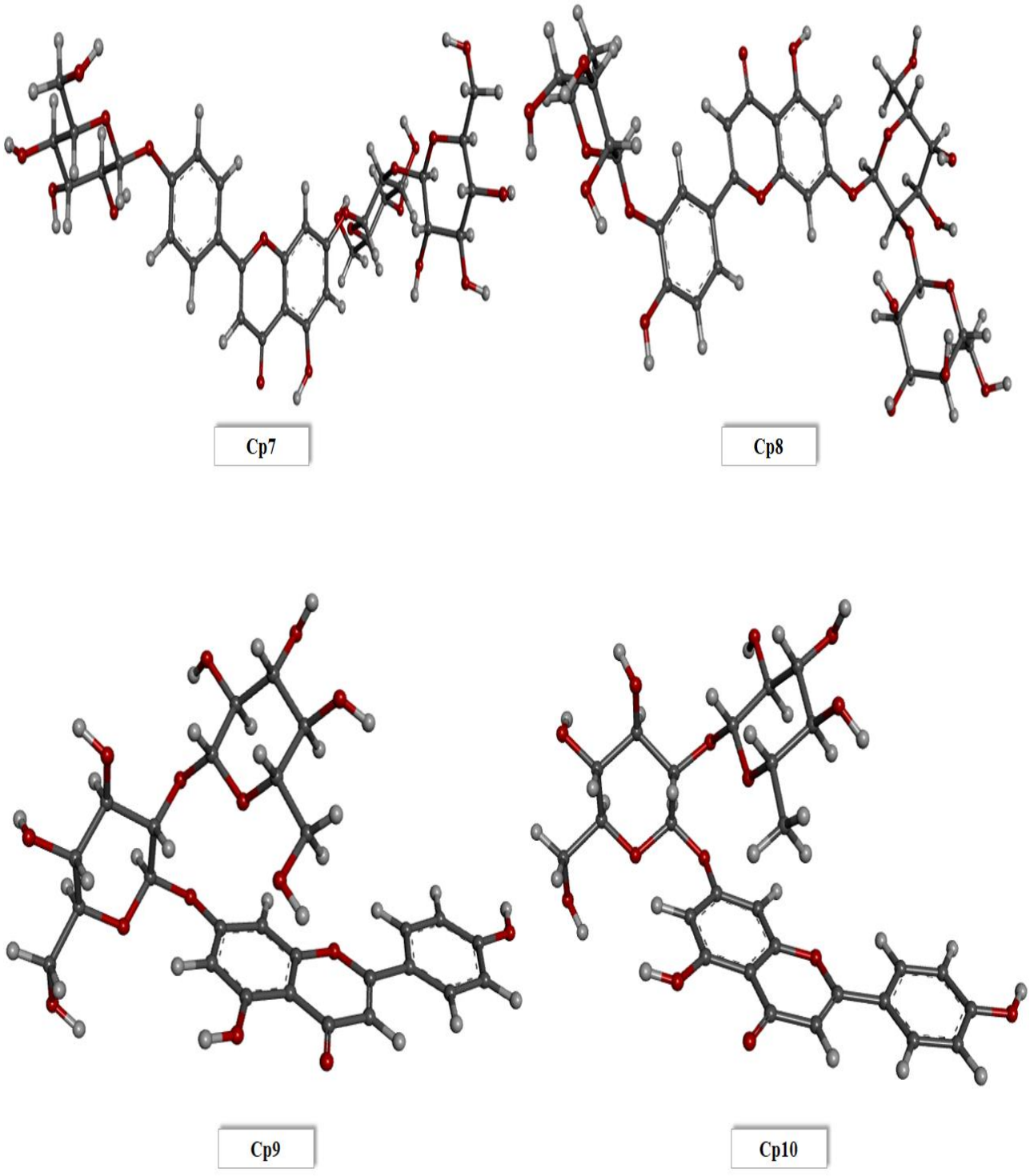

Figure II.5. 3D structure of the compounds Cp7–Cp10 represented in ball and stick

- **Receptor preparation**

The X-ray crystal structures of the selected proteins in the complex state (Table II.2) were retrieved from the RCSB Database (https://www.rcsb.org/pdb) and downloaded as PDB files format. The protein structures were cleaned by removing both water molecules and ligands using BIOVIA Discovery Studio software (Figure II.6, 7). According to the literature data shown in the above website, the active binding site pocket of the target proteins was identified using the same software.

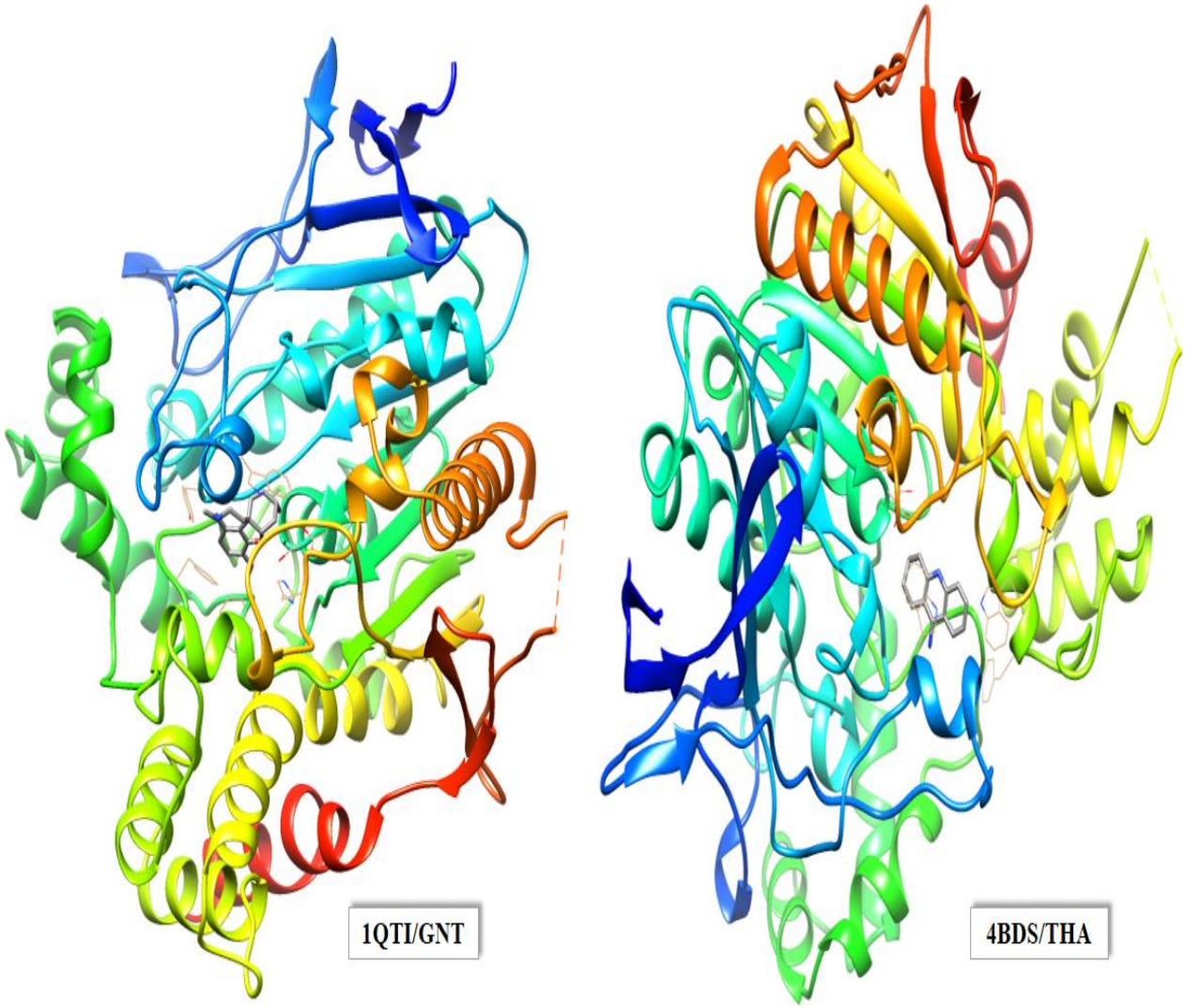

Figure II.6. 3D structures of AChE (at left) and BChE (at right) proteins in complex with their standard inhibitors

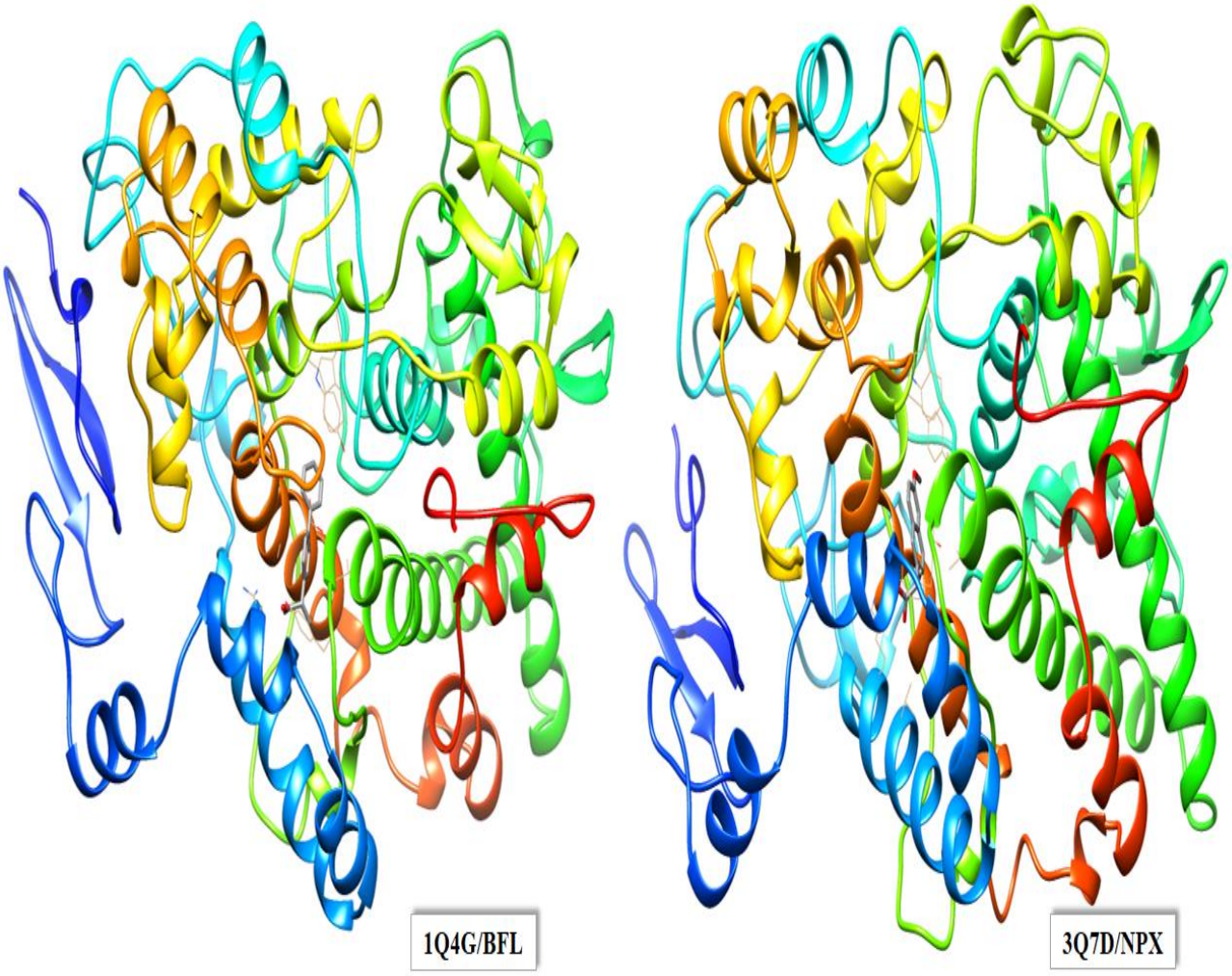

Figure II.7. 3D structures of the isozymes COX-1 (at left) and COX-2 (at right) proteins in complex with their standard inhibitors

Table II.2. Selected complexes for docking studies.

	Cholinesterase activities		Anti-inflammatory activities	
	AChE	***BChE***	***COX-1***	***COX-2***
Complex (PDB ID)	1QTI	4BDS	1Q4G	3Q7D
Docked Ref. ligand	Galanthamine (GNT)	Tacrine (THA)	2-(1,1'-Biphenyl-4-yl)Propanoic acid **(**BFL)	Naproxen (NPX)
Active site residues (Amino acids)	Glc^{199}, Gly^{118}, Ser^{200}, Phe^{331},Trp^{84}, Phe^{330}, Asp^{72}, Gly^{119}, Phe^{288}, Phe^{290}, His^{440}, Ala^{201}, Gly^{117},Tyr^{130}	Trp^{82}, Ser^{79}, Gly^{115}, Gly^{116}, His^{438}, Ser^{198}, Glu^{197}, Gly^{439}, Tyr^{440}, Met^{437}, Trp^{430}, Tyr^{332}, Ala^{328}	Arg^{120}, $Ser^{353, 530}$ Tyr^{385}, Tyr^{355}, Ala^{527}, Val^{349}, Trp^{387}, Leu^{352}, Phe^{381}, Val^{116}, Ile^{523}, Phe^{518}, Met^{522}, Gly^{526}, Leu^{359}, Leu^{384}, Tyr^{348}	Arg^{120}, $Ser^{353, 530}$ Tyr^{385}, Tyr^{355}, Ala^{527}, Val^{349}, Trp^{387}, Leu^{352}, Phe^{381}, Val^{116}, Val^{523}, Phe^{518}, Met^{522}, Gly^{526}, Leu^{359}, Leu^{384}, Tyr^{348}

II.6.2.2 | Docking procedure

According to the docking protocol reported by Muniba **[6]**, the input PDBQT files of ligands and receptors were created by AutoDockTools 1.5.6, then docking calculations were performed using AutoDockVina software **[7]**. Both BIOVIA Discovery Studio and UCSF Chimera were used to analyze and generate illustrations of ligand – receptor complexes (output) in the aim to:

- Find out interactions between ligand atom and active site residues.
- See the formation of complex ligand – receptor and its energy score.
- Compare affinities of the compounds (Cp1– Cp10) to the both receptors in each activity.

References

[1]. Hamouche Y, Amirouche N, Misset MT, Amirouche R. Cytotaxonomy of autumnal flowering species of Hyacinthaceae from Algeria. *Plant Syst. Evol*. **2010**, 285(3-4):177–187

[2]. Dobignard A, Chatelain C. Index synonymique de la flore d'Afrique du nord. Ville de Genéve : Conservatoire et jardin botaniques ; **2010**, p.134

[3]. Chase MW, Reveal JL, Fay MF. A subfamilial classification for the expanded asparagalean families Amaryllidaceae, Asparagaceae and Xanthorrhoseaceae. *J. Linn. Soc. Bot*. **2009**, 161: 132–136

[4]. Byng JW. The Flowering Plants Handbook: A practical guide to families and genera of the world. Hertford, UK: Plant Gateway Ltd.; **2014**. p.92

[5]. Bouaziz M. L'impact de l'extraction sur la composition chimique et l'activité biologique d'une espèce algérienne. L'université M^{ed} Boudiaf-M'sila, **2017**, p. 30–31

[6]. Muniba F. (December 14,2016). How to perform docking in a specific binding site using AutoDock Vina? Bioinformatics review. Retrieved from: https://bioinformaticsreview.com/20161214/how-to-perform-docking-in-a-specific-binding-site-using-autodock-vina/?v=fa3c7f2b5dae

[7]. Trott O, Olson AJ. AutoDock Vina: improving the speed and accuracy of docking with a new scoring function, efficient optimization and multithreading, *J. Comput. Chem*. **2010**, 31(2):455-461

Chapter III

Results and discussions

Spectral analyses of the LC-ESI/MS profiles

Docking results (in silico assays)

Phytochemical study

III.1 | Structural elucidation of the detected compounds in *n*-BuOH extract of S.lingulata using LC-ESI/MS technique

The registered LC-ESI/MS profile revealed the presence of various chromatographic peaks in the studied sample extract (Figure III.1). As a result, forty-one components were detected by MS.

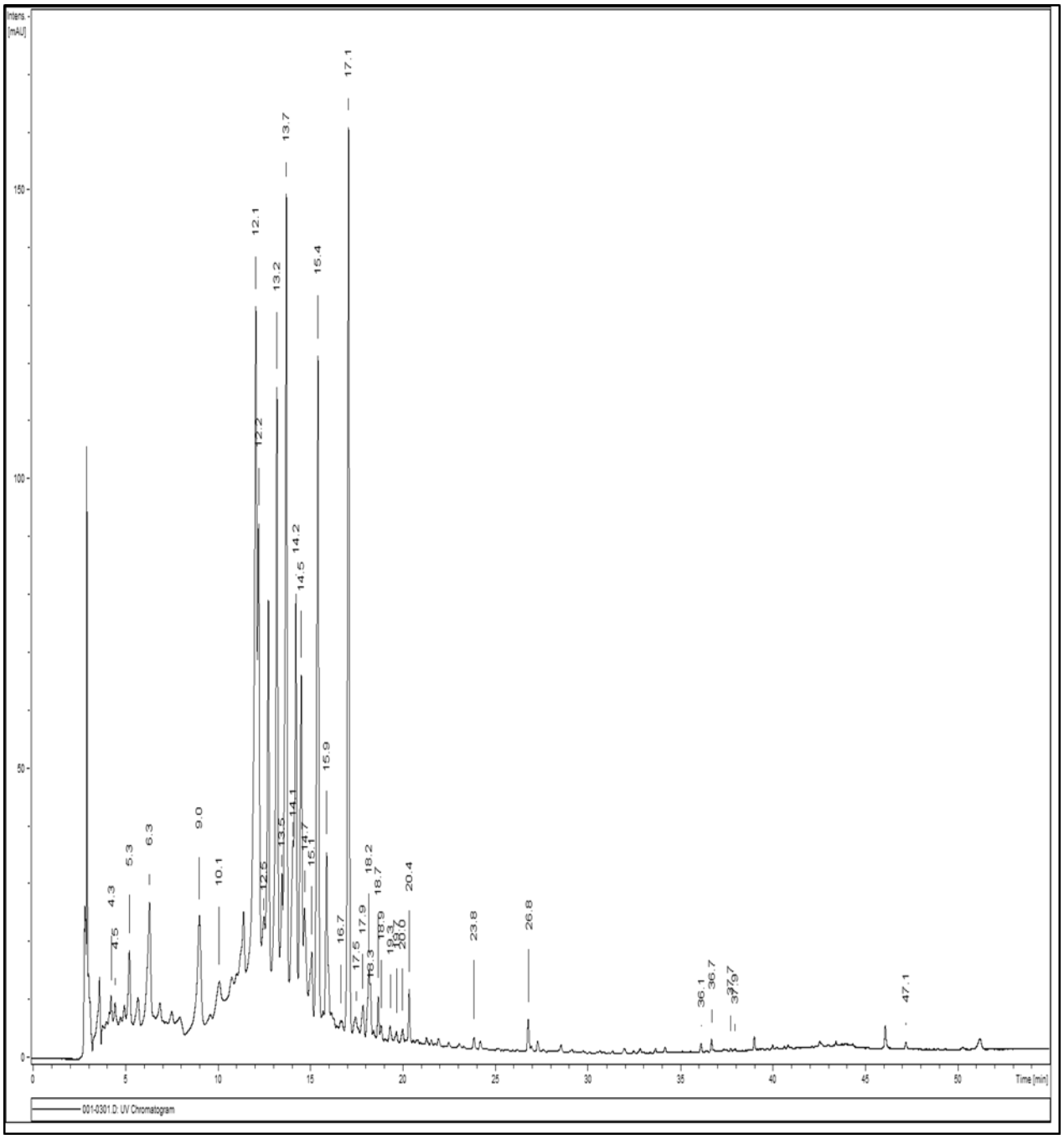

Figure III.1. LC-ESI/MS chromatogram of the *n*-BuOH extract of *S. lingulata* at 296nm.

Ten compounds were identified using ESI mass spectra, UV absorption in MeOH and by the comparison with literature data. The ESI/MS identification method was based on the search of the main molecular ions and also on some of the useful observed fragmentations. All detected compounds showed UV absorptions maxima with three bands (Figure III. 32) close to those of apigenin at 232, 268 and 336 nm as mentioned in literature **[1]**.

The interpretation of the MS spectra are discussed in more detail as below:

- **Compound 1 (t_R =12.4 min)**

The molecular weight of compound **1** was determined from the mass spectral data as 902 Da. This value was confirmed by the presence of representative molecular ion peaks in positive mode (ESI +) at *m/z* 903 $[M+H]^+$, 925 $[M+Na]^+$ and 941 $[M+K]^+$, and at *m/z* 901$[M–H]^-$ detected in negative mode (ESI –) (Figure III.2 and III.3).

This compound was fragmented in ESI/MS (+) by the rupture of glycosidic linkages (the most weak bonds in the molecule) losing sugar units and originating main abundant peaks. In analysis of this spectrum, a high-intensity fragment at *m/z* 595 $[M+H–308]^+$ was observed, indicating two successive losses of sugar residues. The first loss corresponds to a rhamnose (– O)[13] residue $[M+H–146]^+$ giving the *m/z* 757 ion, followed by the elimination of hexose (– O) residue $[M+H–146–162]^+$, where the both are proposed to be linked as (1→2) *O*-diglycosides due to the high intensity of the signal observed at *m/z* 595.1 and the loss of the whole sugar is easier for (1→2) then (1→6) because of the sterical repulsion between the terminal rhamnose and the aglycone part as reported previously **[2]**. The latter peak observed was fragmented to give an aglycone part at *m/z* 287 (suggested to be luteolin) by losing again two successive sugar residues. The signal at *m/z* 433 indicates the loss of hexose (– O) moiety $[M+H–308–162]^+$ followed by the loss of rhamnose residue $[M+H–308–162–146]^+$. Another fragment ion peak at *m/z* 271 (suggested to be apigenin) was shown at high intensity then *m/z* 287 which can yield from losing the entire rhamnose (+ O)[14]. The four sugar units are proposed to be linked at two *O*–positions, in luteolin structure both 7-*O* and 3′-*O* are the preferred positions, as *O*-diglycosides. This result was clearly established by detecting *retro*-Diels Alder (RDA) fragment ion peaks at *m/z* 499 and *m/z* 481.

[13] Without oxygen in anomeric position.
[14] With oxygen in anomeric position.

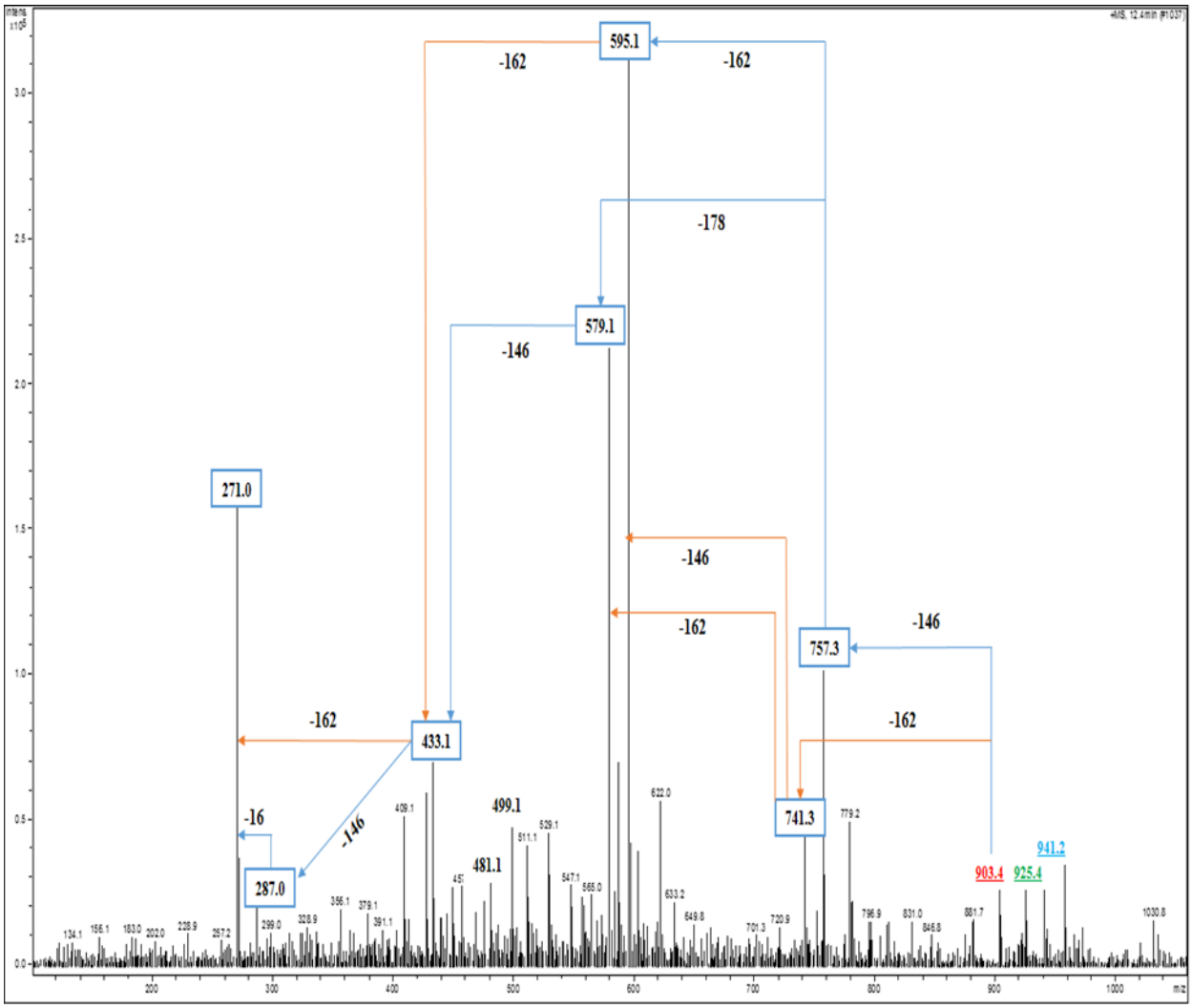

Figure III.2. ESI/MS (+) spectrum of compound **1**.

In negative mode, the MS spectrum exhibited less fragmentation where the useful observed peak ions are listed as *m/z* 755 $[M–H–146]^-$ high-intensity signal, *m/z* 739 $[M–H–162]^-$, *m/z* 593 $[M–H–308]^-$, *m/z* 533 $[M–H–308–60]^-$ indicating the loss of (OH─CH=CH─OH) part from hexose or rhamnose residue and *m/z* 473.6 $[M–H–308–120]^-$ showing the loss of ($^{\bullet}$O─CH─(─CH_2─OH)─CH$^{\bullet}$─OH) which confirms that the 6-OH in hexose was not bonded, this latter was fragmented by losing (OH─CH$^{\bullet}$) from the rest part of hexose yielding a peak ion at *m/z* 443.6. All fragments issue from losing sugars moieties involve hydrogen rearrangement between (glucide–glucide) and (glucide–aglycone). As reported earlier in chapter I (see I.4), all glycosylated flavonoids isolated from *Scilla*, present a hexose residue as glucose.

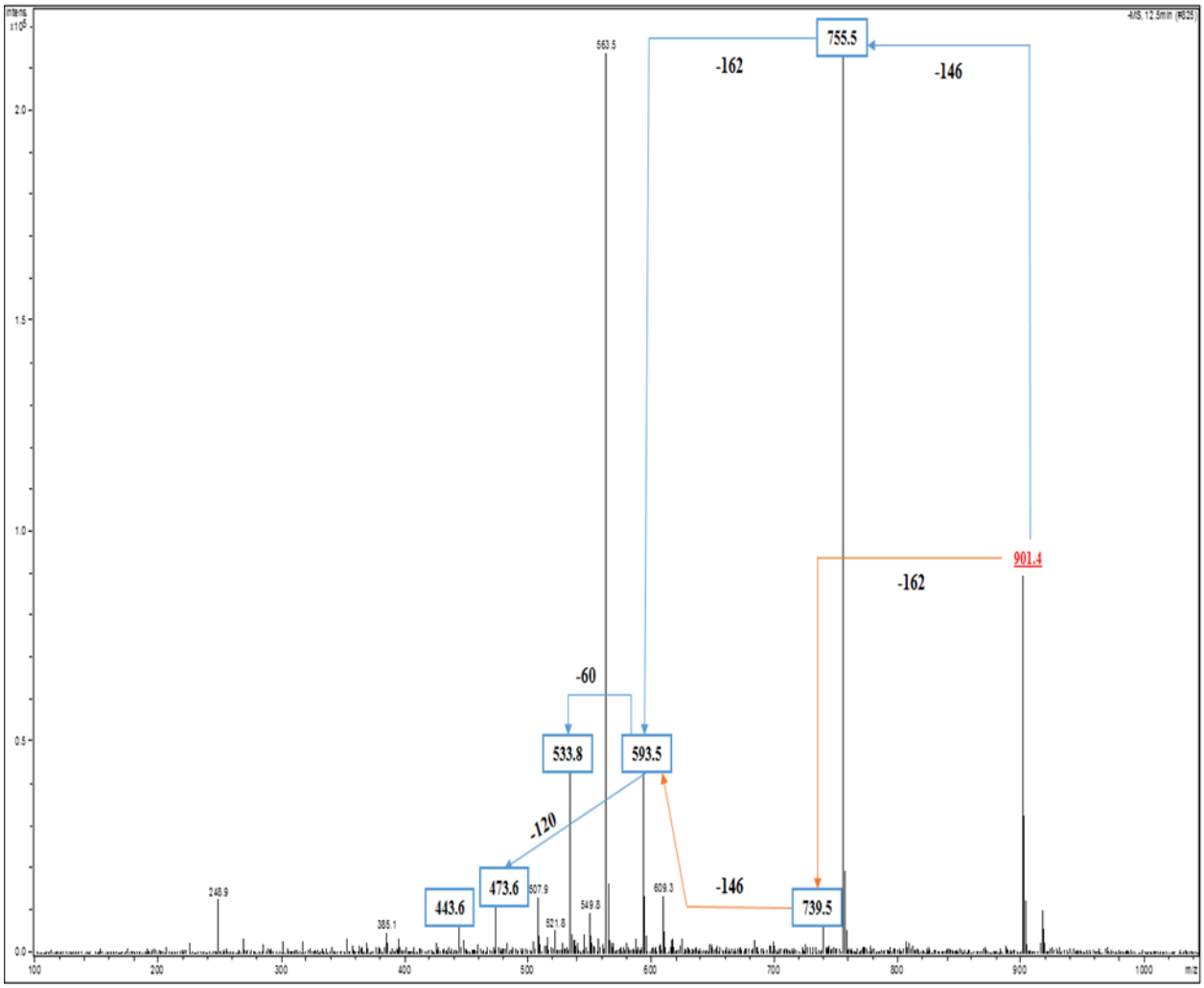

Figure III.3. ESI/MS (–) spectrum of compound **1**.

Therefore, compound **1** is tentatively concluded to be luteolin 7-*O*- (rhamnosyl-(1′′′→2′′)-glucoside)-3′-*O*-(glucosyl-(1′′′′′→2′′′′′)-rhamnoside).

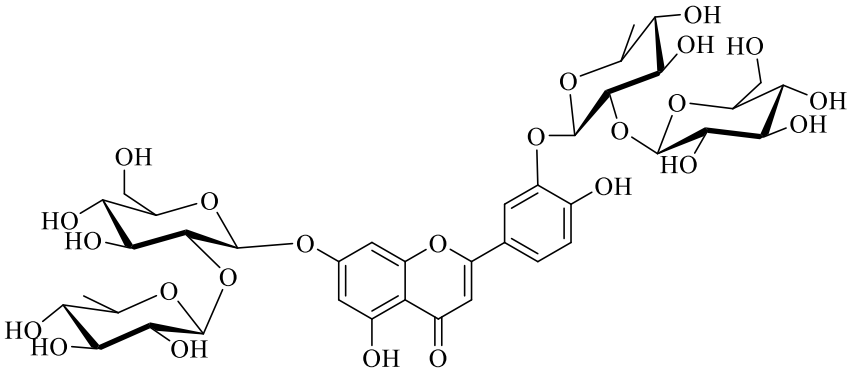

Figure III.4. Chemical structure of compound **1**.

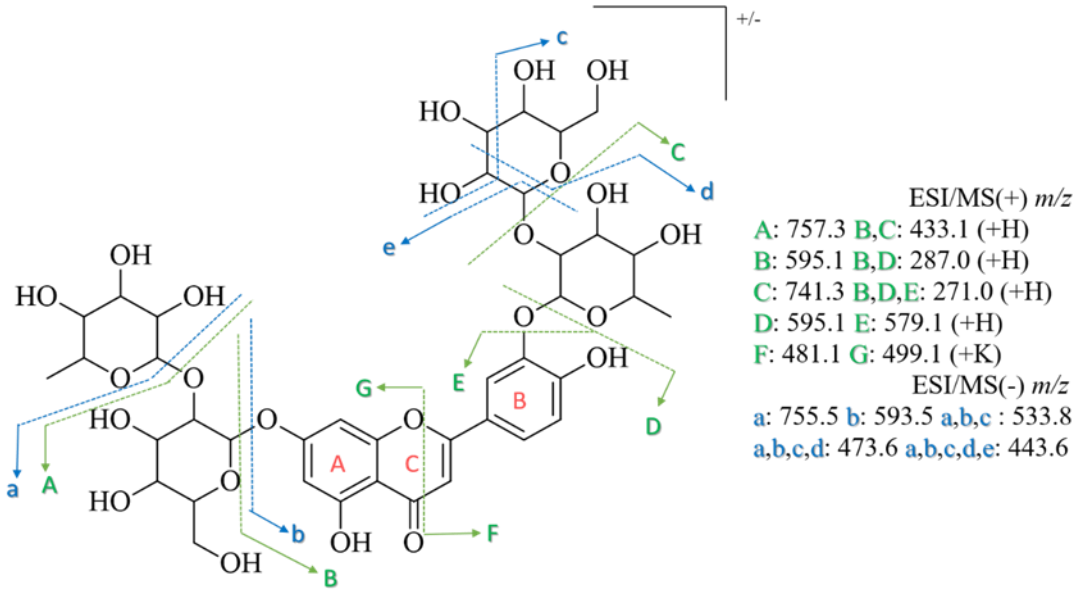

Scheme III.1. Fragmentation pathway of compound **1**.

- **Compound 2 (t_R =12.7 min)**

The molecular weight of compound **2** was deduced from the mass spectral data as 918 Da. This value was confirmed by the presence of representative molecular ion peaks in positive mode (ESI +) at *m/z* 919 $[M+H]^+$, 941 $[M+Na]^+$ and 957 $[M+K]^+$, and at *m/z* 917 $[M–H]^-$ detected in negative mode (ESI –) as base peak (Figure III.5 and III.6).

In positive mode, the MS spectrum revealed only four main product ions demonstrating four successive losses of hexose (– O) units from molecular ion peak at *m/z* 757 $[M+H–162]^+$, *m/z* 595 $[M+H–2\times162]^+$, *m/z* 433 $[M+H–3\times162]^+$ and the last peak at *m/z* 271 $[M+H–4\times162]^+$ identifies the aglycone part of the molecule which was proposed to be apigenin. Additional fragment signals were observed at *m/z* 741 $[M+H–178]^+$ indicating the loss of the entire hexose (+ O) unit followed by the loss of hexose (– O) part at *m/z* 579 $[M+H–178–162]^+$.

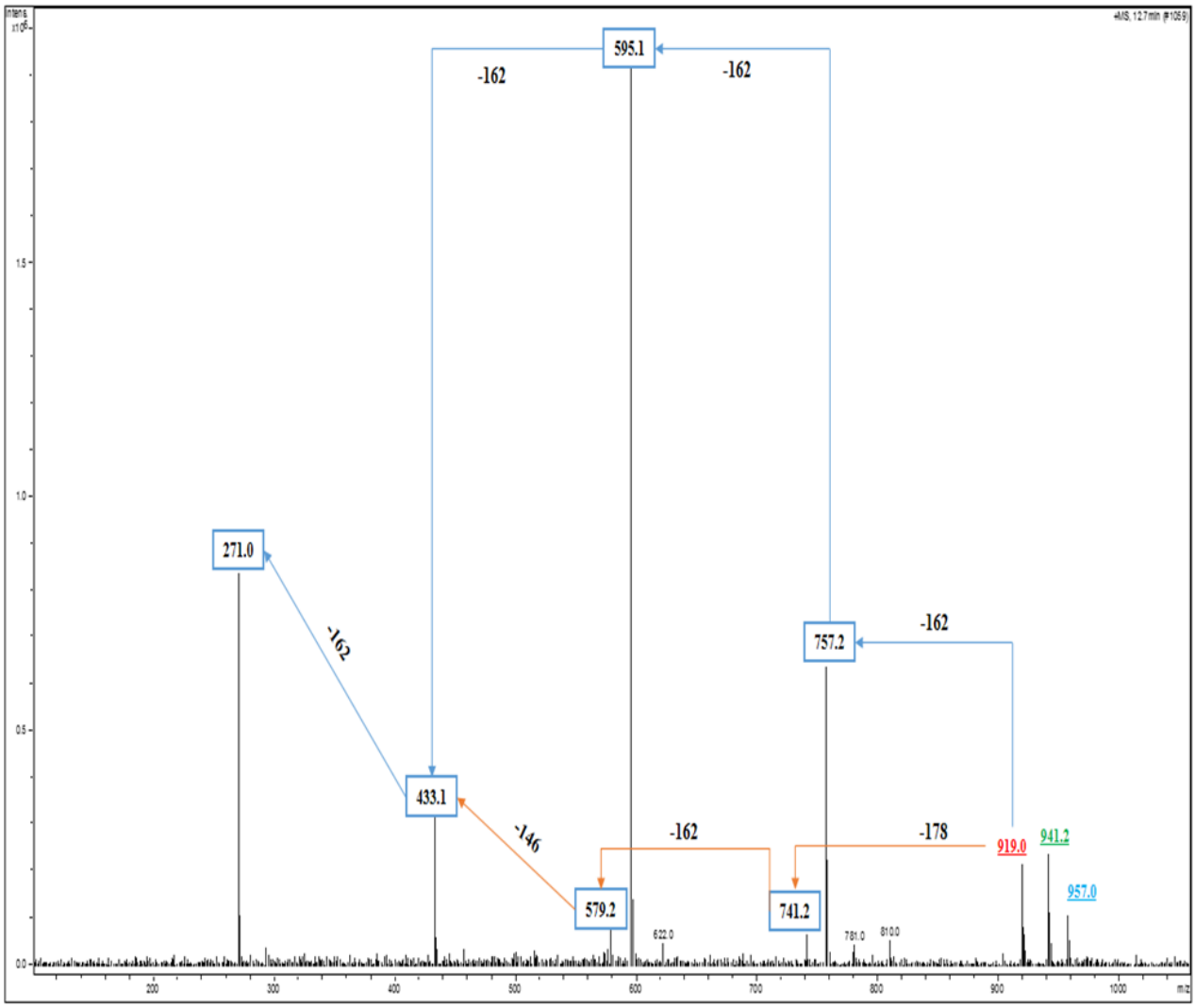

Figure III.5. ESI/MS (+) spectrum of compound **2**.

The ESI/MS (–) spectrum, showed only one useful peak at *m/z* 755 $[M - H - 162]^-$ which confirms the presence of hexose unit yielded from deprotonated molecular ion peak.

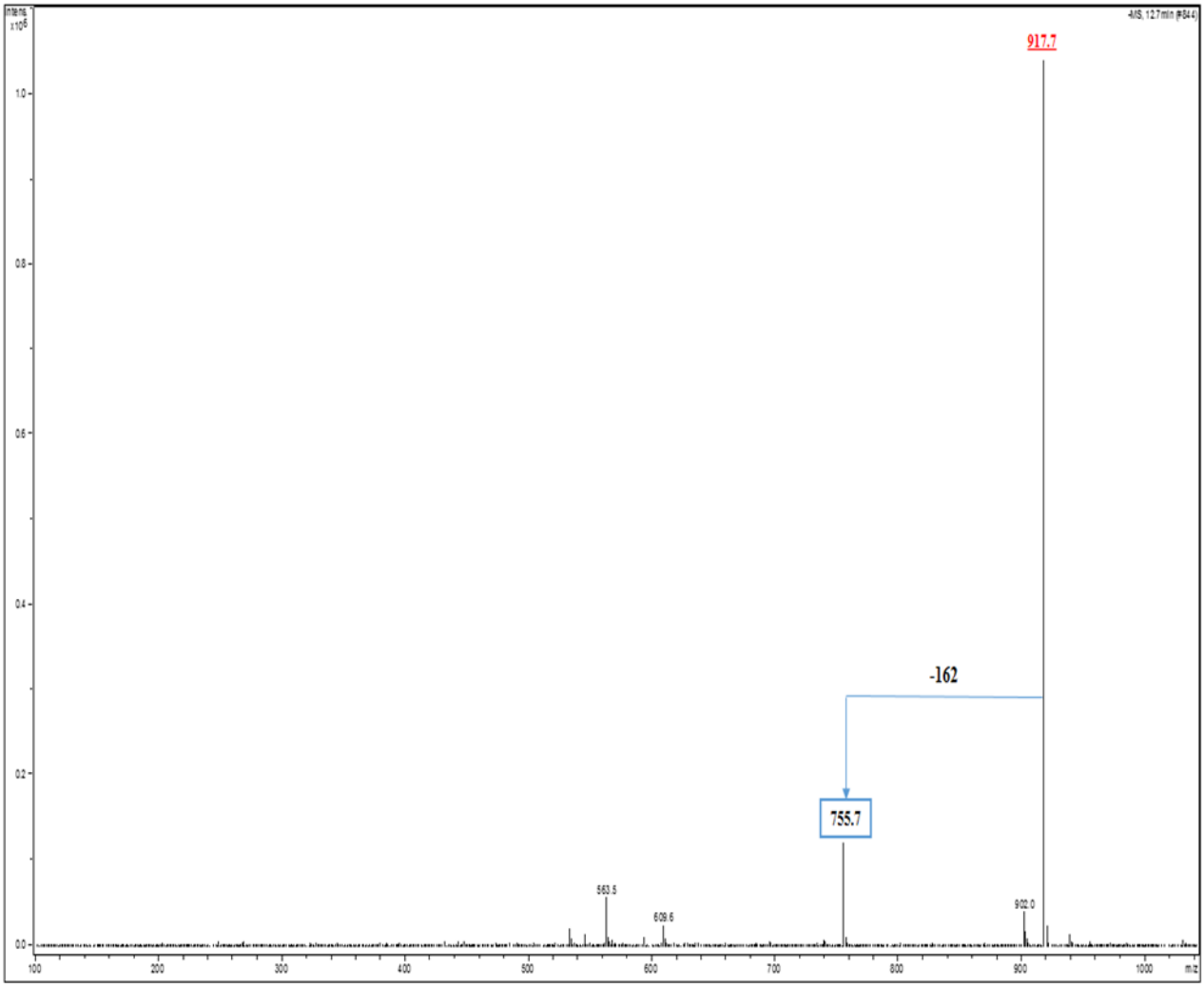

Figure III.6. ESI/MS (–) spectrum of compound **2**.

As a result, compound **2** is tentatively identified as apigenin 7-*O*-(glucosyl-(1´´´→2´´)-glucosyl-(1´´´´→6´´´)-glucosyl-(1´´´´´→2´´´´)-glucoside).

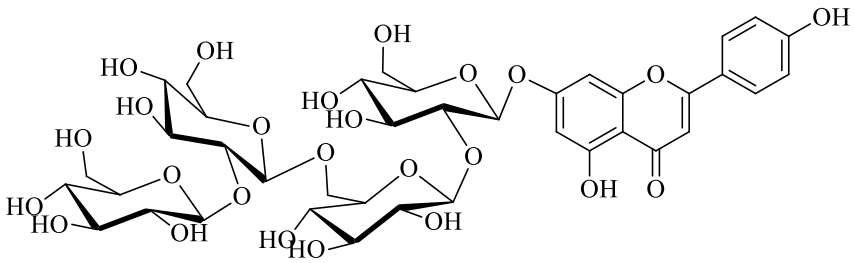

Figure III.7. Chemical structure of compound **2**.

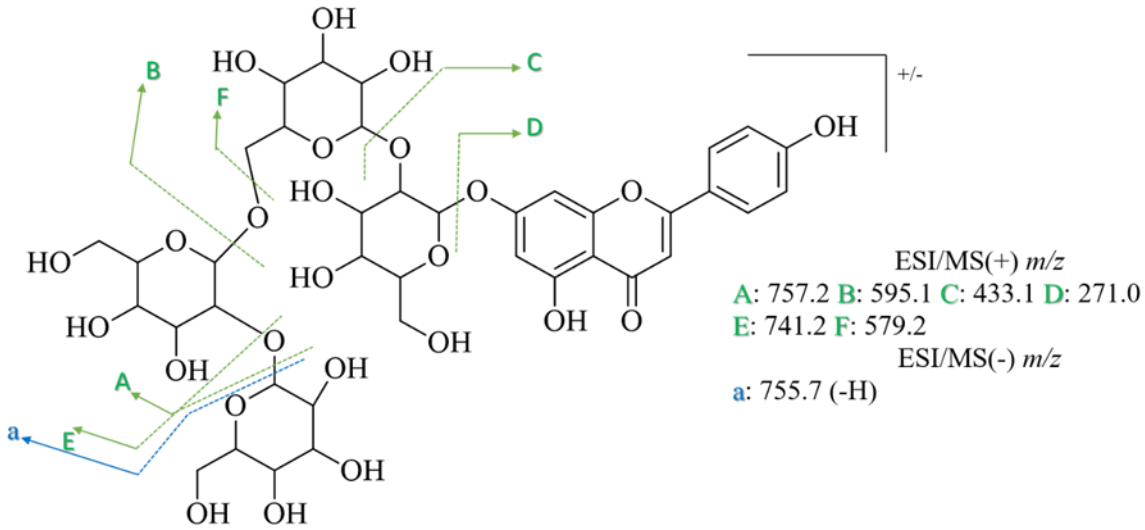

Scheme III.2. Fragmentation pathway of compound **2**.

- **Compound 3 (t_R =13.4 min)**

According to the mass spectral data obtained, the molecular weight of this compound was deduced as 756 Da. The result was confirmed by the presence of pseudo-molecular ion peaks in positive mode (ESI +) at *m/z* 757 $[M+H]^+$, 779 $[M+Na]^+$ and 795 $[M+K]^+$, and at *m/z* 755$[M–H]^-$ detected in negative mode (ESI –) (Figure III.8 and III.9).

In ESI/MS (+) spectrum, compound **3** presented a base peak at *m/z* 595 $[M+H–162]^+$ and three significant fragments at *m/z* 433 $[M+H–324]^+$ corresponding to the successive losses of two hexose (– O) units suggested to be bonded at 3′-*O* position by (1→6) linkage due to the low intensity of the signal observed, *m/z* 287 $[M+H–324–146]^+$ characterizing the aglycone part in the molecular structure which can be suggested as luteolin by losing rhamnose (– O) residue from *m/z* 433. Where the loss of the entire rhamnose unit (+ O) gave an ion at *m/z* 271. A signal at *m/z* 457 which produced from sodiated molecule $[M+Na]^+$ was detected by losing dihydroxylated B ring including the *O*-dihexoses. Therefore, the three sugar residues are fixed at two *O*–positions where the *O*-dihexoses at 3′-*O* and rhamnose unit at 7-*O* which detected also by the presence of *m/z* 633 $[M+Na–146]^+$ generated from sodiated molecule.

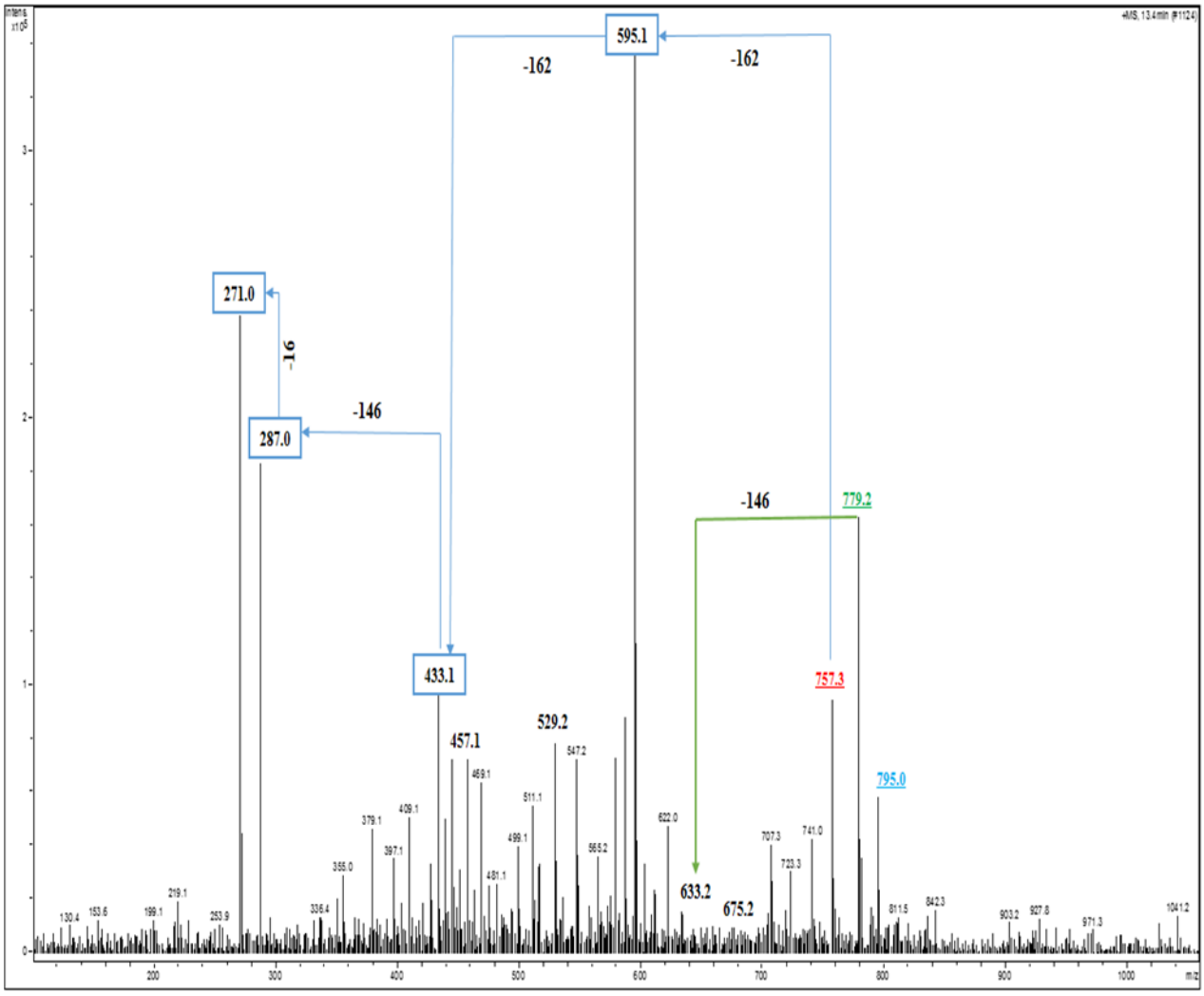

Figure III.8. ESI/MS (+) spectrum of compound **3**.

In negative mode, the MS spectrum exhibited less fragmentation where the useful observed peaks are listed as *m/z* 609 $[M–H–146]^-$, a high-intensity signal at *m/z* 563 $[M–H–(162+30)]^-$ indicating the loss of the terminal hexose unit carrying with it the (─O─CH_2─) moiety of the first hexose unit which confirms that both hexose units are bonded through an interglycosidic (1→6) linkage, this latter was fragmented by losing the rest part of hexose yielding a peak ion at *m/z* 443.8 $[M–H–(162+30)–120]^-$.

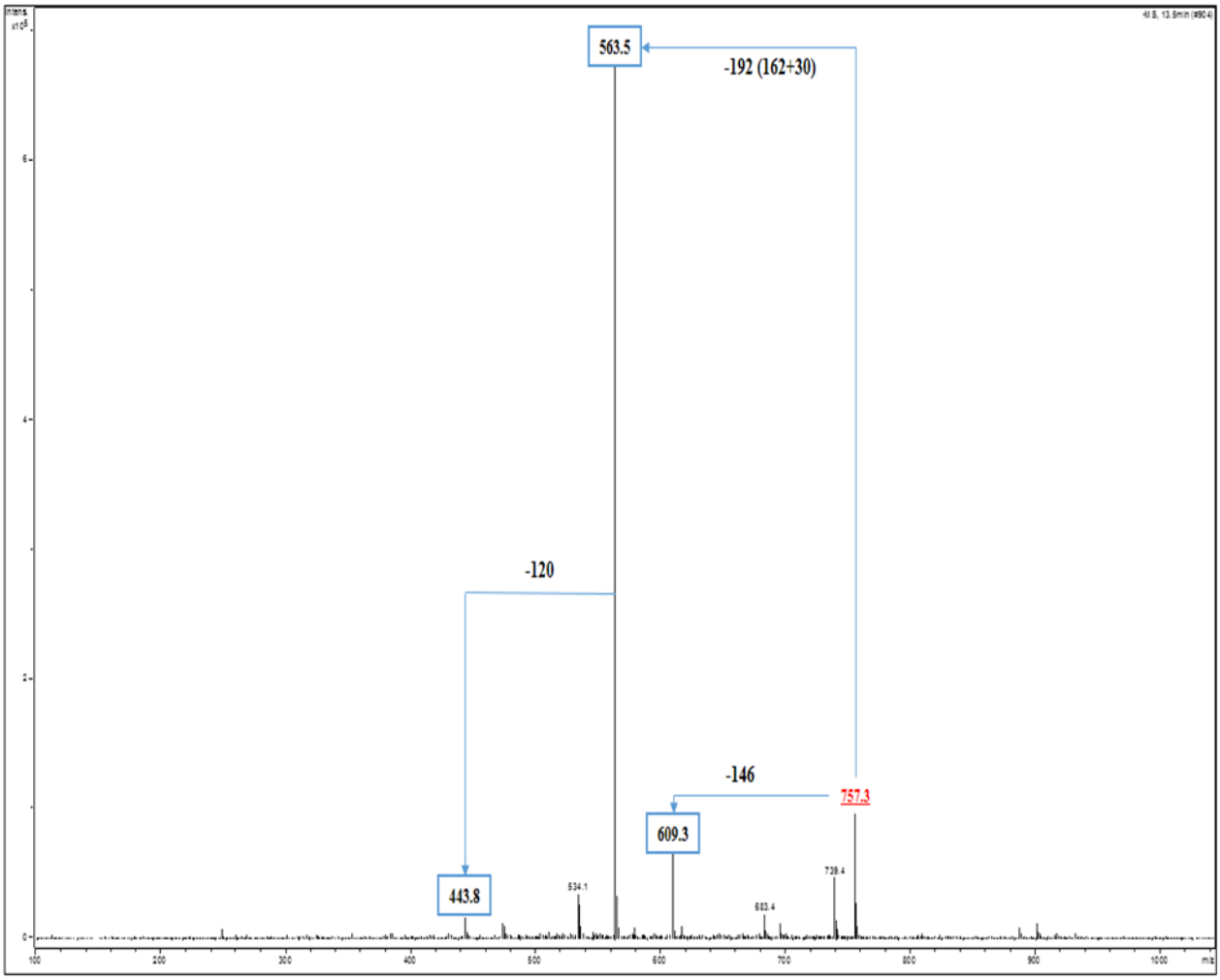

Figure III.9. ESI/MS (–) spectrum of compound **3**

The collected data of compound **3** conclude tentatively its structural elucidation as luteolin 7-*O*-rhamnoside-3′-*O*-(glucosyl-(1′′′′→6′′′)-glucoside).

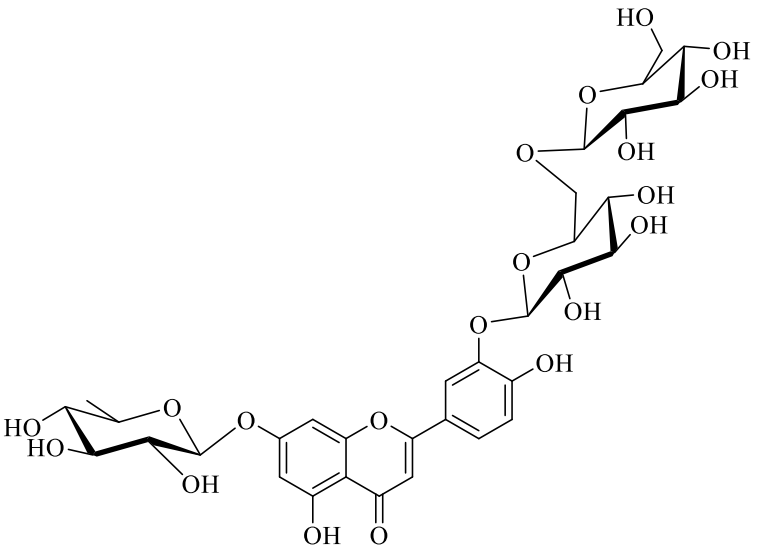

Figure III.10. Chemical structure of compound **3**.

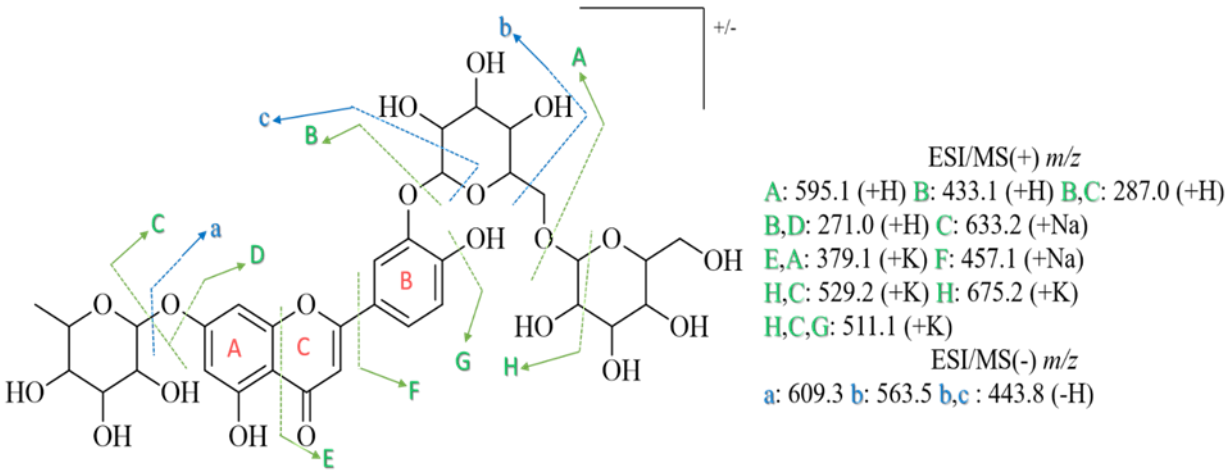

Scheme III.3. Fragmentation pathway of compound **3**

- **Compound 4 (t_R =13.7 min)**

The molecular weight of compound **4** was determined from the mass spectral data as 756 Da. This value was confirmed by the presence of pseudo-molecular ion peaks in positive mode (ESI +) at *m/z* 757 $[M+H]^+$, 779 $[M+Na]^+$ and 795 $[M+K]^+$. Besides, one peak detected with high-intensity in negative mode (ESI –) at *m/z* 755 $[M–H]^-$ (Figure III.11 and III.12).

In positive mode, the MS spectrum revealed only three main product ions demonstrating three successive losses of hexose (– O) units from molecular ion peak at *m/z* 595 $[M+H–162]^+$ as a base peak, *m/z* 433 $[M+H–2\times162]^+$ with a low intensity suggesting that the two hexose moieties are linked through (1→6) bond. The final product ion at *m/z* 271 $[M+H–3\times162]^+$ characterizes the aglycone part of the molecule which is proposed to be apigenin according to the UV data obtained. The first hexose linked to the aglycone part is proposed to be bonded *via* (1→2) to the other units due to the high intensity of the last signal observed.

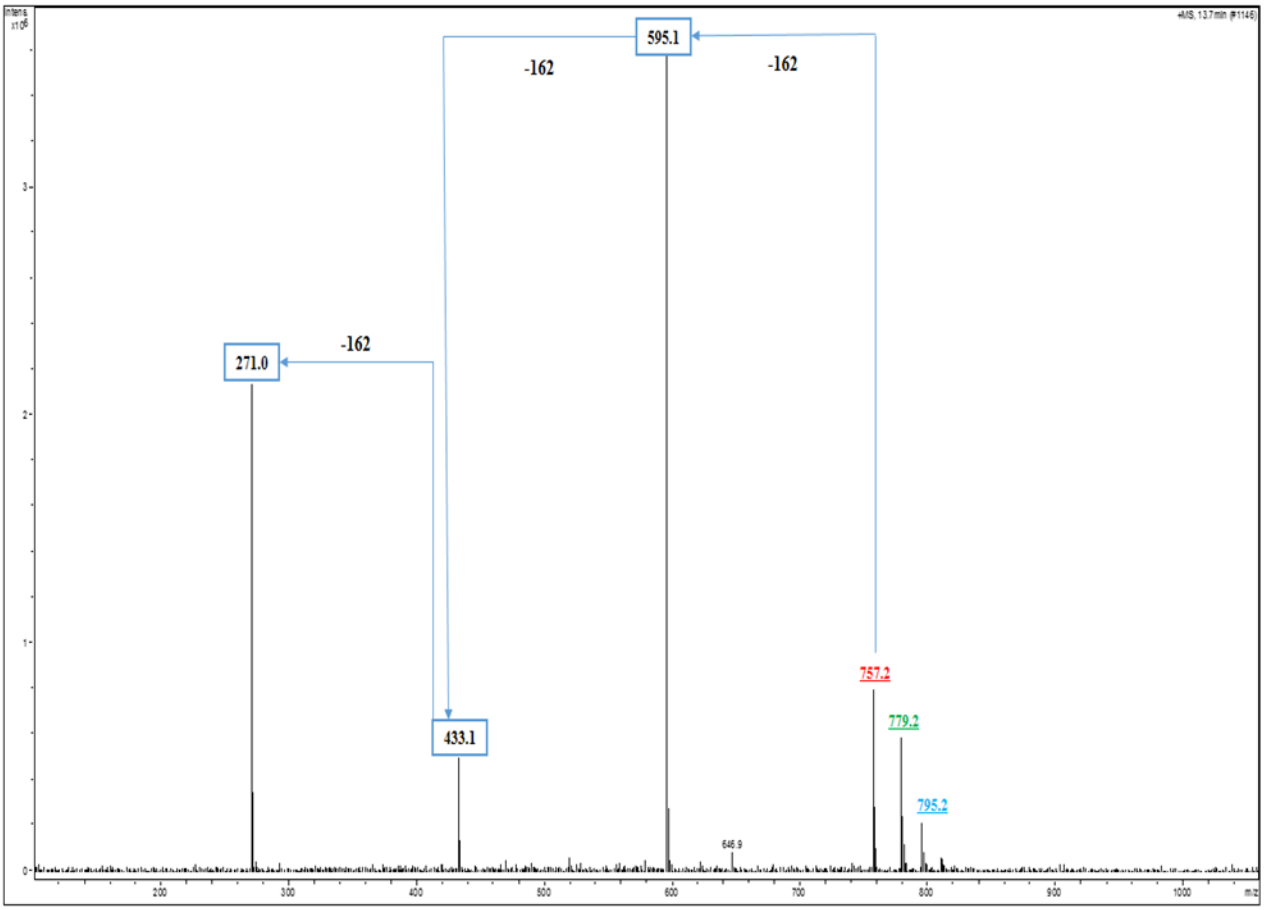

Figure III.11. ESI/MS (+) spectrum of compound **4**.

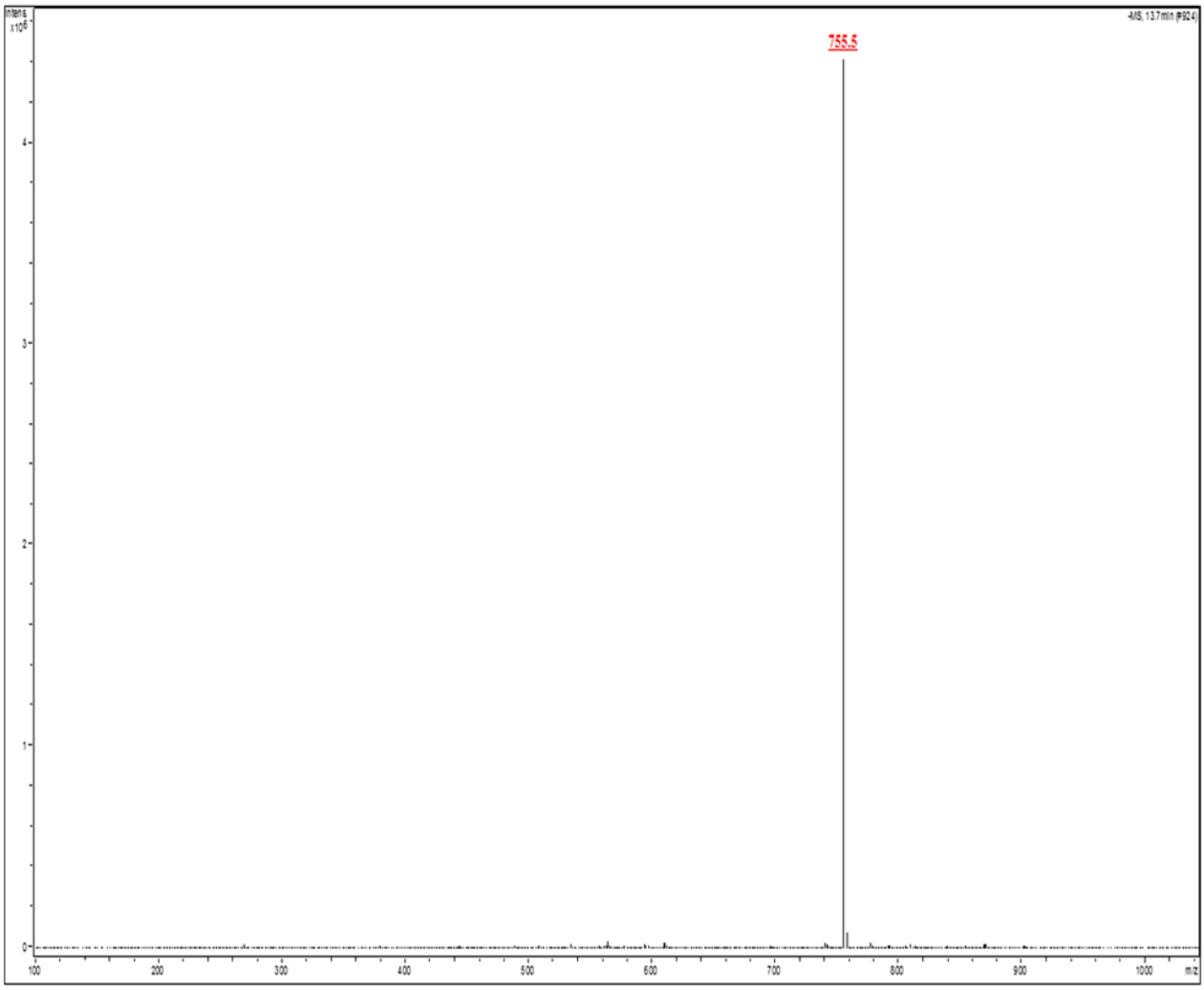

Figure III.12. ESI/MS (–) spectrum of compound **4**

The obtained results suggest that compound **4** is tentatively structurally identified as apigenin 7-*O*-glucosyl-(1′′′→2′′)-glucosyl-(1′′′′→6′′′)-glucoside.

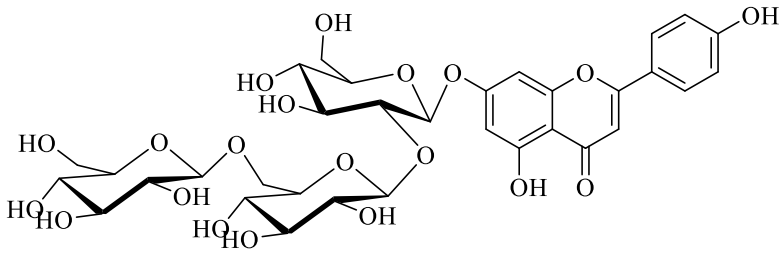

Figure III.13. Chemical structure of compound **4**

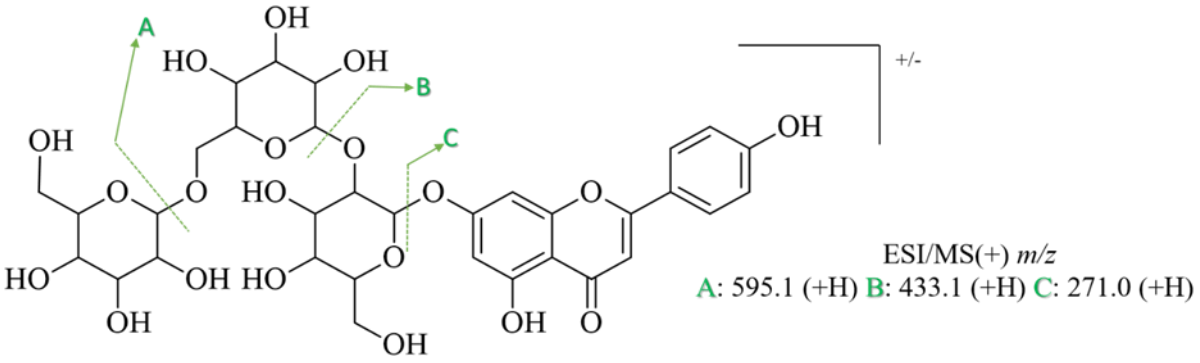

Scheme III.4. Fragmentation pathway of compound **4**

- **Compound 5 (t_R =14.0 min)**

According to the mass spectral data obtained, the molecular weight of this compound was deduced as 740 Da. The result was confirmed by the presence of pseudo-molecular ion peaks in positive mode (ESI +) at *m/z* 741 $[M+H]^+$, 763 $[M+Na]^+$ and 779 $[M+K]^+$,and at *m/z* 739.5 $[M-H]^-$ detected in negative mode (ESI –) (Figure III.14 and III.15).

In analysis of ESI/MS (+) spectrum, compound **5** showed a base peak at *m/z* 579 $[M+H-162]^+$ and other significant fragments at *m/z* 433 $[M+H-162-146]^+$, *m/z* 271 $[M+H-162-146-162]^+$ characterized the apigenin structure. From this analysis, the molecule must be contained two hexose (– O) units and one part of rhamnose (– O) with an ambiguous glycane sequence deduced from the presence of this proposition: *m/z* 595 $[M+H-146]^+$, *m/z* 433 $[M+H-146-162]^+$ and *m/z* 271 $[M+H-146-162-162]^+$. An additional fragment signal was observed at *m/z* 481 $[M+Na-(163+119)]^+$ indicating the loss of the terminal hexose unit carrying with it the (OH─CH•─CH (OH)─CH (─CH_2─O•)─O•) moiety of the first hexose unit attached to the apigenin which proves that both hexose units are bonded through (1→6) linkage and the second position of first hexose unit is occupied by rhamnose part as (1→2) linkage (branched tri-saccharide).

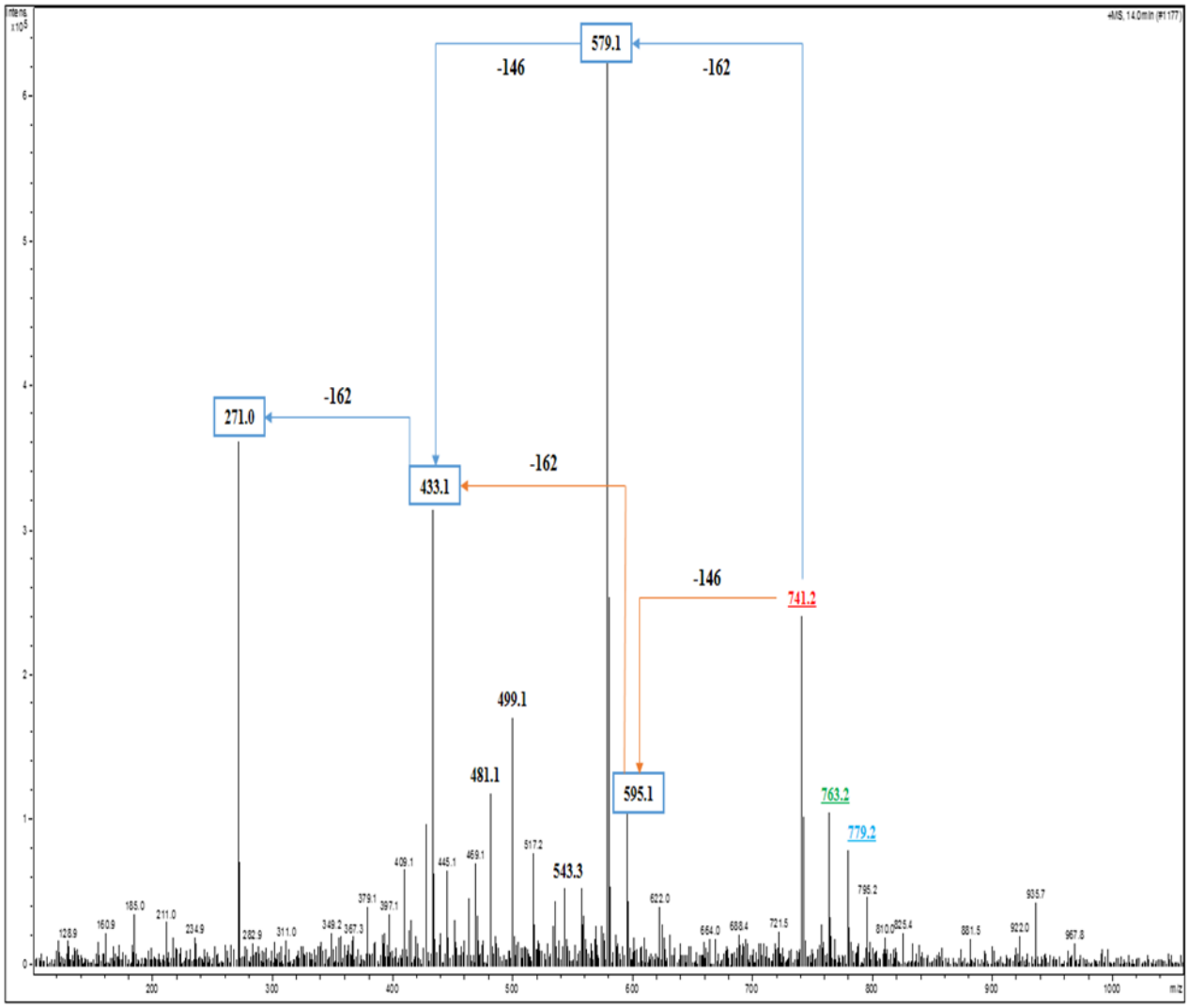

Figure III.14. ESI/MS (+) spectrum of compound **5**

The ESI/MS (–) spectrum, showed two useful peaks at *m/z* 533 $[M–H–206]^-$ (206 = 146+60) with a high intensity, indicating the loss of terminal rhamnose unit carrying with it the (OH─CH=CH─O─) part of the first hexose, this latter was fragmented by losing (•O─CH(─CH_2─OH)─CH•─OH) part of the terminal hexose unit yielding a peak at *m/z* 443 $[M–H–206–90]^-$ which confirms the above result of sugar linkages.

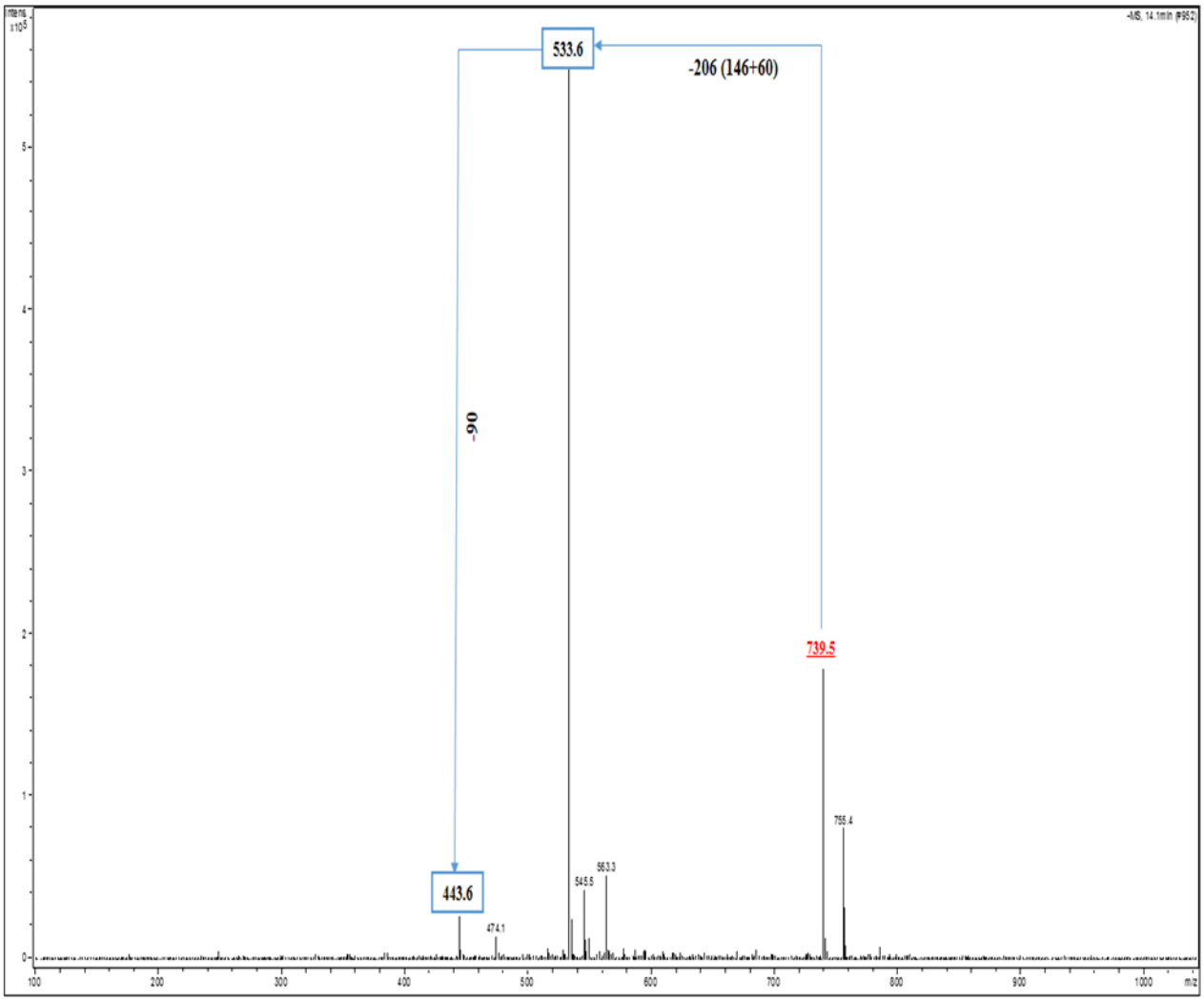

Figure III.15. ESI/MS (–) spectrum of compound **5**

According to the obtained interpretations, compound **5** is tentatively identified as apigenin 7-*O*-glucosyl-(1´´´→2´´)-rhamnoside-(1´´´´→6´´)-glucoside.

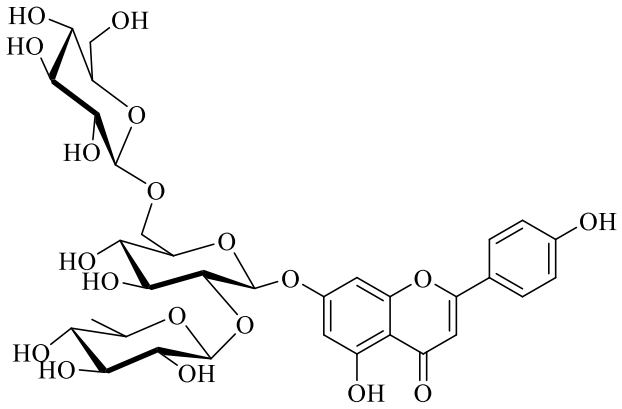

Figure III.16. Chemical structure of compound **5**

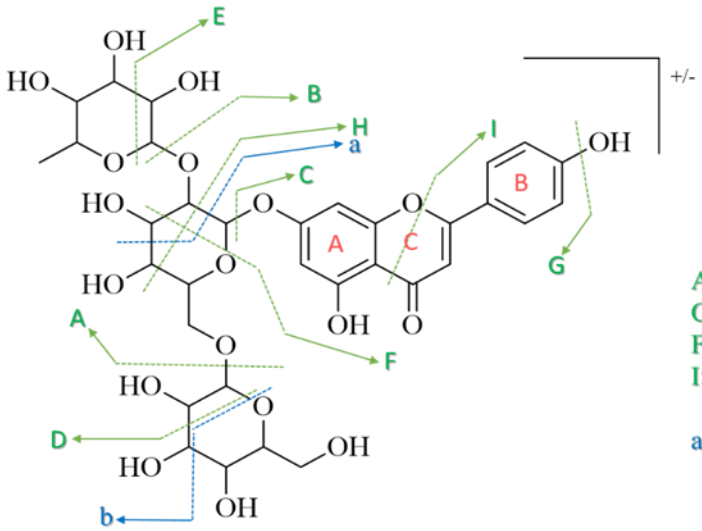

ESI/MS(+) *m/z*
A: 579.1 (+H) B: 595.1 (+H) B, A: 433.1 (+H)
C: 271.0 (+H) D: 622.0 (+H) E,D: 517.2 (+H)
F: 481.1 (+Na) E,D,G: 499.1 (+H) H: 543.3 (+K)
I: 185.0 (+K)

ESI/MS(-) *m/z*
a: 533.6 a,b: 443.6 (-H)

Scheme III.5. Fragmentation pathway of compound **5**

- **Compound 6 (t_R =14.2 min)**

In comparison with the previous obtained MS data for compound **5**, compound **6** produced the same pseudo-molecular ion peaks in both negative and positive mode (Figure III.17 and III.18). Thus, the two compounds are considered as isomers (identical molecular mass).

The ESI/MS (+) spectrum of this detected compound, revealed the same main peaks that observed for compound **5** which are: *m/z* 595 $[M+H–146]^+$ as a base peak, *m/z* 579 $[M+H–162]^+$ with a low intensity, *m/z* 433 $[M+H–146–162]^+$ or *m/z* 433 $[M+H–162–146]^+$ and the final product ion at *m/z* 271 $[M+H–162–146–162]^+$ or *m/z* 271 $[M+H–146–162–162]^+$ characterized the apigenin structure. The presence of two peaks generated from $[M+H]^+$ indicating the loss of either hexose (– O) or rhamnose (– O) unit with different intensities, gave the following glycan sequence suggestion $[M+H–162–162–146]^+$. This means that the base peak observed at *m/z* 579 refers to the phenomenon of internal hexose residue loss as reported in literature **[3]**, not to the loss of terminal hexose. All detected sugar residues are proposed to be linked through (1→2) interglycosidic linkages.

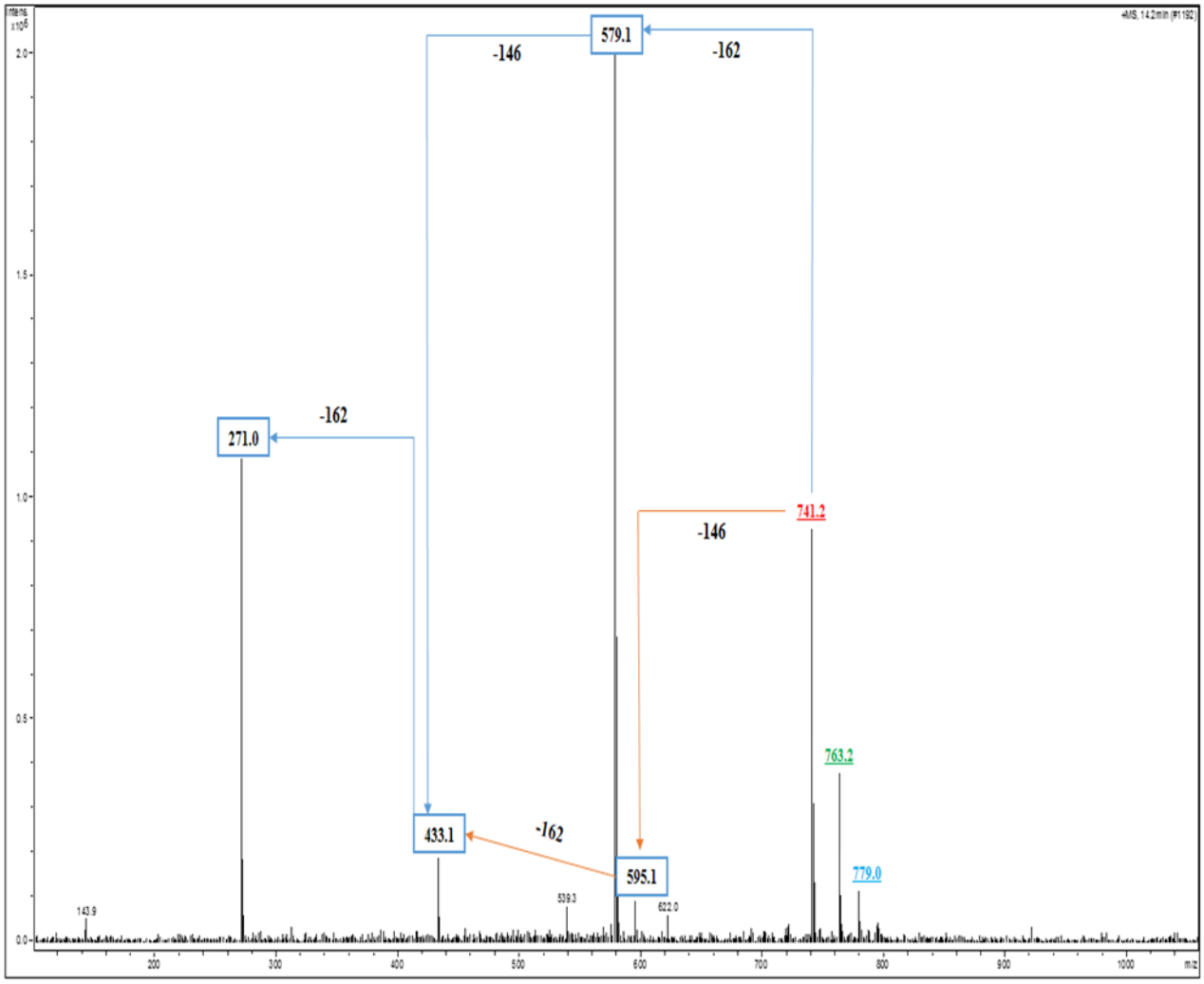

Figure III.17. ESI/MS (+) spectrum of compound **6**

The ESI/MS (–) spectrum showed only one peak at *m/z* 739.5 $[M–H]^-$ with high-intensity. The absence of other fragmentations in both spectra indicates that the *O*-tri-saccharide is fixed at one position as a linear sequence.

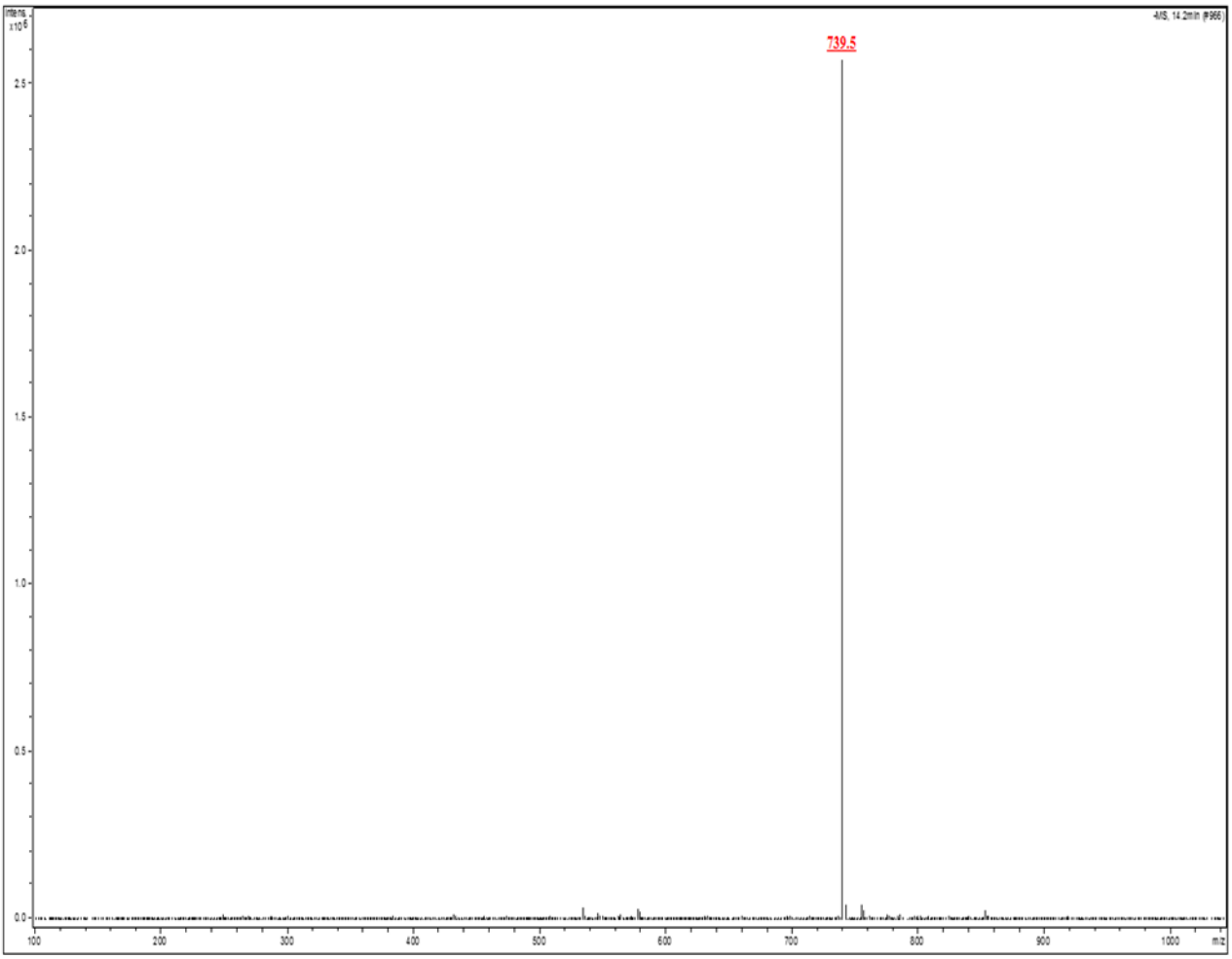

Figure III.18. ESI/MS (–) spectrum of compound **6**

Thus, compound **6** is tentatively identified as apigenin 7-*O*-glucosyl-(1´´´→2´´)-glucosyl-(1´´´´→2´´´)-rhamnoside.

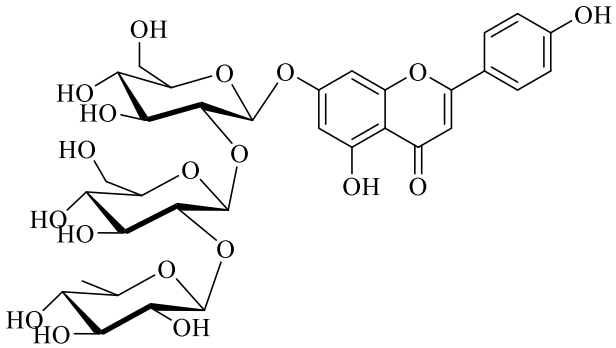

Figure III.19. Chemical structure of compound **6**

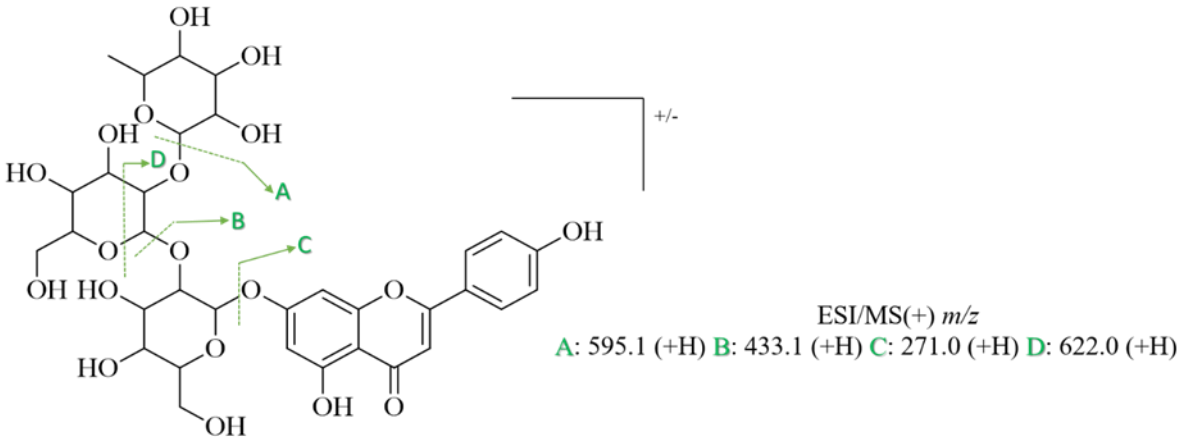

Scheme III.6. Fragmentation pathway of compound **6**

- **Compound 7 (t_R =14.7 min)**

The molecular weight of compound **7** (an isomer of the 4th compound) was determined from the mass spectral data as 756 Da. This value was found by the presence of pseudo-molecular ion peaks in positive mode (ESI +) at *m/z* 757 $[M+H]^+$, 779 $[M+Na]^+$ and 795 $[M+K]^+$, and at *m/z* 755 $[M–H]^-$detected with a high abundance in negative mode (ESI –) (Figure III.20 and III.21).

In positive mode, the MS spectrum showed several fragmentation peaks. The most representative are those observed at *m/z* 595 $[M+H–162]^+$, *m/z* 433 $[M+H–2\times162]^+$ as a base peak and the final product ion at *m/z* 271 $[M+H–3\times162]^+$ proposed to be the structure of apigenin according to the UV data acquired. These registered peaks are yielded from the elimination of three successive hexose (– O) units from molecular ion peak. A signal at *m/z* 499 which produced from potassiated molecule $[M+K]^+$ characterizes the loss of B ring including a part of C ring and 4′-*O*-hexose, another signal at *m/z* 297 indicates the loss of A ring including a part of C ring and 7-*O*-dihexose. The elimination of the whole *O*-dihexose was observed at *m/z* 325.

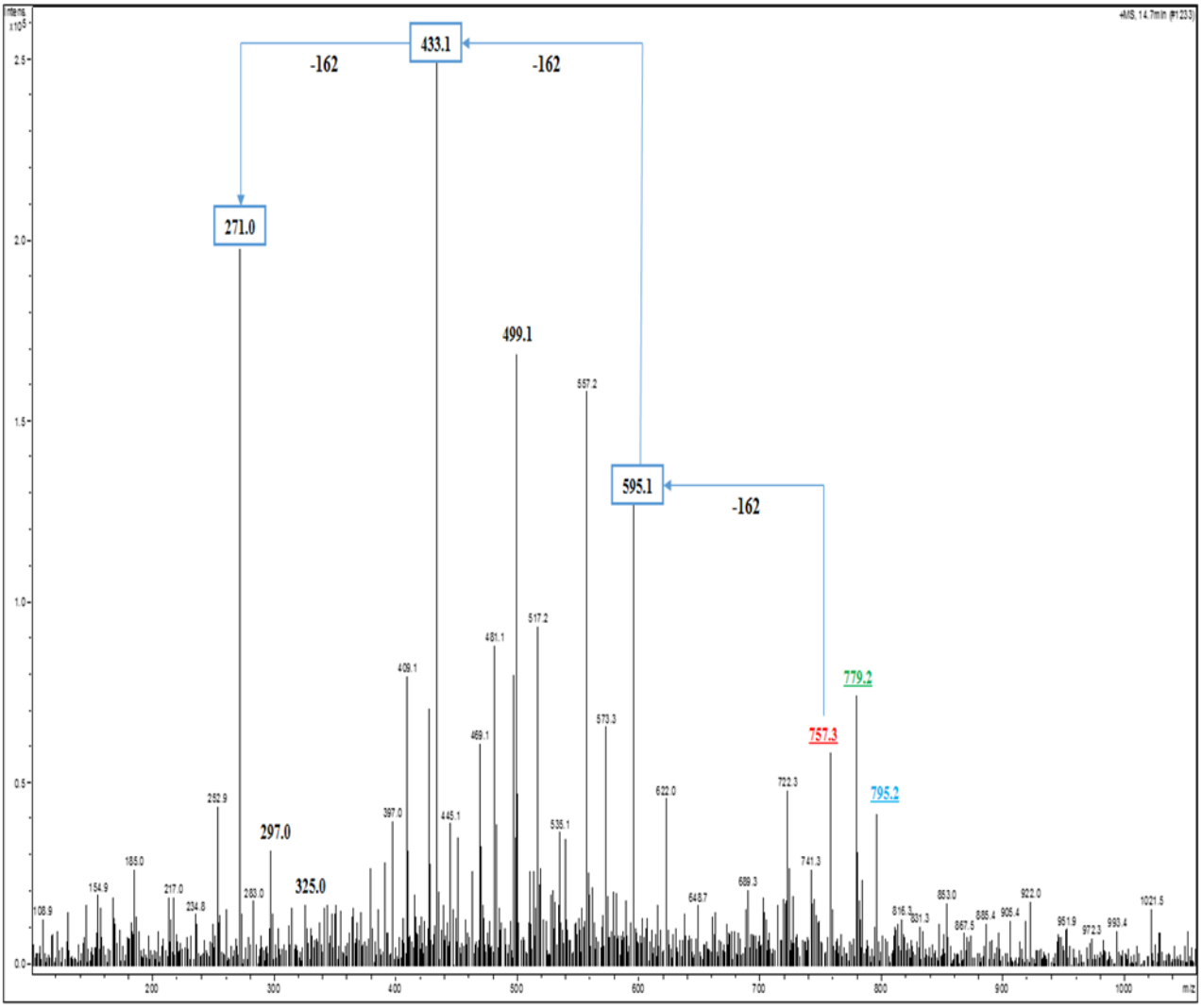

Figure III.20. ESI/MS (+) spectrum of compound **7**

The ESI/MS (–) spectrum, displayed three significant peaks listed as *m/z* 577 $[M–H–178]^-$ showing the loss of the entire hexose residue, *m/z* 533 $[M–H–222]^-$ (222 = 163+59) indicating the loss of hexose (– O) unit carrying with it (OH─CH=CH─O─) part, which means that both hexose moieties are bonded through (1→2) linkage. This latter was fragmented by losing the (OH─CH•─CH(OH)─O•) part from hexose moiety yielding a peak at *m/z* 443 $[M–H–222–90]^-$.

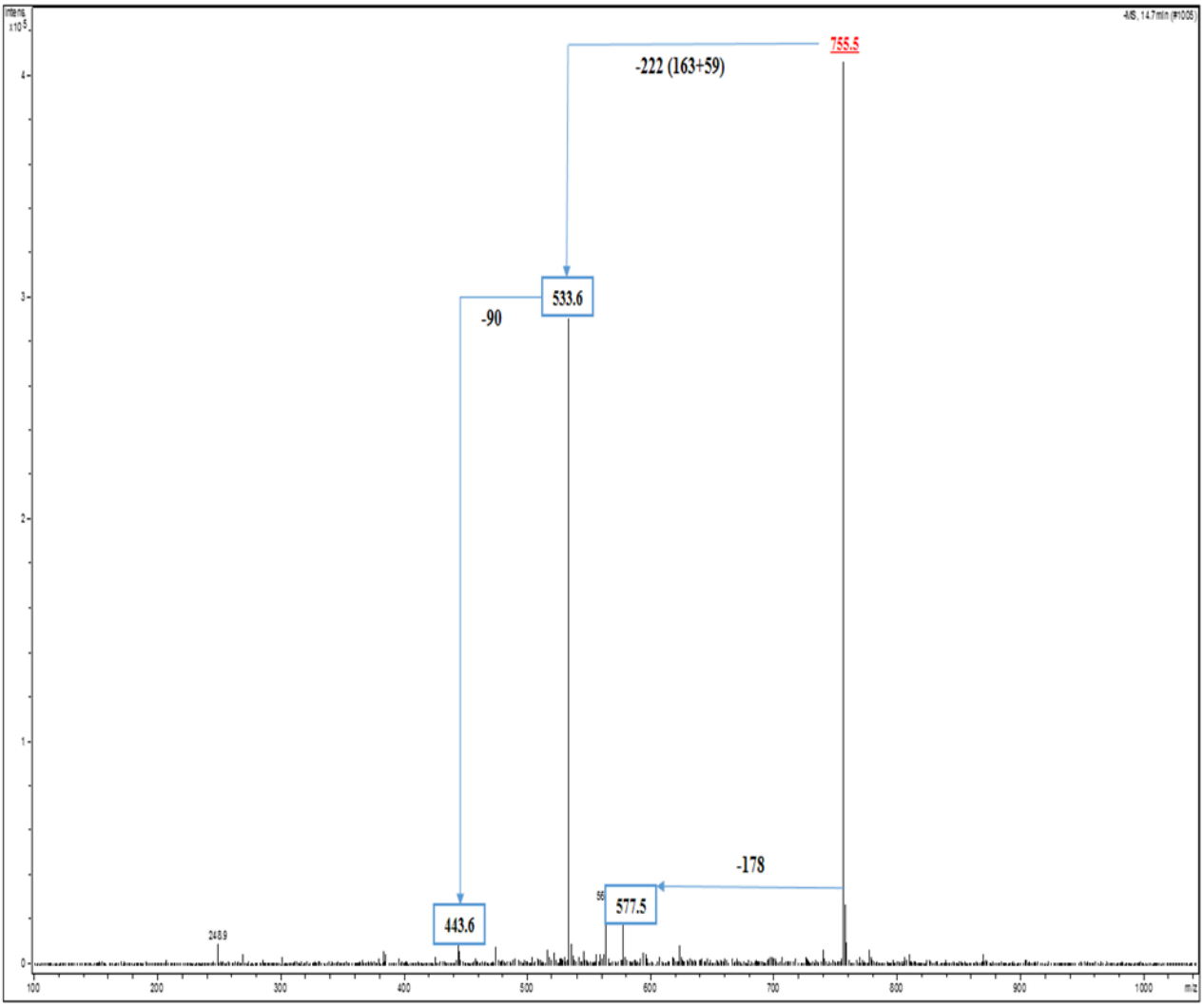

Figure III.21. ESI/MS (–) spectrum of compound **7**

Consequently, compound **7** is tentatively identified as apigenin 7-*O*-(glucosyl-(1´´´→2´´)-glucoside)-4´-*O*-glucoside.

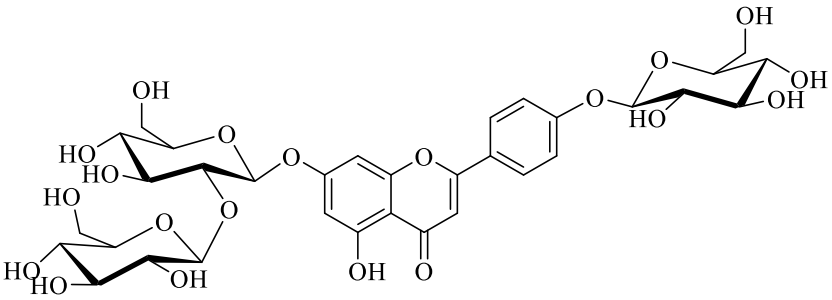

Figure III.22. Chemical structure of compound **7**

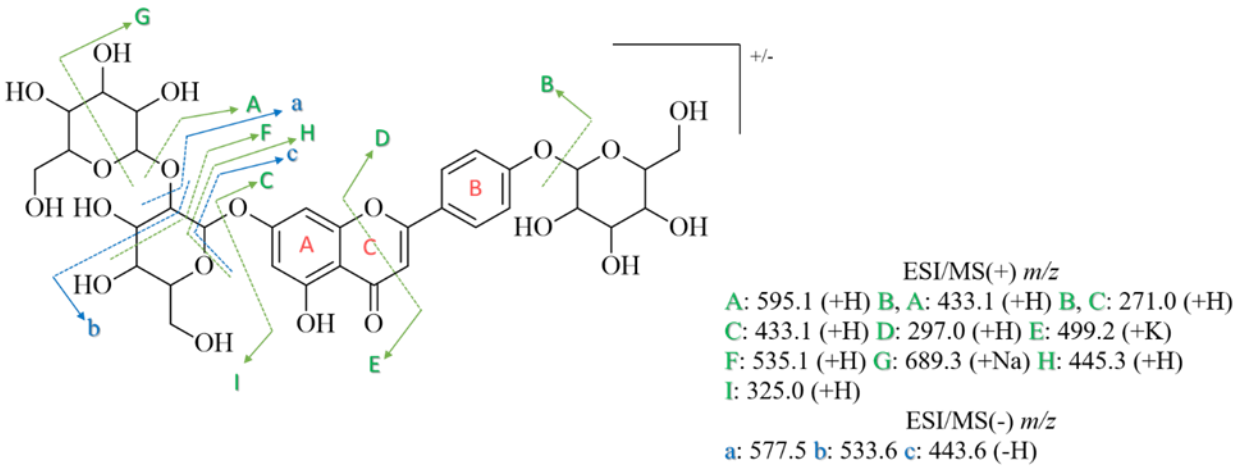

Scheme III.7. Fragmentation pathway of compound **7**

- **Compound 8 (t_R =15.0 min)**

In comparison with the previous obtained MS data for compound **3**, compound **8** shared the same molecular weight which is 756 Da (757 $[M+H]^+$ in (ESI +) and 755 $[M–H]^-$in (ESI –)) (Figure III.23 and III.24). Thus, the two compounds are considered as isomers.

The ESI/MS (+) data, showed four significant fragment ion signals at *m/z* 595 $[M+H–162]^+$, *m/z* 433 $[M+H–2\times162]^+$ with a high-intensity, *m/z* 287 $[M+H–324–146]^+$ suggested to be luteolin structure. A base peak observed at *m/z* 271 $[M+H–324–162]^+$ indicates the loss of the entire rhamnose unit giving the apigenin fragment ion which characterized by producing *m/z* 253 and *m/z* 152.9 fragment ion peaks. The moieties of rhamnose and *O*-dihexose are proposed to be fixed at 3′-*O* and 7-*O* respectively, concluded from registered peak at *m/z* 297 showing the loss of B ring including a part of C ring and 3′-*O*-rhamnose.

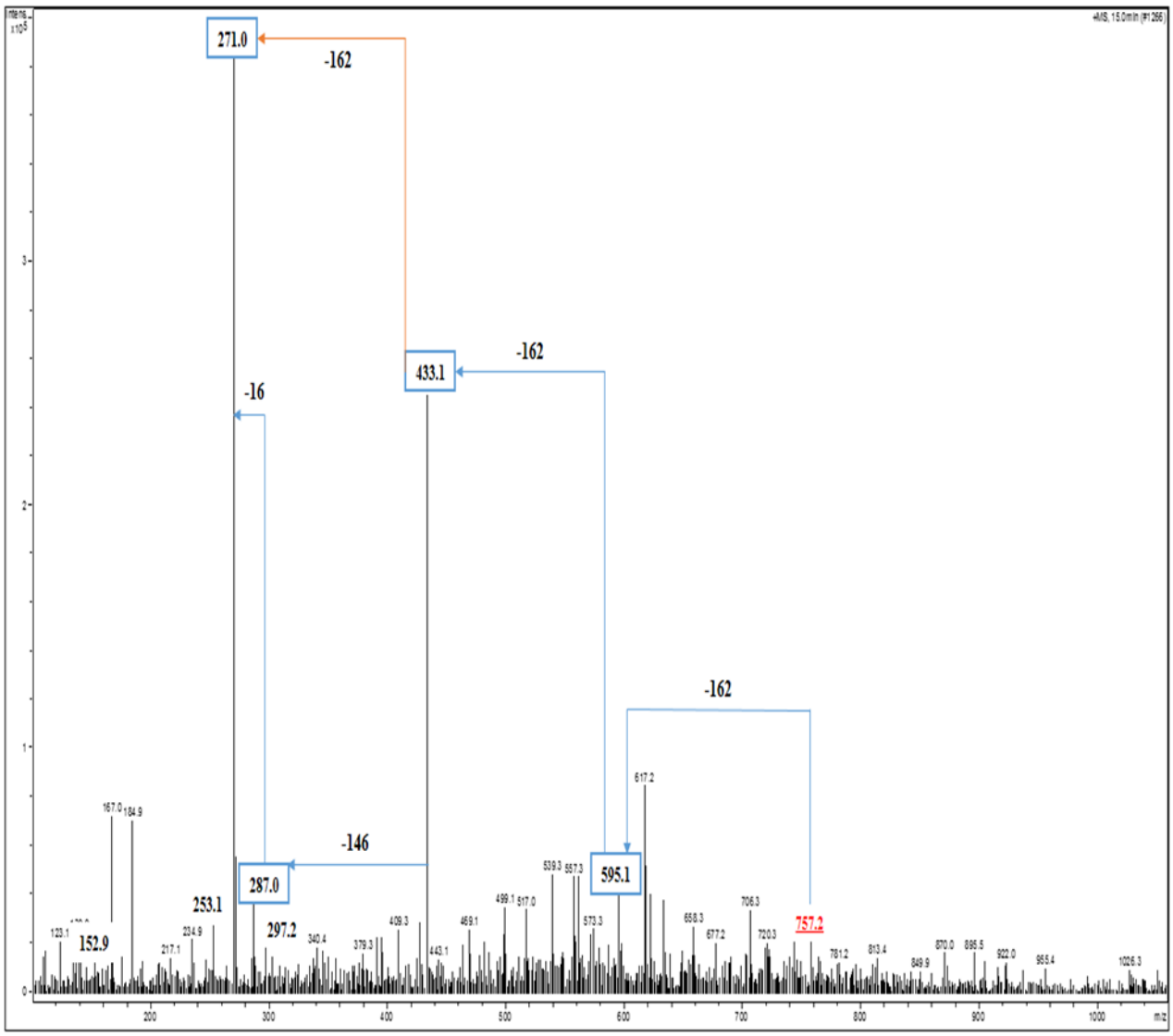

Figure III.23. ESI/MS (+) spectrum of compound **8**

The above result is confirmed by investigating the ESI/MS (–) spectrum, which shows the following useful fragment ion peaks: *m/z* 609 $[M–H–146]^-$, *m/z* 593 $[M–H–162]^-$ indicates the loss of either hexose (– O) part or the entire rhamnose unit, *m/z* 533 $[M–H–162–60]^-$ showed as base peak, *m/z* 474 $[M–H–162–119]^-$ indicating the loss of (•O─CH(─CH_2─OH)─CH(OH)─CH•─OH) part with H-rearrangement, *m/z* 443 $[M–H–162–60–90]^-$, *m/z* 269 $[M–H–162–324]^-$ indicates the direct loss of the whole *O*-dihexoe which is more abundant then the observed peak at *m/z* 285 $[M–H–162–308]^-$ produced from losing both hexose (– O) and rhamnose (– O) units.

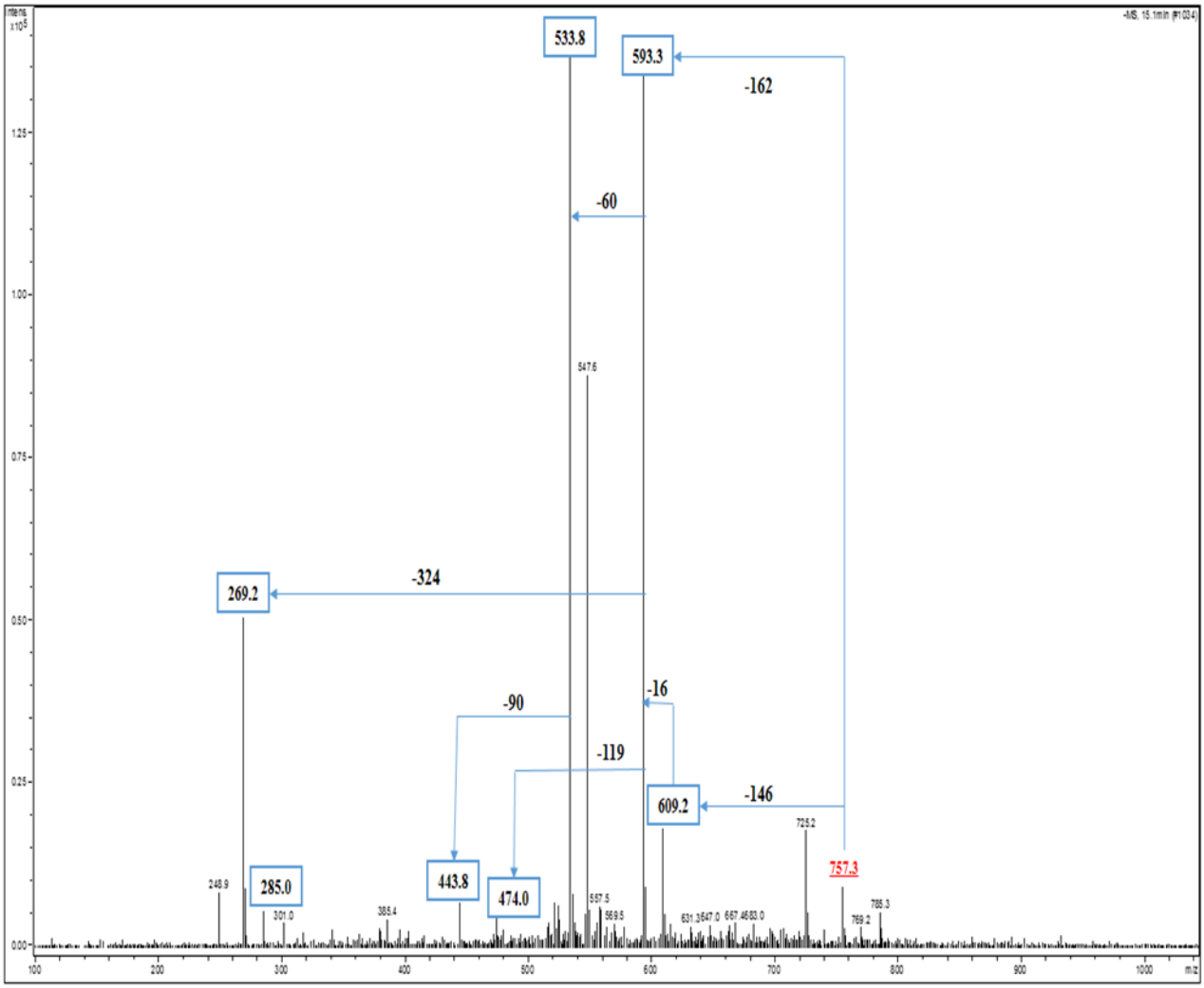

Figure III.24. ESI/MS (–) spectrum of compound **8**

As a result, compound **8** can be identified as luteolin 7-*O*-(glucosyl-(1´´´→2´´)-glucoside)-3´-*O*-rhamnoside.

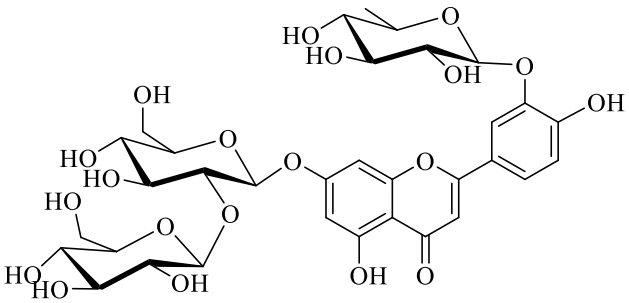

Figure III.25. Chemical structure of compound **8**

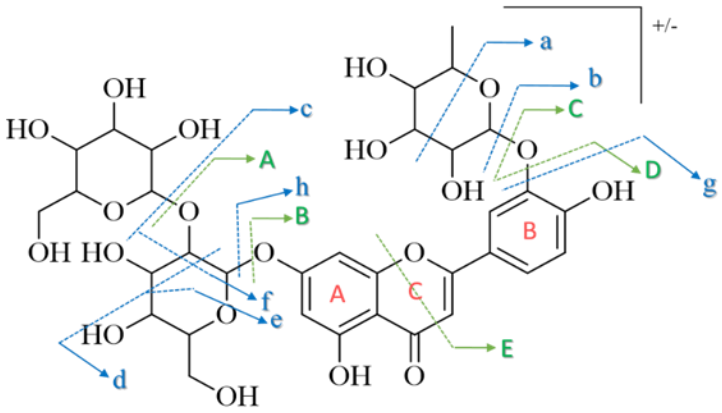

Scheme III.8. Fragmentation pathway of compound **8**

- **Compound 9 (t_R =15.4 min)**

According to the obtained mass spectral data, the molecular weight of this compound was deduced as 594 Da. The value was confirmed by the presence of pseudo-molecular ion peaks in positive mode (ESI +) at *m/z* 595 $[M+H]^+$ and 617 $[M+Na]^+$,and at *m/z* 593 $[M–H]^-$ in negative mode (ESI –) (Figure III.26 and III.27).

In positive mode, the MS spectrum revealed only two main product ions demonstrating two successive losses of hexose (– O) units from molecular ion peak at *m/z* 433 $[M+H–162]^+$ and the last peak at *m/z* 271 $[M+H–2\times162]^+$ suggested to be the fragment ion of apigenin. These two hexose units are proposed to be bonded through (1→2) linkage.

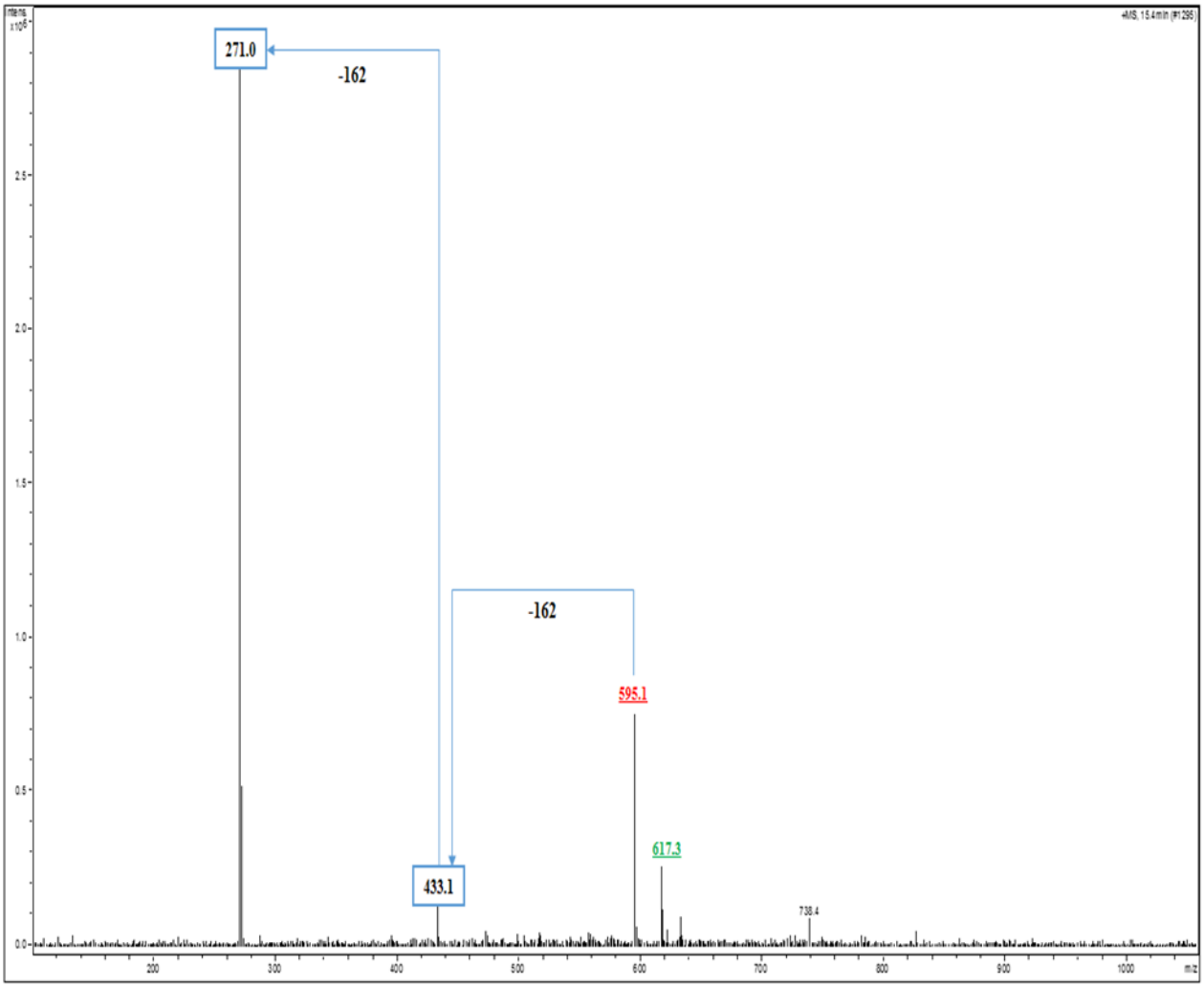

Figure III.26. ESI/MS (+) spectrum of compound **9**

This result was supported by losing the whole *O*-dihexose part yielding a small peak at *m/z* 269 $[M–H–324]^-$ in ESI/MS (–).

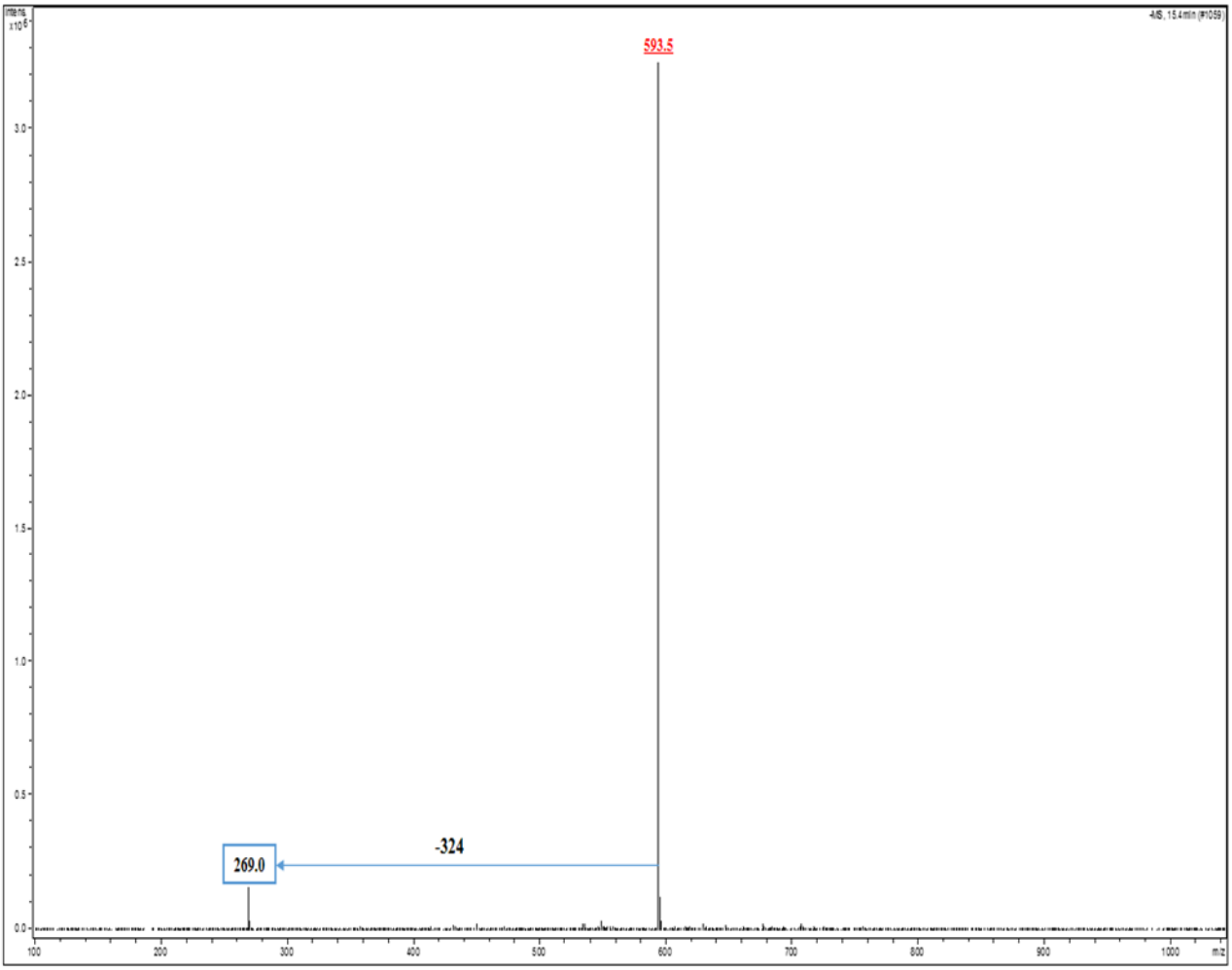

Figure III.27. ESI/MS (–) spectrum of compound **9**

According to the literature data **[4]**, compound **9** was formerly identified in *Scilla maderensis* Menezes as apigenin 7-*O*-(glucosyl-(1´´´→2´´)-glucoside).

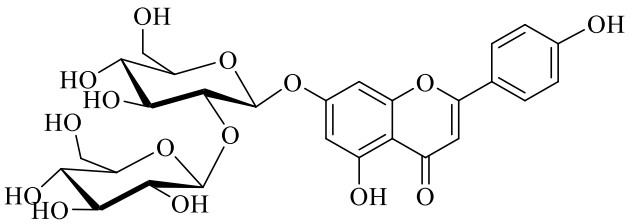

Figure III.28. Chemical structure of compound **9**

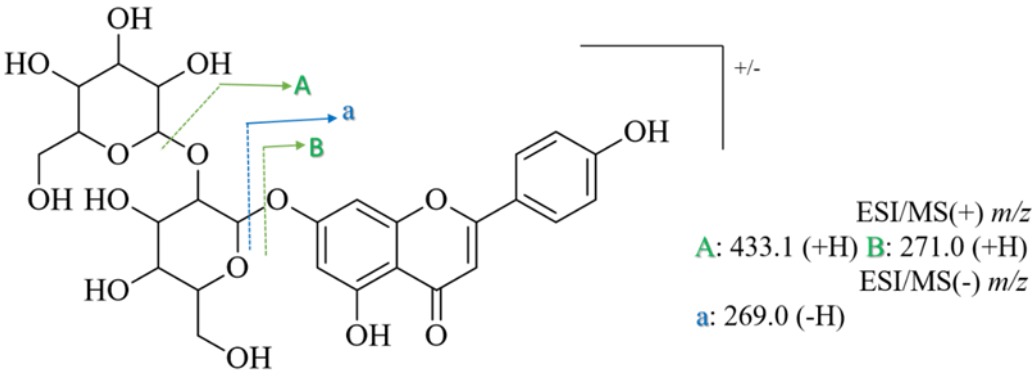

Scheme III.9. Fragmentation pathway of compound **9**

- **Compound 10 (t_R =17.1 min)**

The molecular weight of compound **10** was deduced from the mass spectral data as 578 Da basing on the presence of representative molecular ion peaks at *m/z* 579 $[M+H]^+$ and 601 $[M+Na]^+$ in ESI/MS (+), and at *m/z* 577 $[M–H]^-$ detected by ESI/MS (–) (Figure III.29 and III.30).

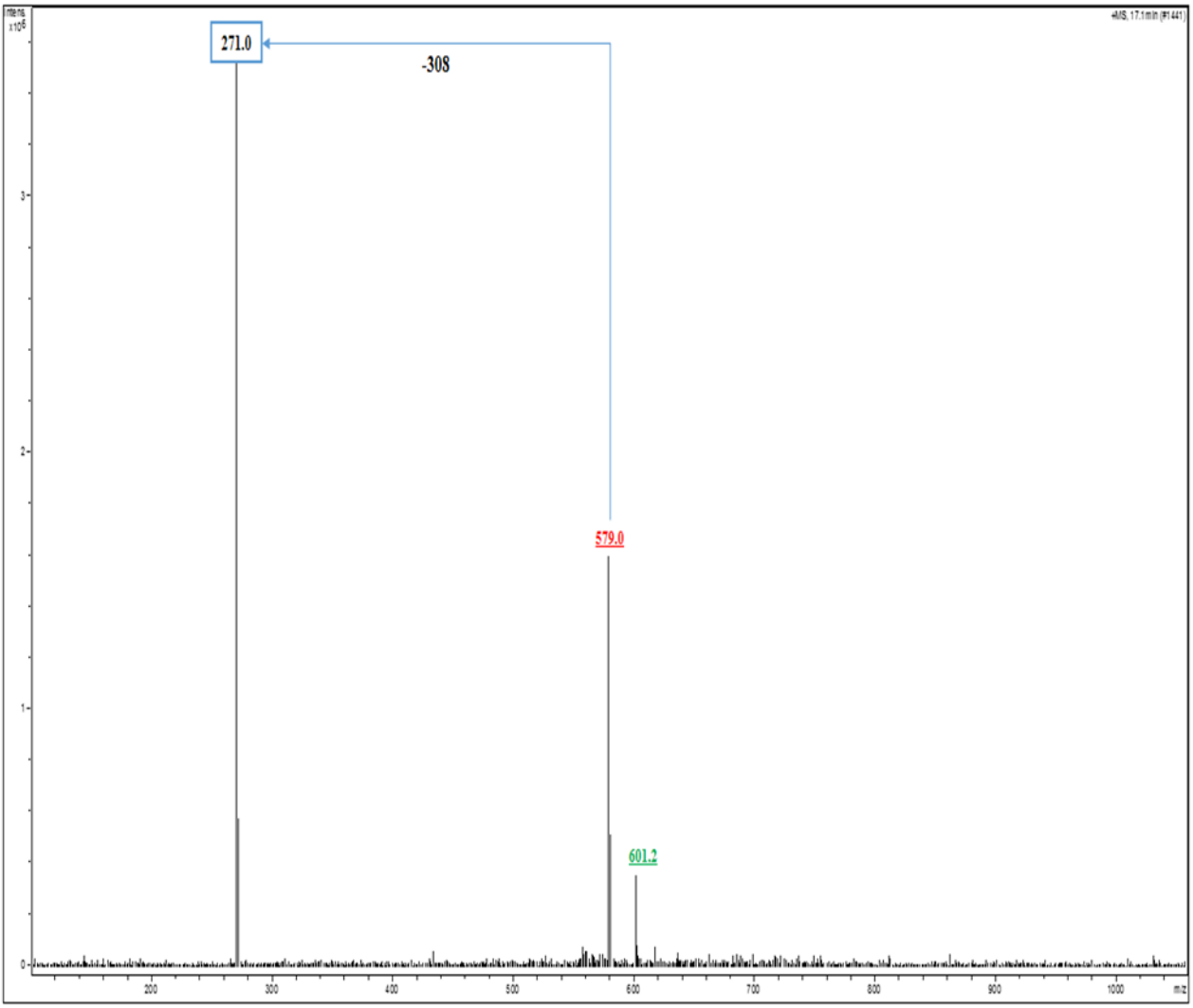

Figure III.29. ESI/MS (+) spectrum of compound **10**

Only one diagnostic fragment at *m/z* 271 $[M+H–308]^+$ is observed as a base peak in ESI/MS (+) spectrum or at *m/z* 269 $[M–H–308]^-$ in ESI/MS (–) data, indicates the elimination of rhamnose (– O) and hexose (– O) residues as one part.

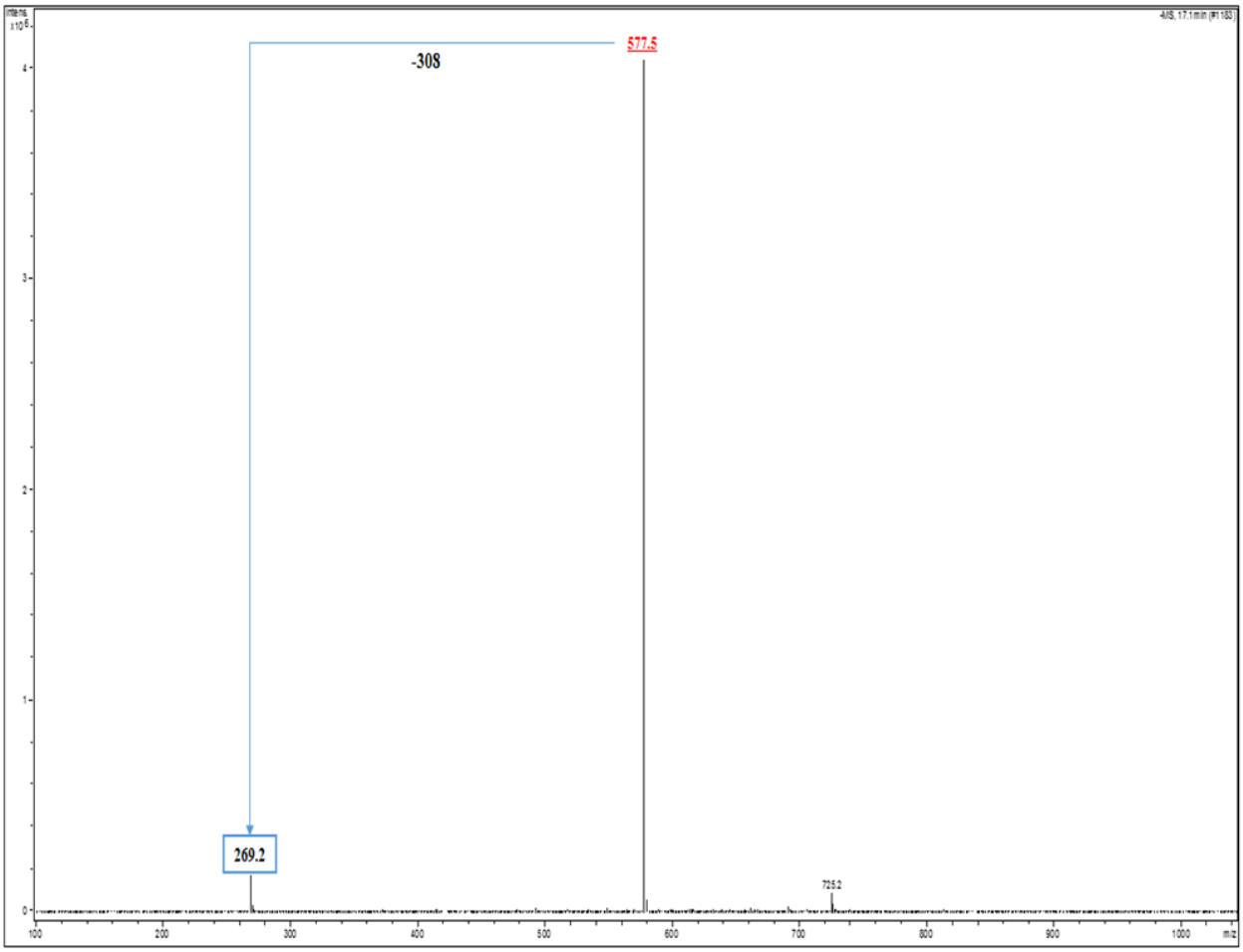

Figure III.30. Fragmentation pathway of compound **10**

As a result, compound **10** can be tentatively identified to be apigenin 7-*O*-(glucosyl-(1´´´→2´´)-rhamnoside).

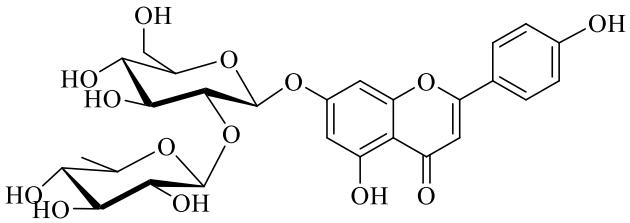

Figure III.31. Chemical structure of compound **10**

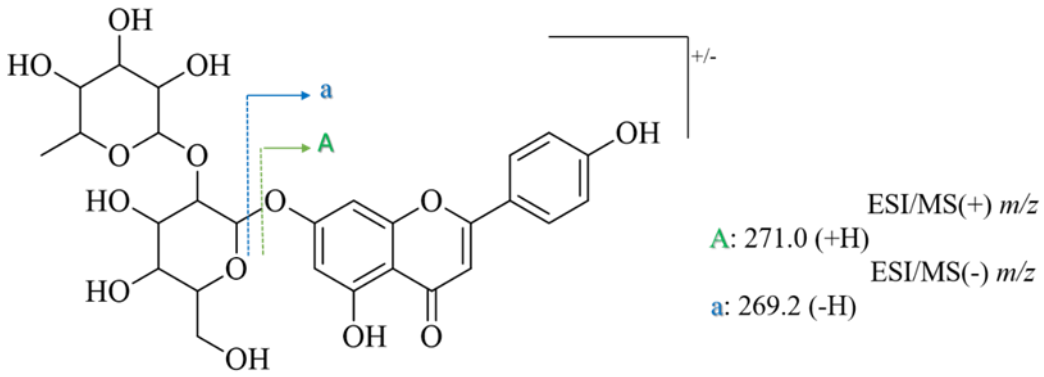

Scheme III.10. Fragmentation pathway of compound **10**

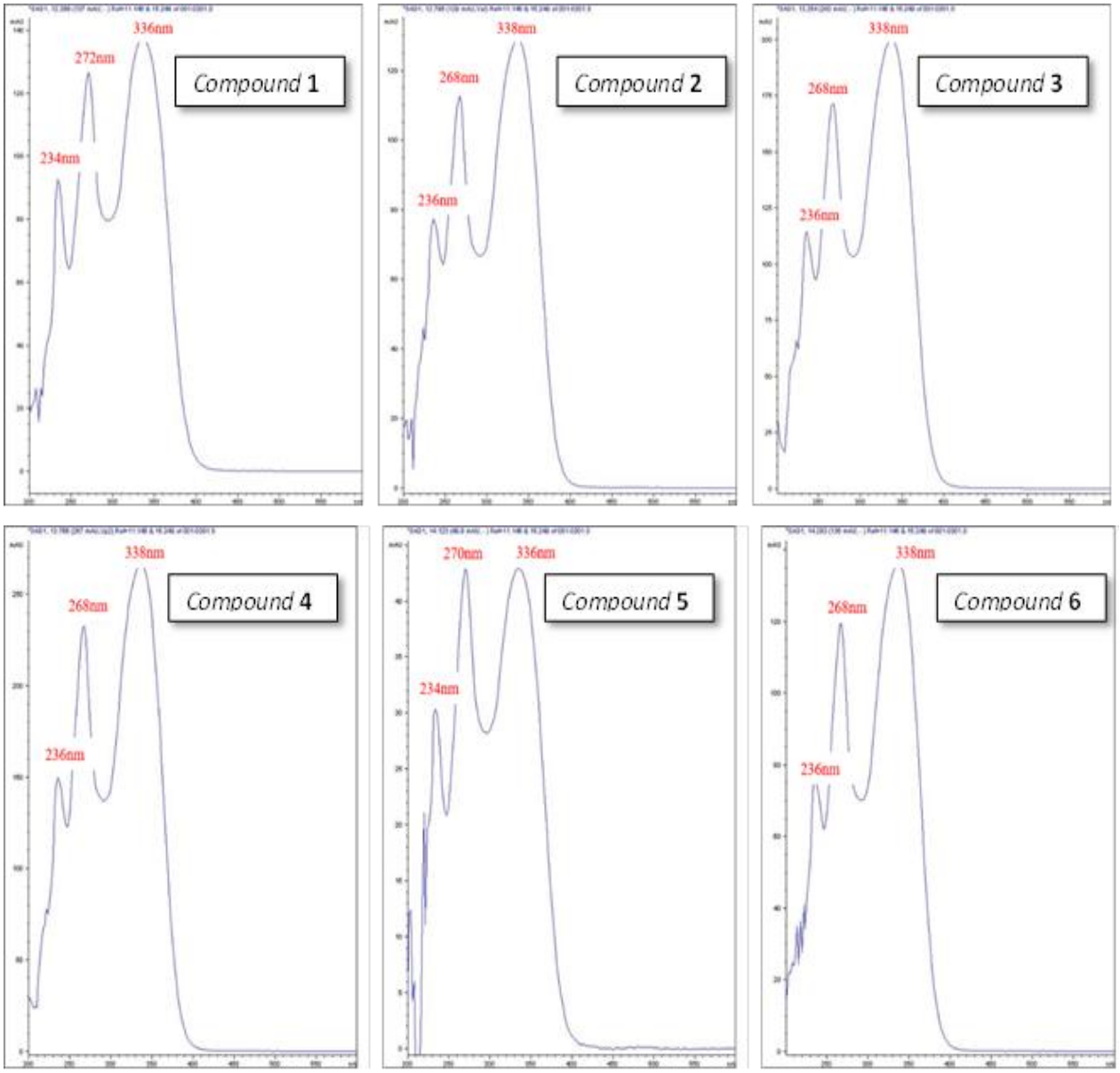

Figure III.32. UV spectra of the detected compounds (from 1 to 10)

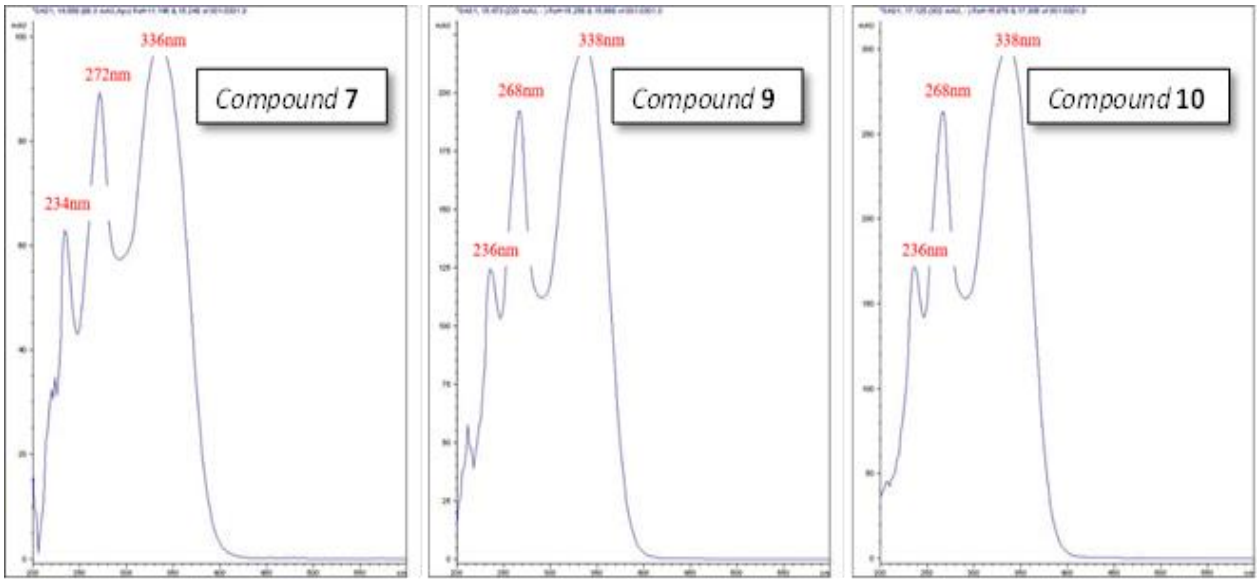

Figure III.32. (Continued)

Molecular docking studies

III.2 | Cholinesterase activities

III.2.1 | Background

Alzheimer's disease (AD) is a progressive neurodegenerative disorder characterized by the loss of cognition and impaired intellectual ability and functionality **[5]**. Herein, acetylcholinoesterase (AChE) and butylrylcholinoesterase (BChE) are some of the keys targets of drugs for treating AD **[6]**.

III.2.2 | Vina results interpretation

III.2.2.1 | Re-docked reference ligands

The re-docking results recapitulate that the standard inhibitors GNT and THA show an orientation similar to that mentioned in the literature **[7–10]** inside the active site pocket of the AChE (Trp^{84}, Glu^{199}, Ser^{200}, and His^{440}) and BChE enzymes (Trp^{82}, Ala^{328}, and His^{438}) respectively.

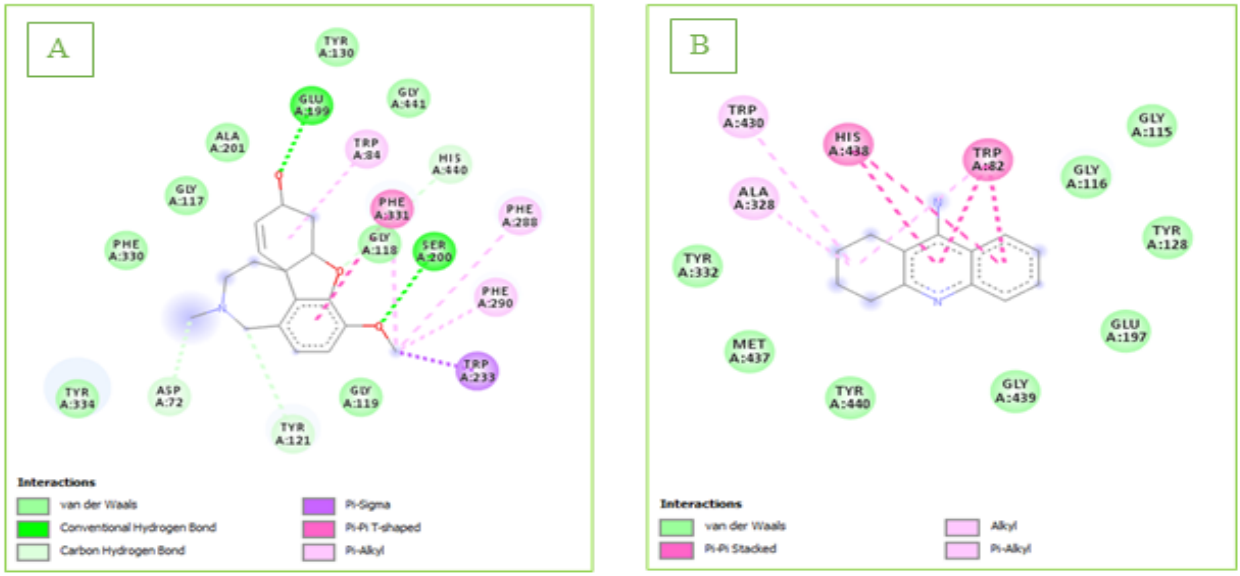

Figure III.33. 2D view of the binding poses of GNT in AChE (**A**) and THA in BChE (**B**).

III.2.2.2 | Binding affinities of the elucidated compounds into the chosen receptors

The docking calculations yielded several conformations with different energy values of the protein – ligand complexes. Thus, the minimum binding energy indicates the preferred docked ligand conformation with receptor as listed in (Table III.1).

Table III.1: Top binding affinities of the isolated compounds to the receptors.

	AChE	BChE
Compounds	Binding energy (kcal/mol)	
Ref.	-10.4	-8.4
Cp1	-10.6	-10.0
Cp2	-10.1	-11.2
Cp3	-11.2	-10.2
Cp4	-8.7	-10.3
Cp5	-10.8	-11.3
Cp6	-9.0	-11.3
Cp7	-11.1	-10.5
Cp8	-11.2	-10.4
Cp9	-11.6	-9.8
Cp10	-11.6	-10.2

The docking calculations of each compound produced several conformations. Among them, we had chosen the conformation that has low binding energy. Next, the above-outlined compounds are ranked in ascending order, where the compound with high energy in negative value has a good affinity to the receptor.

AChE: Cp10 = Cp9 < Cp 8 = Cp3 < Cp 7 < Cp5 < Cp1 < Ref < Cp 2 < Cp6 < Cp4

BChE: Cp6 = Cp5 < Cp2 < Cp7 < Cp8 < Cp4 < Cp3 = Cp10 < Cp1 < Cp9 < Ref

- ## AChE – Compounds interactions

In comparison with the above figure (A) and reported data **[7, 8]**, the binding mode observed for Cp1 shows that the hydroxyl (OH) group of the glycosidic part forms a hydrogen-bond (H-bond) with Glu^{199} and carbon-hydrogen bond (C-H bond) with Trp^{84}. Three Van Der Waals (VDW) interactions with Ser^{200}, Phe^{288} and His^{440} were observed. Besides, benzyl rings form two π- π stacking interactions with Trp^{279} and Tyr^{334} (Figure III.34).

The glycosidic OH groups of Cp2 interact with Trp^{84}, Glu^{199}, and Ser^{200} by forming H-bonds. The benzyl ring forms π- π stacking interaction with Trp^{279} (Figure III.34).

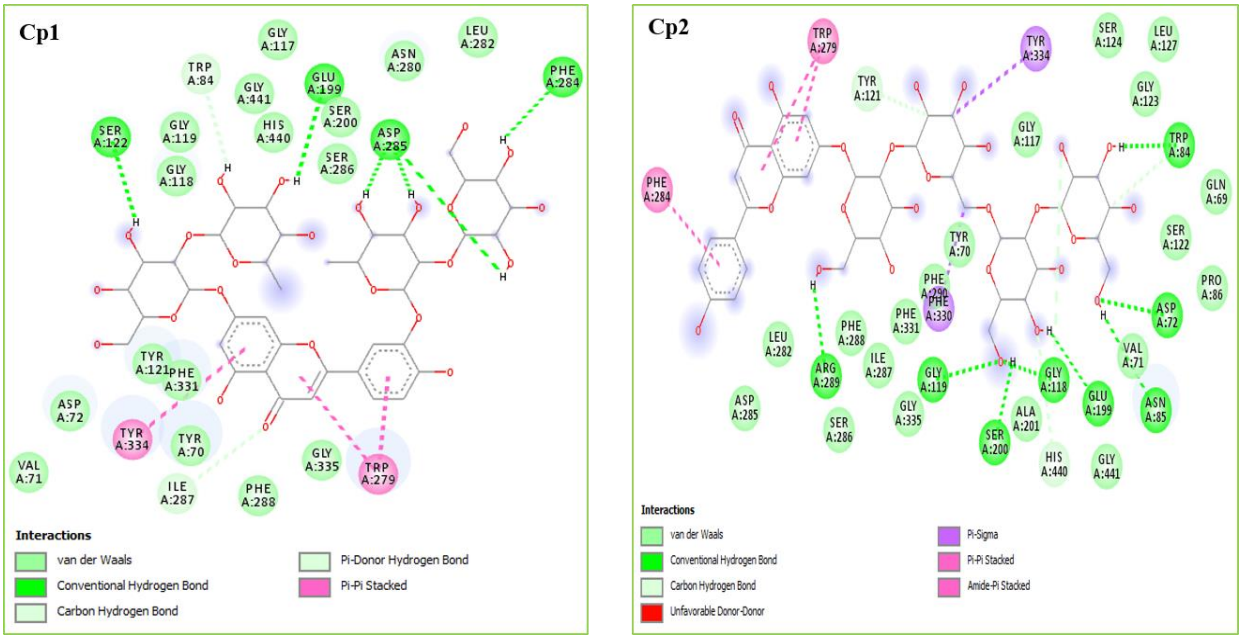

Figure III.34. 2D view of the binding poses of Cp1 and Cp2 in AChE enzyme.

Note 1: These results indicate that Cp1 and Cp2 may exhibit an inhibitory effect on the AChE enzyme by creating the main bonds with the amino acids of the pocket.

The Cp3 diagram displays that both OH-flavone and OH-sugar form H-bonds with Phe^{330} and Ser^{200} respectively. Two π- π stacking interactions with Trp^{279} and Tyr^{334} created by the benzyl rings. One VDW interaction and one C-H bond were observed for the sugar moiety with Trp^{84} and His^{440} individually. Two unfavorable interactions were created with $Gly^{118, 119}$ (Figure III.35).

The binding mode observed for Cp4 shows that both OH groups of the glycosidic part and OH-flavone form H-bonds with Trp^{84}, Phe^{330}, Phe^{331} and Trp^{279}, respectively (Figure III.35)

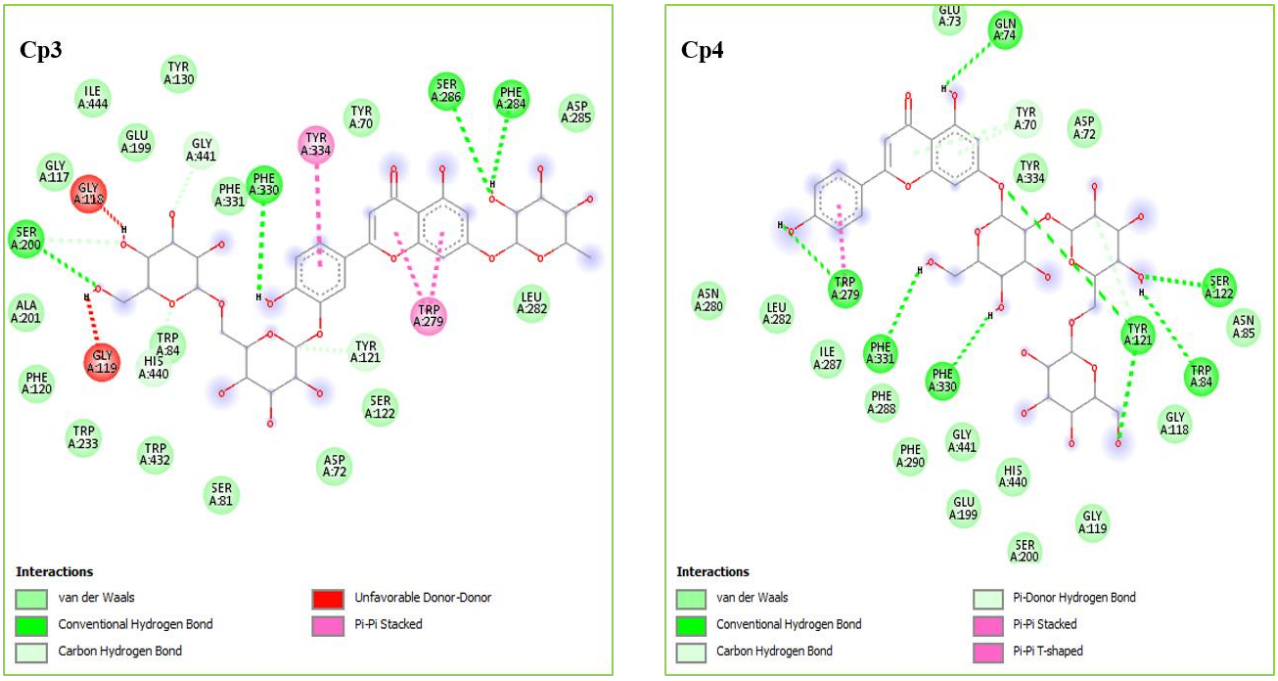

Figure III.35. 2D view of the binding poses of Cp3 and Cp4 in AChE enzyme.

Note 2: In this case, Cp3 and Cp4 may exhibit an inhibitory effect on the AChE enzyme according to the interactions receptor-ligand observed (either H-bond or π- π stacking interactions). Because of the unfavorable Donor – Donor interactions observed for Cp3 in the AChE pocket, this model seems to be unsuitable for AChE inhibitory activity.

The analyses of the following 2D digrams (Figure III.36) showed that:

The δ-bond in (–CH_2–OH) of the glucose (Glc) unit in Cp5 creates a π-δ interaction with Phe^{330}. An H-bond was formed between the OH-flavone group and Tyr^{334}. A π- π stacking interaction with Trp^{279} resulted by chromone rings.

The molecular docking result of Cp6 exhibited no interactions between ligand parts and the key amino acids of the target protein.

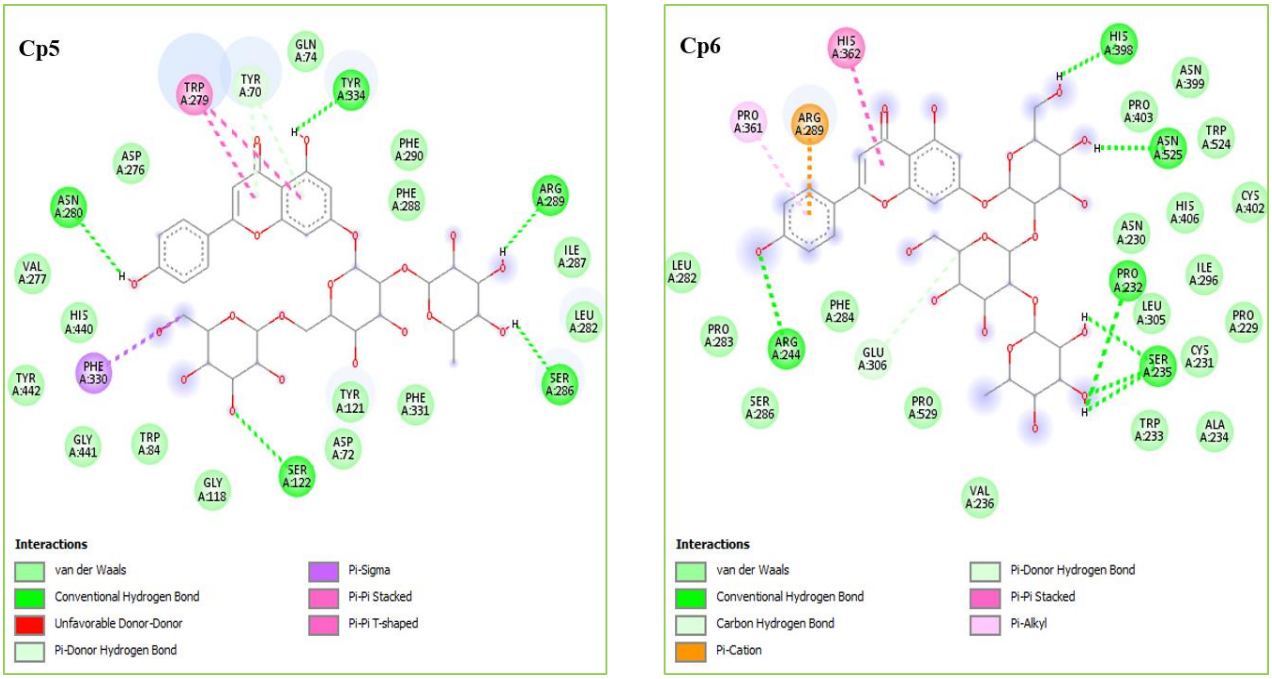

Figure III.36. 2D view of the binding poses of Cp5 and Cp6 in AChE enzyme.

Note 3: Upon the above results, Cp5 is predicted to block the action of the AChE enzyme by establishing different bond types with the active site residues, while Cp6 have no inhibitory effect against AChE enzyme.

As it is shown in Figure III.37, Cp7 forms various interactions with the target protein pocket. The aglycone part interacts with Tyr^{334}, Phe^{330}, Phe^{331} and Trp^{279} by including its OH group in H-bond and its benzyl rings in either π- π stacking interactions or C-H bond. While the glycan part interacts with Tyr^{121} by forming H-bond and C-H bond, the VDW interaction was observed only with Trp^{84}.

The 2D diagram of Cp8 shows the formation of two H-bonds with His^{440} and Ser^{200} *via* OH-sugar groups. In addition, the glycan part interacts by its OH groups with Tyr^{334} and Trp^{279} (Figure III.37).

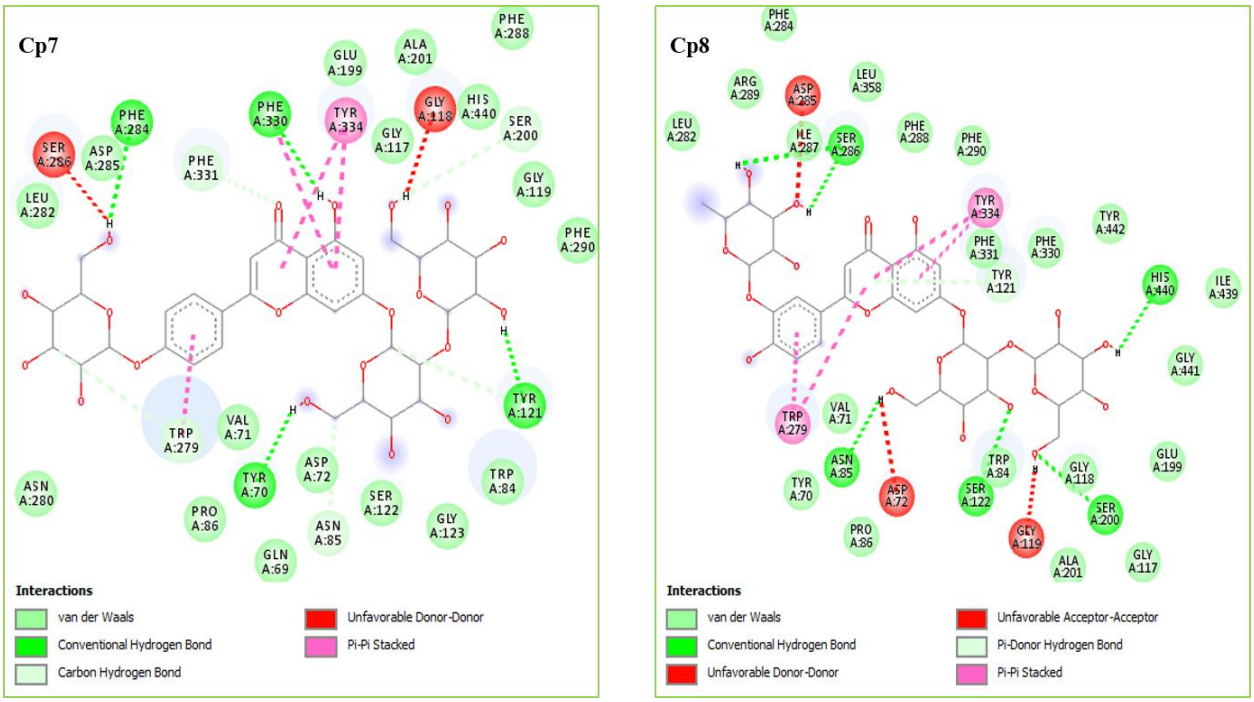

Figure III.37. 2D view of the binding poses of Cp7 and Cp8 in AChE enzyme.

Note 4: Both Cp7 and Cp8 may exhibit an inhibitory effect on the AChE enzyme by creating main bonds with the key amino acids of the pocket. On the other hand, each compound reveals unfavorable Donor-Donor or Acceptor-Acceptor interactions which can decrease their inhibitory effect.

The 2D interactions of Cp9 show three main H-bonds with Ser^{200}, Gly^{118}, and Tyr^{121} focused on the glycosidic part. Furthermore, the aglycone part interacts with Tyr^{334}, Trp^{279} and Phe^{330} by involving its benzyl rings in π- π stacking interactions. The Phe^{331} residue interacts with both carbonyl group by forming π-Donor-H bond and OH-group by creating C-H bond.

In the 2D view of Cp10, the aglycone part forms four π- π stacking interactions with Tyr^{334}, Trp^{279} and Phe^{330} in which one H-bond created by OH group with Phe^{330}, and one C-H bond between carbonyl group and Phe^{331}. Moreover, the OH groups of the glycan part interact with Ser^{200}, $Gly^{118, 119}$ and Trp^{84} by forming H-bond (Figure III.38).

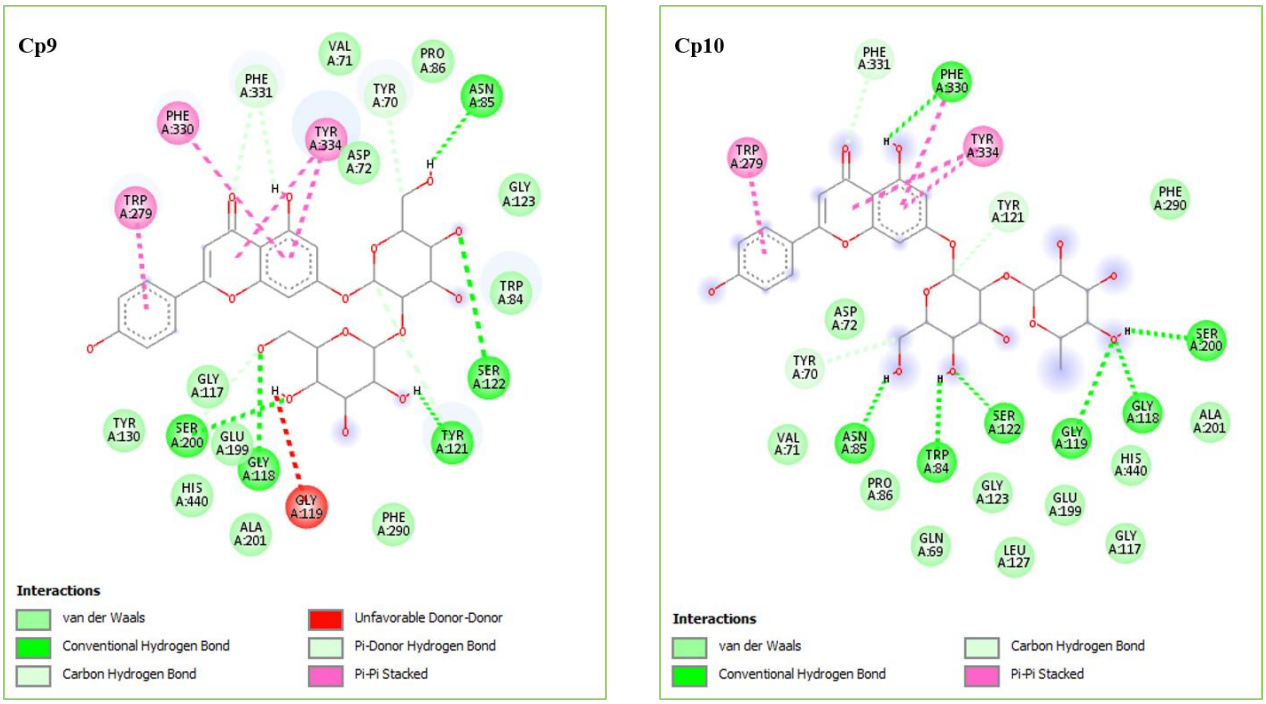

Figure III.38. 2D view of the binding poses of Cp9 and Cp10 in AChE enzyme.

Note 5: Although Cp9 and Cp10 may exhibit an inhibitory effect on the AChE enzyme by forming significant bonds with the key amino acids of the pocket, Cp9 seems to be inappropriate to the AChE inhibitory activity due to the unfavorable Donor-Donor observed interaction.

Deductive remarks

In comparison with the standard AChE inhibitor GNT, the docking study revealed that all docked compounds excepting Cp6, have an acceptable alignment at the active site by interacting with the most crucial amino acid residues of the target protein pocket, which gave them an AChE inhibitory effect. Herein, both of flavonoid and glycosidic moieties are played a role in blocking AChE enzyme. Among these 9 active compounds, **Cp10** presents a top pose inside the enzyme pocket by giving the lowest binding affinity at (-11.6 Kcal/mol) comparing to the native ligand at (-10.4 kcal/mol). Our choice was supported by the following data:

The docked free OH-groups apigenin has been previously presented an inhibitory effect against AChE enzyme **[11]** by establishing π-π stack to Phe^{330} as mentioned in literature **[12]**. Previous study revealed that the presence of 7-*O*-glycosylation can be enhanced the AChE inhibitory effect of the flavonoid **[13]**, which make our result in agreement with the reported data due to the presence of H-bindings between glycosidic moieties (OH-groups) and the key amino acid of the AChE enzyme.

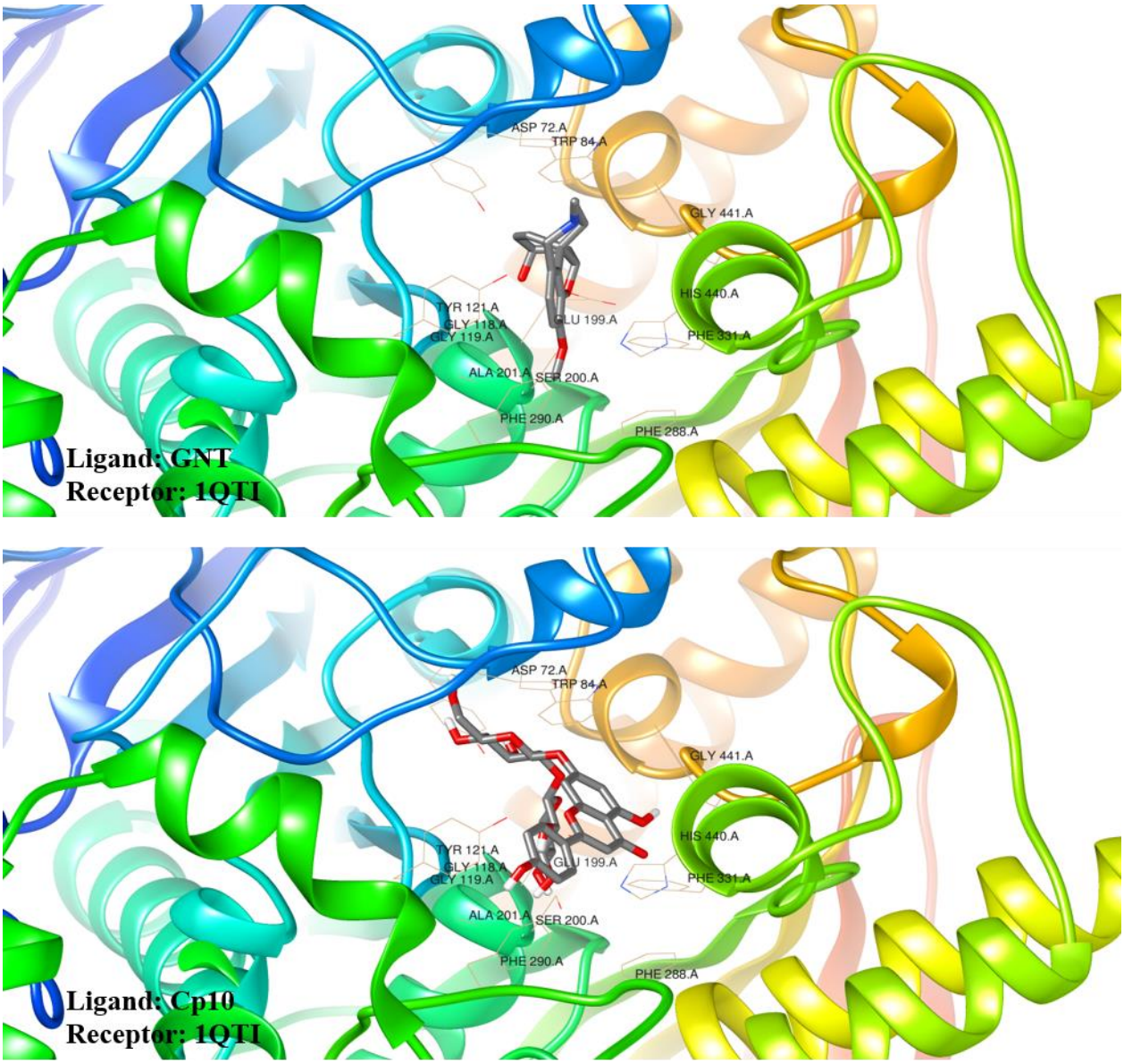

Figure III.39. 3D alignment of Cp10 inside the AChE (1QTI) pocket.

- **BChE – Compounds interactions**

Based on the previous literature data **[7, 9]** and re-docking result that showed in Figure III.34.B, the binding mode observed for Cp1 shows that the OH group of the glycosidic part forms H-bonds with Trp^{82}, Tyr^{440} and C-H bond with His^{438}. Three VDW interactions formed with Trp^{430}, Ala^{328} and Gly^{116}. Besides, chromone rings form π- anion interactions with Asp^{70} (Figure III.40).

The glycosidic OH groups of Cp2 interact with $Gly^{115, 116}$, $Tyr^{440, 332}$, Asp^{70} and Ser^{198} by forming H-bonds. It shows also hydrophobic interactions (π- Donor H-bond, C-H bond) with Trp^{82}, Gly^{439}, Ser^{198} and His^{438} (Figure III.40).

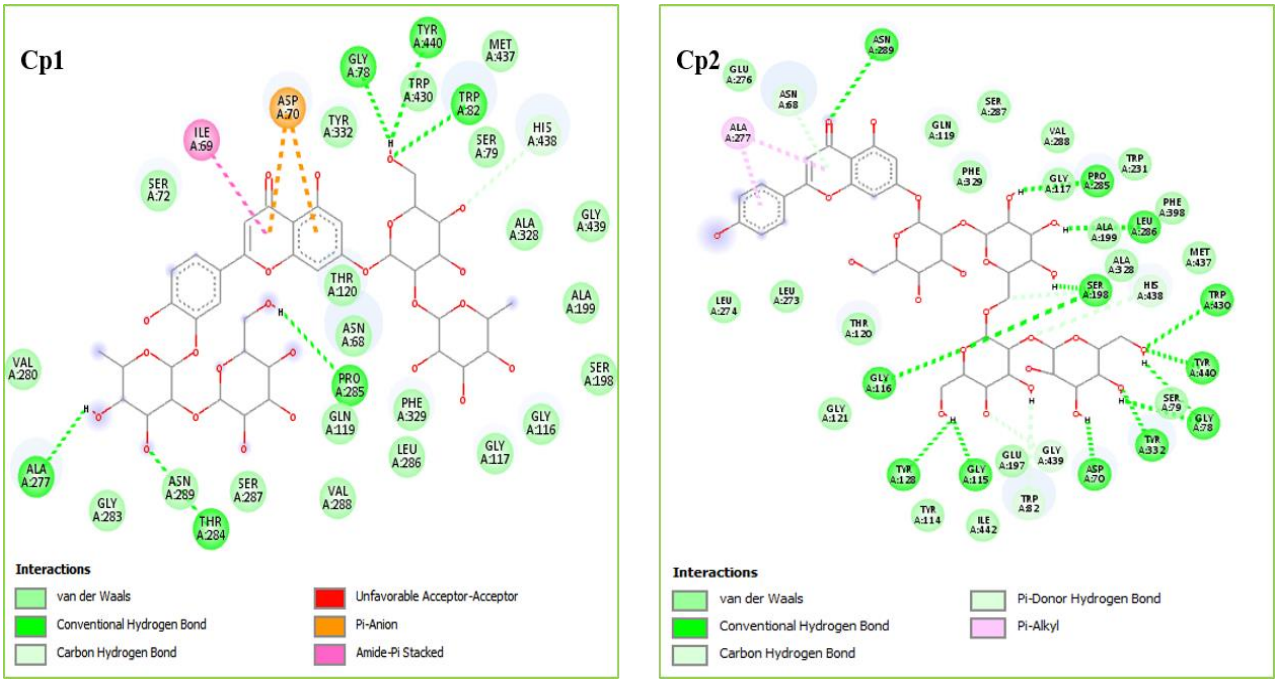

Figure III.40: Intra-molecular interactions of Cp1 and Cp2 with BChE enzyme in 2D.

Note 1: These investigations reveal that Cp1 interacts with the key amino acids by introducing its chromone rings and glycosidic moiety, and Cp2 interacts by involving only its glycosidic moieties. Both compounds may exhibit an anti-BChE activity.

The Cp3 diagram presented in figure III.41, displays that this compound establishes no associations with the key amino acid residues of the active site.

The 2D analysis of Cp4 reveals several types of associations. Ser^{198}, His^{438}, $Tyr^{440, 332}$ and Trp^{430} share H-bonding with 4′-OH group in flavonoid skeleton, and with OH groups of the glycosidic part. Asp^{70} showed π- anion associations with chromone rings. Unfavorable interactions were observed between Trp^{82} and glycosidic side (Figure III.41).

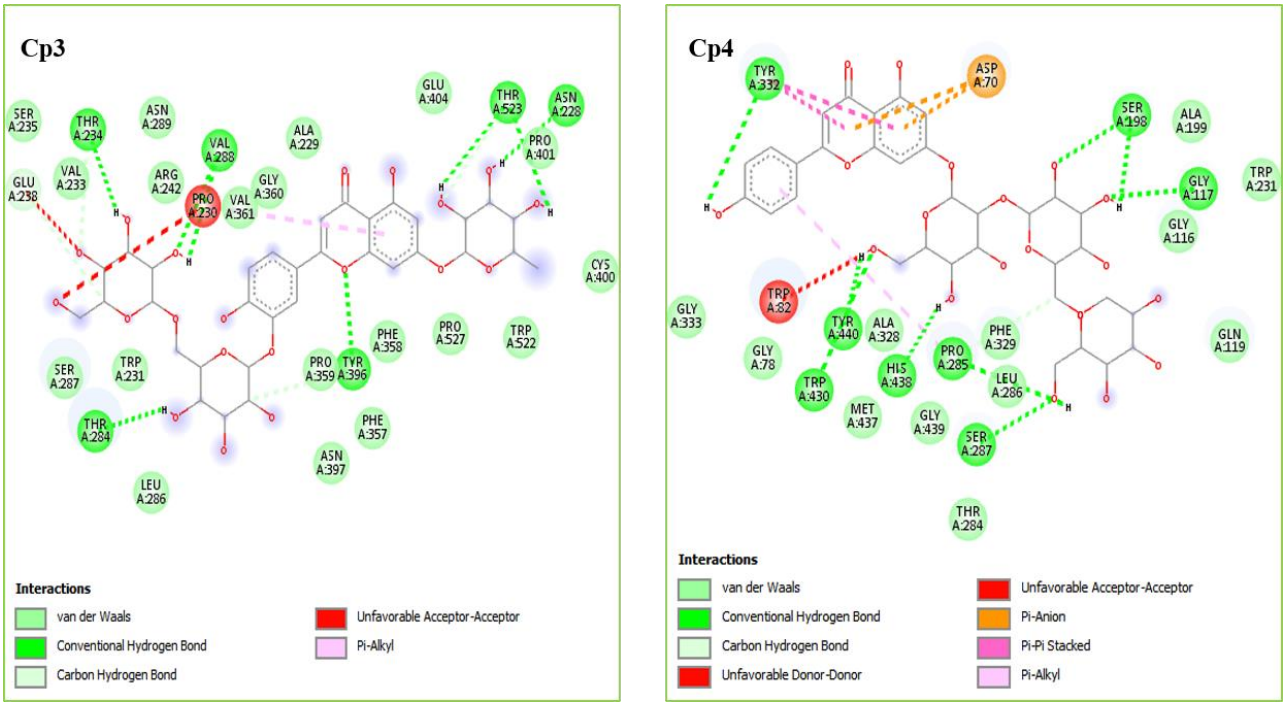

Figure III.41. Intra-molecular interactions of Cp3 and Cp4 with BChE enzyme in 2D.

Note 2: Upon the above investigations, Cp4 is predicted to block the action of the BChE enzyme by establishing different bond types with the active site residues. On the other hand, this compound displayed an unfavorable interaction with the Trp^{82} which can decrease its inhibitory effect.

As seen in Figure III.42, Cp5 forms H-bond with Ser^{198}, Glu^{197} and His^{438} by comprising OH-groups of the flavonoid skeleton and glycosidic moieties. B-ring of flavonoid part shares a π-δ interaction with Trp^{82}. Three unfavorable interactions were detected for this compound.

The molecular docking result of Cp6 showed the formation of H-bonds between OH-sugar groups and $Ser^{198,}$ Glu^{197} and Tyr^{332}. It shows also hydrophobic interactions (VDW, C-H bond) with $Trp^{82, 430}$, Tyr^{440} and Gly^{439} (Figure III.42).

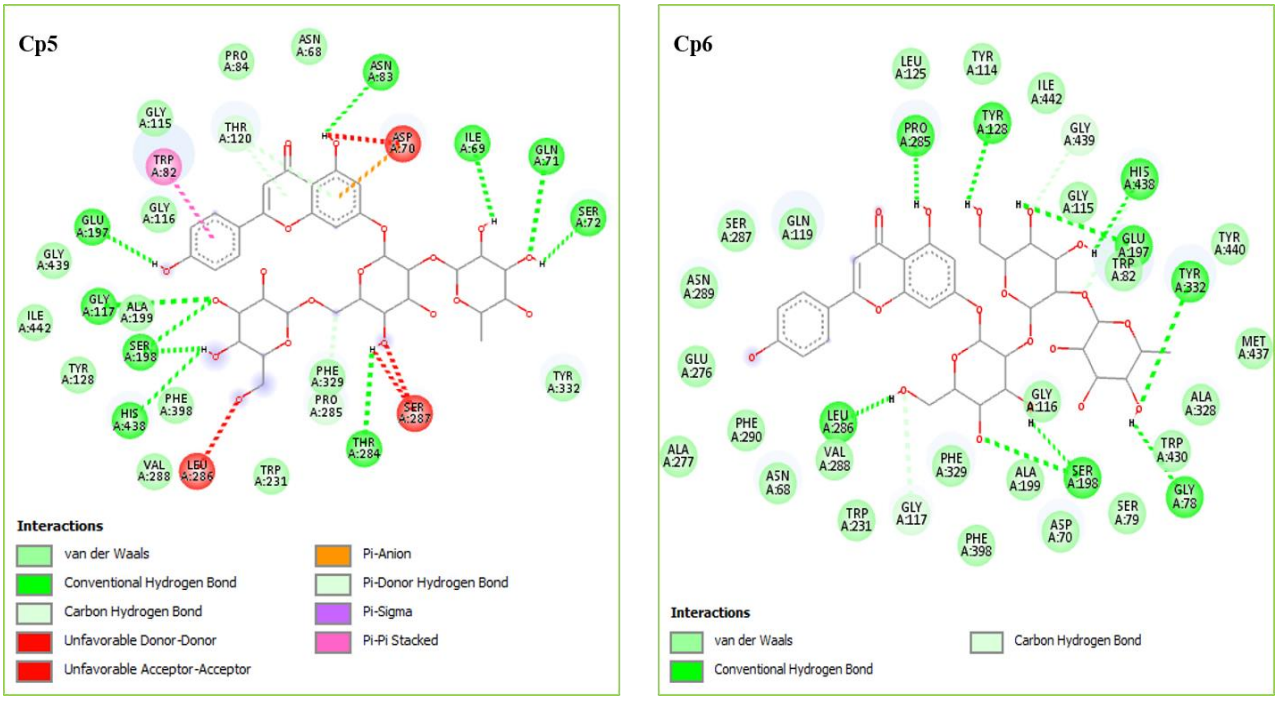

Figure III.42. Intra-molecular interactions of Cp5 and Cp6 with BChE enzyme in 2D.

Note 3: The docking study of these compounds revealed that they create several associations with the key amino acids of the enzyme pocket. As a result, Cp5 and Cp6 may exhibit an inhibitory effect on the BChE enzyme. Besides, the Cp5 predicted to be unfitting as an inhibitor for the BChE protein due to the unfavorable interactions.

The analyses of the following 2D illustrations (Figure III.43) showed that:

The two linked glucose units of Cp7 create different associations with the key amino acids by forming H-bonds with Glu^{197}, Ser^{198}, His^{438}, Trp^{82}, Tyr^{332} and Asp^{70}, hydrophobic interaction with Gly^{439}, His^{438}, Tyr^{440}, Ala^{328} and Trp^{430} besides to the unfavorable interaction on the 4′-*O*-Glc. Gly^{116} shows amide-π stacking interaction with chromone rings.

The B-ring of Cp8 forms π-π stacking interaction with Trp^{82} and H-bond between 4′-OH and Glu^{197}. The A-ring creates an π- anion interaction with Asp^{70} and H-bond between the same amino acid and 5-OH. A number of hydrophobic interactions were observed on the monoglycodic side with Ala^{328}, Tyr^{332} and His^{438} besides the H-bindiging on the bi-saccharide parts with Pro^{285} and Ser^{287}.

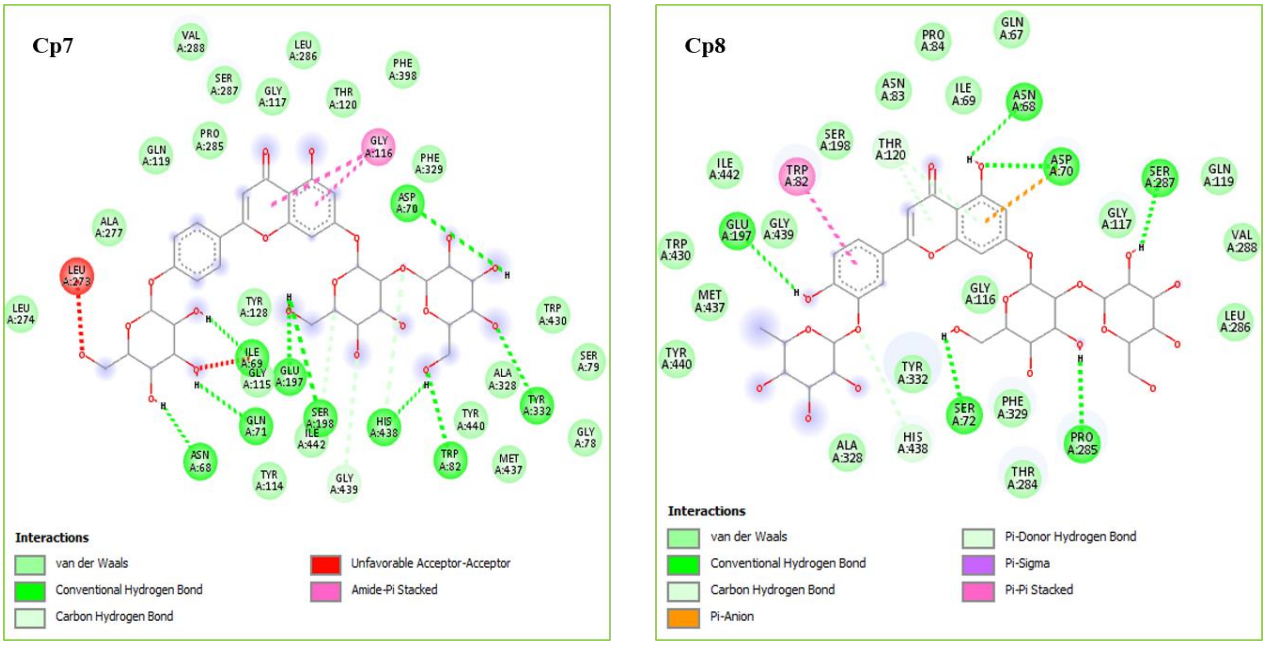

Figure III.43. Intra-molecular interactions of Cp7 and Cp8 with BChE enzyme in 2D.

Note 4: These results indicate that Cp7 and Cp8 may exhibit an inhibitory effect on the BChE enzyme by creating the main bonds with the amino acids of the pocket. Despite the main interactions with the active site associated with Cp7, the presence of the unfavorable interactions makes it less active as an inhibitor.

As shown in Figure III.44, both Cp9 and Cp10 share the same interactions with the following residues: Trp^{82} (π-π stacking interaction), Asp^{70} (as π- anion interaction with A-ring and as H-bonding with 5-OH). A number of VDW interactions were also observed with His^{438}, Phe^{329}, $Gly^{115,116}$ and Tyr^{332}. Additionnel H-bond with $Glu^{197}$was observed for Cp10.

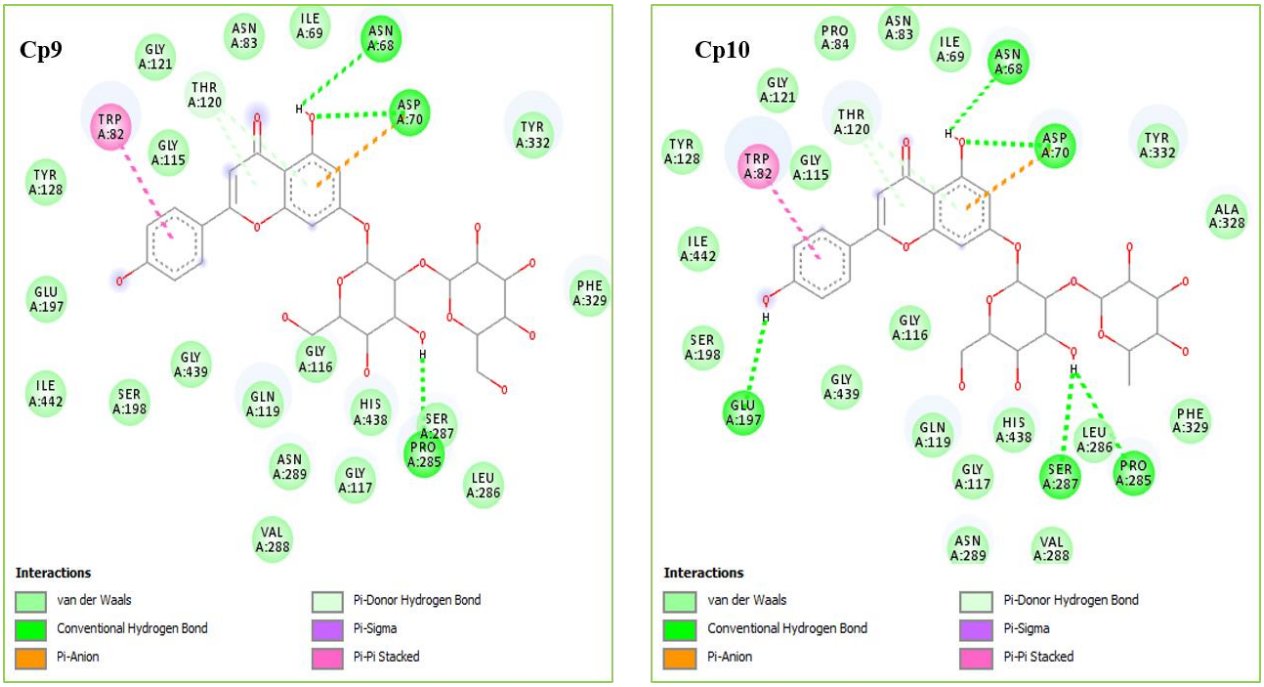

Figure III.44. Intra-molecular interactions of Cp9 and Cp10 with BChE enzyme in 2D.

Note 5: According to the docking analyzed data, Cp9 and Cp10 are predicted to inhibit the action of the BChE enzyme by interacting with the most important amino acid residues of the target protein.

Deductive remarks

Based on the binding energies illustrated in (Table III.1), all docked compounds showed a higher affinity to the binding site of the BChE enzyme compared to the native ligand THA. The 2D interactions diagram revealed that all docked compounds excluding Cp3, have a satisfactory alignment at the active site by interacting with the most crucial amino acid residues. This result can lead to the bioactivity of these compounds against BChE. Profound analysis revealed that the active compounds were **Cp6** (-11.3 Kcal/mol), where the inhibitory activity was focused only on the tri-saccharide part, besides **Cp8** (-10.4 Kcal/mol), **Cp9** (-9.8 Kcal/mol) and **Cp10** (10.2 Kcal/mol). Basing on their binding energy the best inhibitor is **Cp8**. This compound interacts by involving its aglycone part (A, B rings and OH-groups at 5, 4′ position) and glycosidic moeities. Our result and also previously published docking studies of flavonoid derivatives **[14, 15]** support the idea about inhibition *via* the aglycone part.

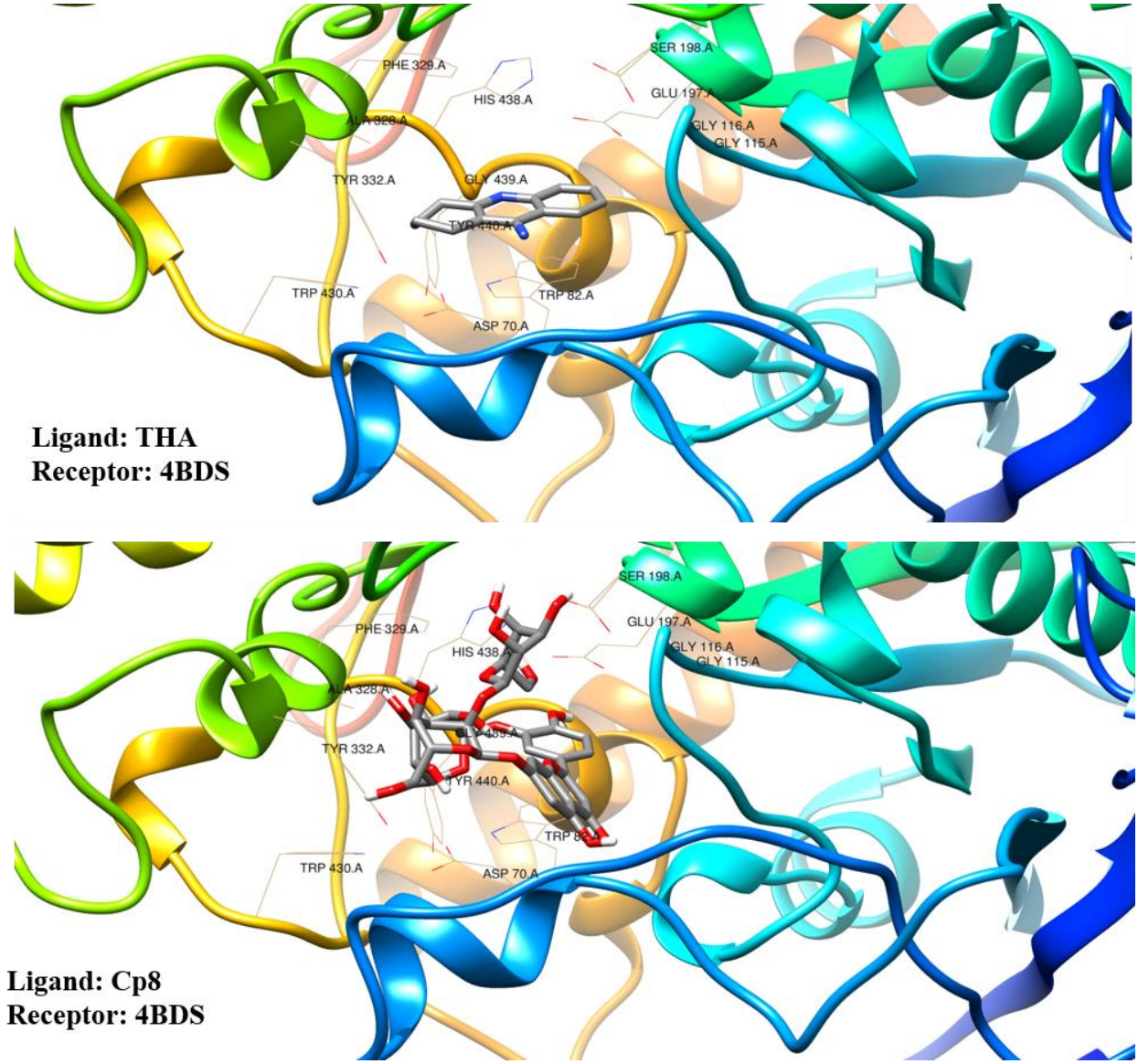

Figure III.45. 3D alignment of Cp8 inside the BChE (4BDS) pocket.

III.3 | Anti-inflammatory activity

III.3.1 | Background

Inflammation is a dynamic process that is elicited in response to mechanical injuries, burns, microbial infections, and other noxious stimuli that may threaten the well-being of the host. Non-steroidal anti-inflammatory drugs (NSAIDs) are widely used for the treatment of inflammatory ailments such as: rheumatism diseases (rheumatoid arthritis). The pharmacological effects of NSAIDs are due to the inhibition of a membrane enzyme called cyclooxygenase (COX) **[16, 17]**.

III.3.2 | Vina results interpretation

III.3.2.1 | Re-docked reference ligands

Through the results shown by the re-docking studies, the standard ligands BFL and NPX reveal approximately the same interactions with the key amino acids, into COX-1 and COX-2 respectively. These results are in agreement with the online models **[18, 19]** and literature **[20, 21]**.

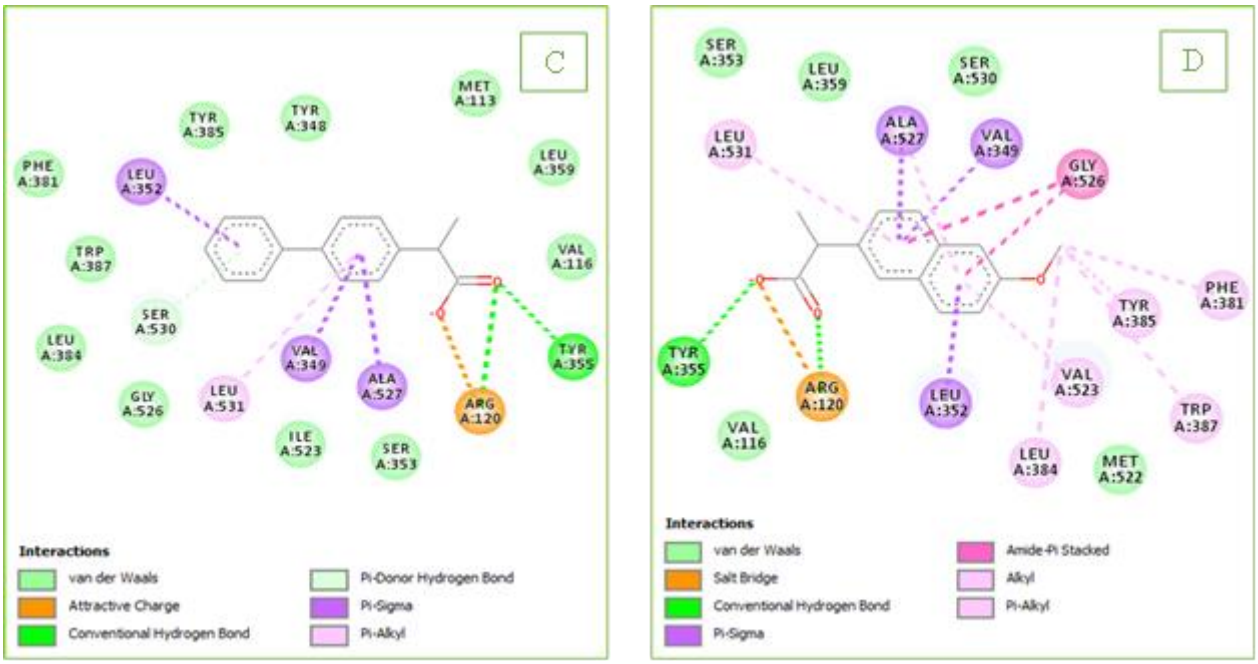

Figure III.46. 2D view of the binding poses of BFL in COX-1 (**C**) and NPX in COX-2 (**D**).

Note 1: Because COX-1 and 2 are isozymes, they share a similar key amino acid residues in their active site (see chapter II .Table II.2). Only one difference was detected at position 523. So, this latter was defined as Ile in COX-1 and as Val in COX-2 **[22, 23]**.

III.3.2.2 | Binding affinities of the elucidated compounds into the chosen receptors

The docking calculations yielded several conformations with different energy values of the protein – ligand complexes. Therefore, the minimum binding energy indicates the preferred docked ligand conformation with receptor as listed in (Table III.2).

Table III.2: Top binding affinities of the isolated compounds to the receptors.

	COX-1	COX-2
Compounds	Binding energy (kcal/mol)	
Ref.	-8.9	-9.0
Cp1	-9.0	10.8
Cp2	-9.1	6.1
Cp3	-8.9	4.6
Cp4	-8.5	0.7
Cp5	-9.4	-0.7
Cp6	-8.8	0.7
Cp7	-9.0	3.8
Cp8	-9.1	3.1
Cp9	-8.8	-3.2
Cp10	-9.2	-3.4

From the binding energy point of view, the compound with lower binding energy was selected to be the preferred inhibitor. Which means it has a higher affinity to the pocket of the target protein. The affinity of the tested compounds to the receptor are ranked in descending order as below:

COX-1: Cp5 > Cp10 > Cp2 = Cp8 > Cp7 = Cp1 > Ref = Cp3 > Cp6 = Cp9 > Cp4

COX-2: Ref > Cp10 > Cp9 > Cp5> Cp6 = Cp4 > Cp8> Cp7 > Cp3 > Cp2 > Cp1

- **(COX-1) – Compounds interactions**

Despite the low registered energy in compounds Cp1, Cp2, and Cp3, the 2D visualization of them revealed no interactions with the key amino acid residues of the target COX-1 enzyme (Figure III.47). By doing so, these compounds have no inhibition activity against the COX-1 enzyme.

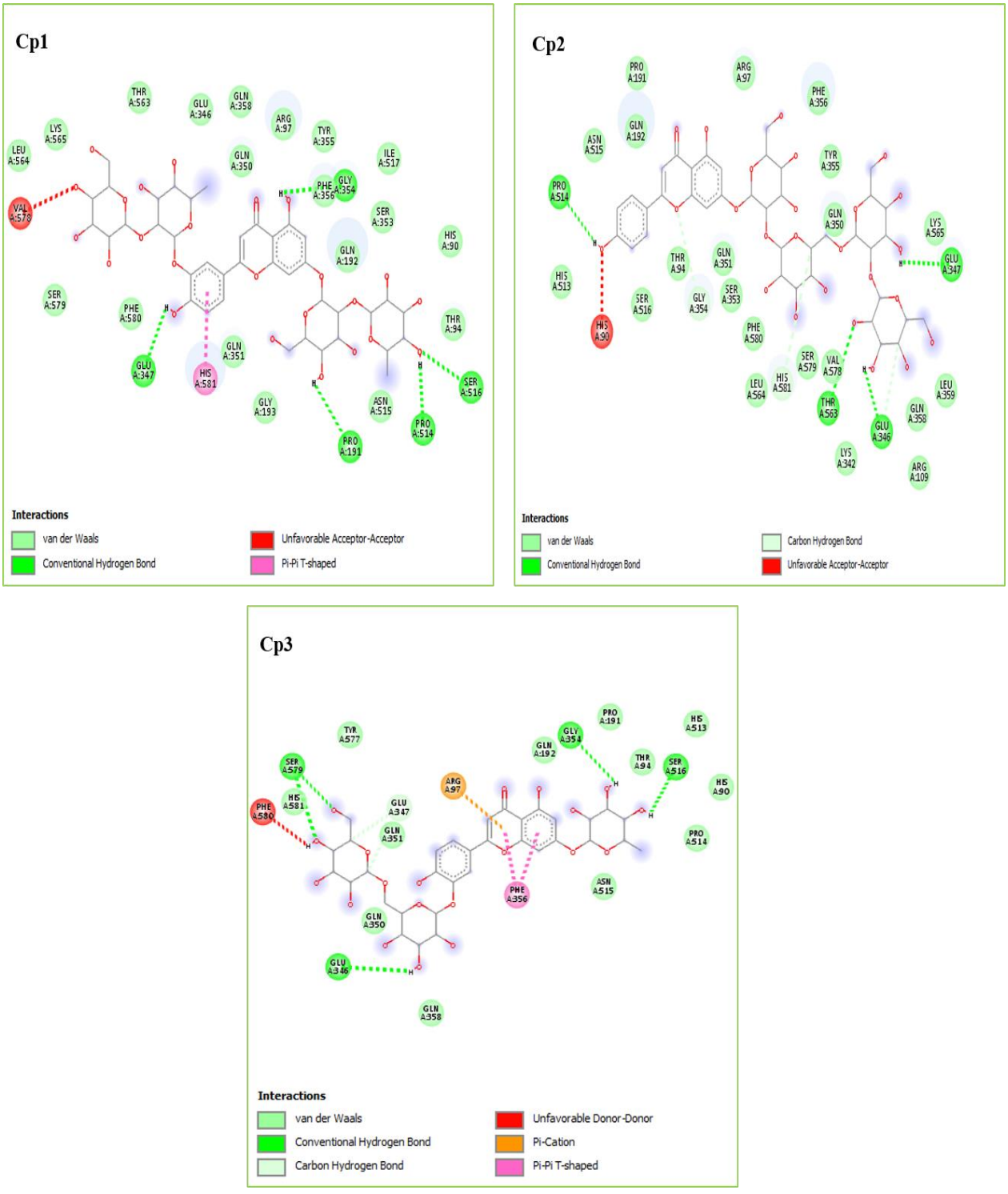

Figure III.47. 2D view of the binding poses of Cp1, Cp2, and Cp3 in COX-1 enzyme.

The compounds Cp4, Cp5, Cp6 and Cp7 show only one association with Tyr^{355} by involving their 5-OH group of the flavonoid skeleton. An H-bonding is observed for Cp4 and Cp6, while Cp5 and Cp7 create a hydrophobic interaction (VDW type) with the same amino acid (Figure III.48).

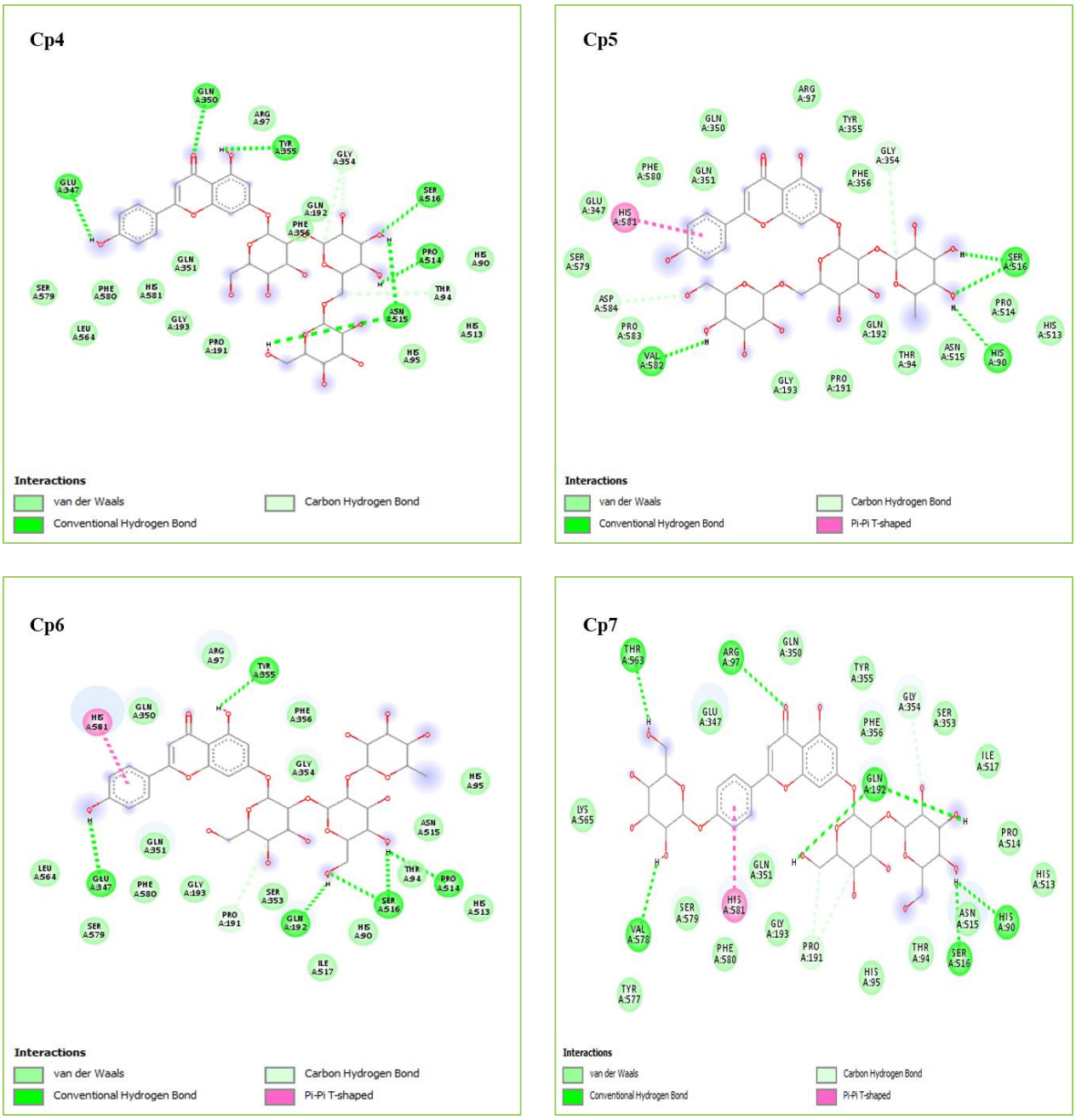

Figure III.48. 2D view of the binding poses of Cp4, Cp5, Cp6 and Cp7 in COX-1 enzyme.

Note 2: As a result, the above compounds are predicted to block the action of the COX-1 enzyme by establishing an H-bond or a VDW interaction with Tyr^{355} in the active site.

The analyses of following 2D digrams (Figure III.49) showed that:

The 5-OH group of the flavonoid part in Cp8 creates an H-bond with Tyr^{355}. Another H-bond was formed between the OH group of Glc moiety and Ser^{353}. The compound Cp9 creates two VDW interactions with Tyr^{355} and Ser^{353}. Moreover, the compound Cp10 shows an H-bond with Trp^{387} by involving its 4′-OH group in the interaction.

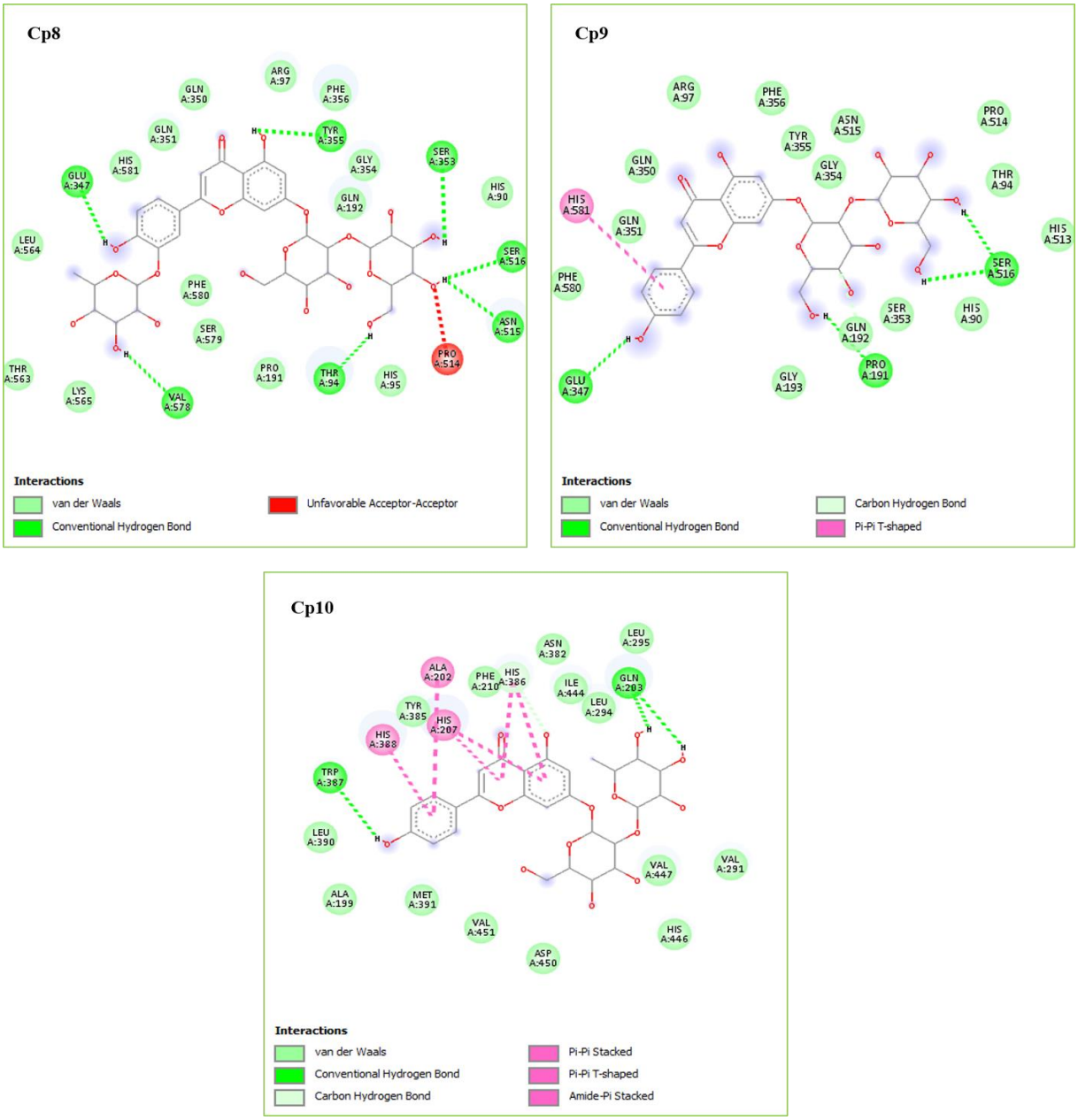

Figure III.49. 2D view of the binding poses of Cp8, Cp9, and Cp10 in COX-1 enzyme.

Note 3: According to the docking analyses, Cp8, Cp9, and Cp10 are predicted to inhibit the action of the COX-1 enzyme by interacting with the most important amino acid residues of the target protein such as Ser^{353}, Tyr^{355} and Trp^{387}.

Deductive remarks

In comparison with the standard COX-1 inhibitor BFL, the 3D visualization revealed that although the docked compounds Cp4–Cp10 present an association with some amino acid of the active site, they do not bind to the active site pocket of the target protein as observed for the re-docked BFL inhibitor. By doing that, the tested compounds may exhibit no inhibitory effect against the COX-1 enzyme. Our results were closely accorded with literature **[24]** where the docked flavonoids, apigenin and luteolin, show interactions out of the pocket of target COX-1 enzyme.

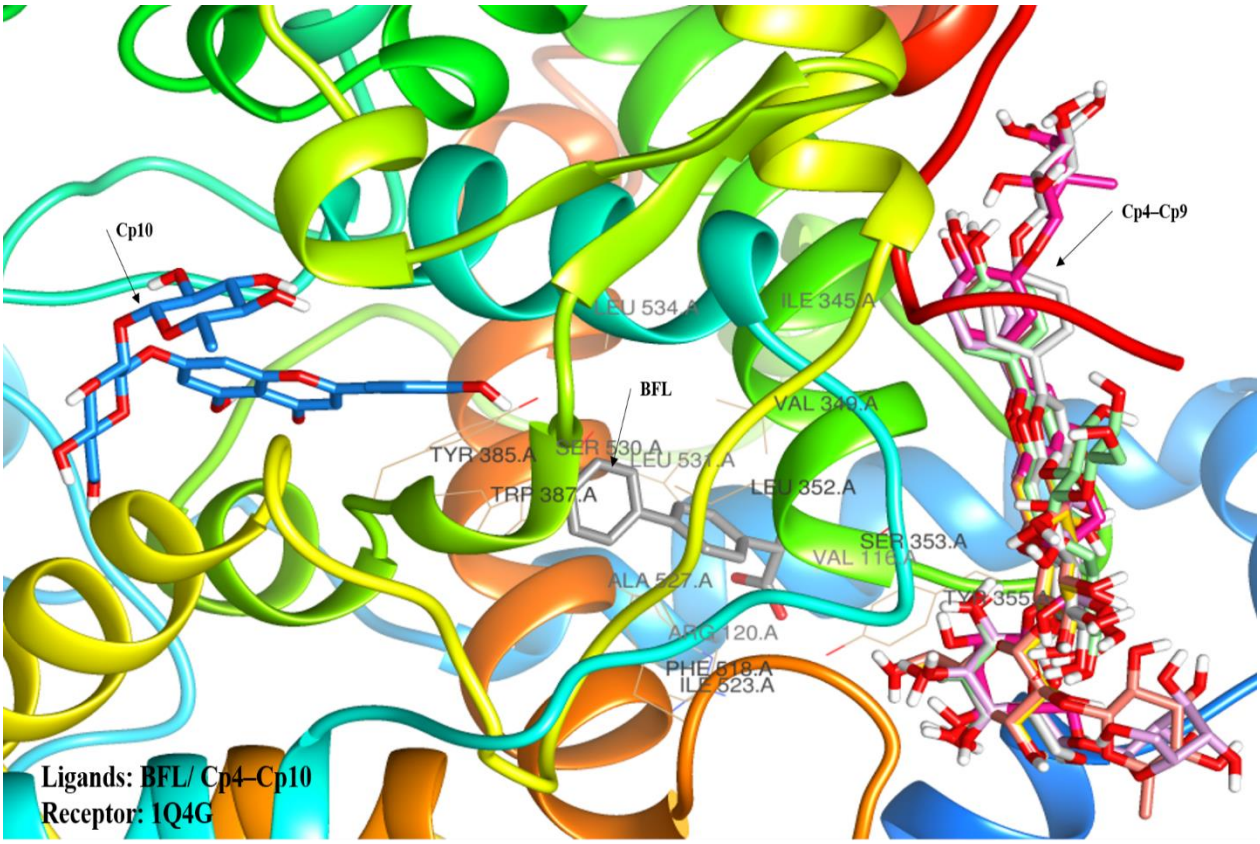

Figure III.50: 3D view of the binding poses of BFL and Cp4–Cp10 in COX-1 enzyme.

- **(COX-2) – Compounds interactions**

The 2D complexes generated by docking the compounds Cp1–Cp4 into the COX-2, illustrated in (Figure III.51), show that:

The OH groups of the glycosidic part in Cp1 form H-bonds with Arg^{120}, Gly^{533} and Ser^{353}, while, the flavonoid part interacts by involving its rings in hydrophobic interactions with $Leu^{352,534}$, Ala^{527}, Gly^{526}. In addition to the H-bond observed between 5-OH group and Met^{522} residue.

The tri-saccharide part of Cp2 form an H-bonds with Arg[120], and Ala[527]. And C-H bond with Tyr[355], Ser[353], Val[523], and Leu[352], this latter presents also a VDW interaction. Moreover, the flavonoid part interacts by involving its rings in hydrophobic interactions (such as π-π stacking, π-alkyl, π-lone pair, and VDW) with the following amino acid residues: Tyr[348, 385], Ser[530], Leu[534] and Phe[205, 209].

The bi-saccharide moiety of compound Cp3, create different associations with Ala[527], Leu[352], and Ser[353] by forming H-bonds. As well, it shows hydrophobic interactions VDW type with Val[523], Met[522] and Phe[518] residues. Furthermore, the aglycone part involves interaction with Val[116, 349], Leu[531], in addition to H-bonding focused on the 4′-OH group with Ser[530].

The glycosidic part in Cp4 creates two H-bonds with Arg[120] and Ser[353] in addition to the hydrophobic interactions with Tyr[355]. On the other side, a number of hydrophobic interactions were observed on the flavonoid skeleton by intruding all rings in association with Leu[352], Phe[518], Ser[530], Tyr[385] besides to the interaction observed between carbonyl group (C=O) and Gly[526].

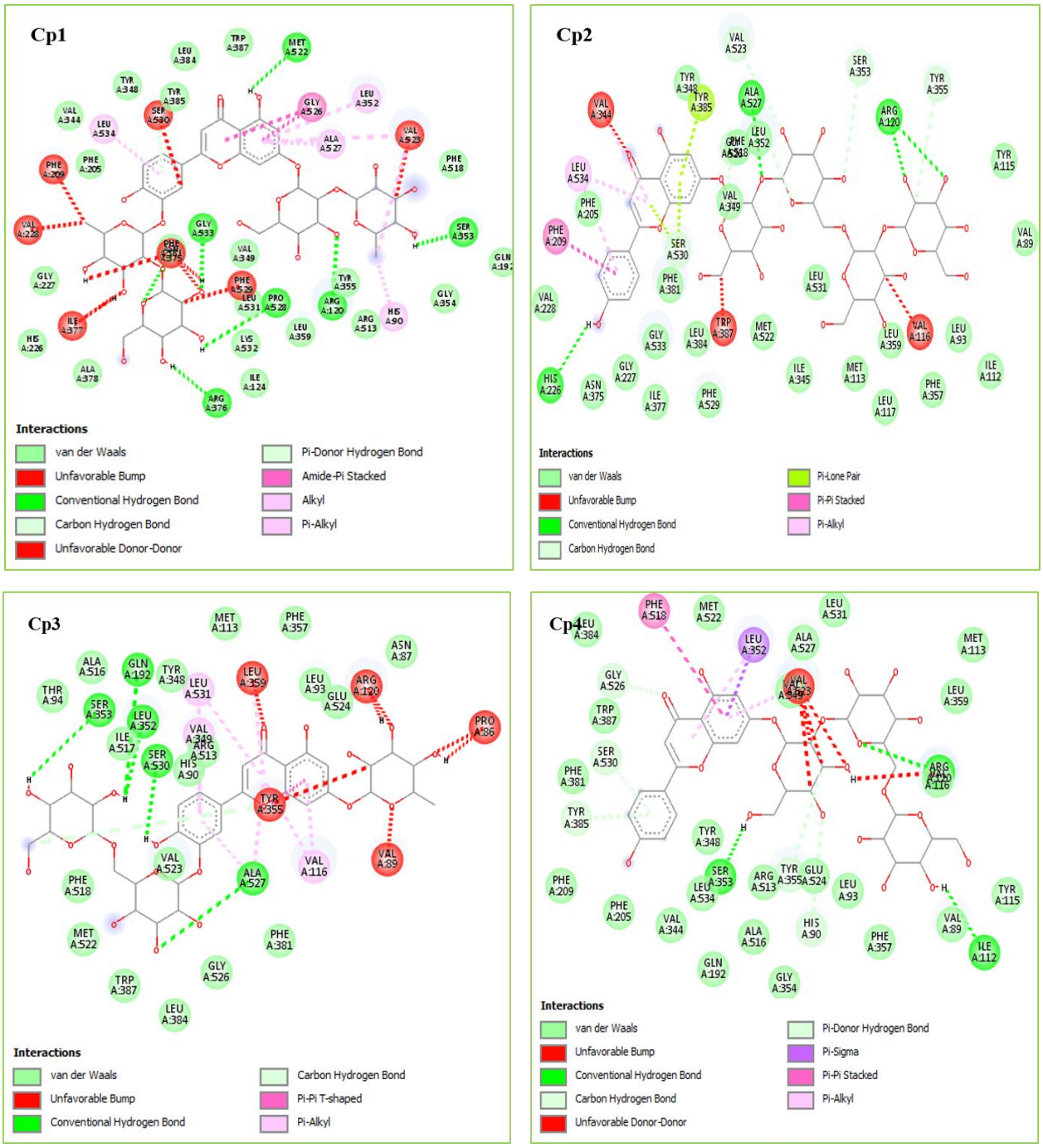

Figure III.51. Intra-molecular interactions of compounds Cp1–Cp4 with COX-2 enzyme in 2D.

Note 1: According to the docking analyses, the tested compounds exhibited several linkages with the most key amino acids in the active site. Nevertheless, numerous clashes were created into the pocket of the target protein as unfavorable bumping or Donor-Donor interactions, presented in the red label on the 2D diagram. By doing so, these types of interactions can make those compounds non-active as inhibitors against the COX-2 enzyme. Moreover, this result is supported by the high positive values of the binding energies (Table III.2) yielded by the studied compounds.

As seen in Figure III.52, Cp5 forms various interactions with the target protein pocket. The glycan part interacts with Arg^{120}, Ser^{530} by forming H-bonds besides to the hydrophobic interactions with $Val^{116, 349}$, Leu^{531}, Ala^{527} and Gly^{526}. The aglycone part creates linkages with Val^{523}, Ala^{527} and Leu^{352} by introducing its chromone rings. Similarly, the compound Cp6 made an H-bonding between its glycosidic side and Arg^{120}, Ser^{530} and Leu^{352} residues. Also, it is bound to the active site with the rings of the aglycone part, which interact with Arg^{120} (π- cation interactions) and Val^{116} (hydrophobic interaction). Then, the luteolin skeleton of the Cp7 (Figure III.52) introduced its rings in several hydrophobic interactions with Leu^{352}, Val^{523}, Gly^{526} and Ser^{530}. It also creates a C-H bond between 5′-OH and Phe^{518}. Two significant H-bonds were observed on the glycosidic side with Ser^{353} and Gly^{533}, besides the VDW interactions with Arg^{120}, Val^{116} and Tyr^{355}.

Eventually, the most hydrophobic interaction of compound Cp8 with the key amino acids $Val^{116, 349}$, Ala^{527}, $Leu^{359, 531}$ and Tyr^{355} were centered on the flavonoid rings. Besides, the H-bonds were observed between bi-saccharide, $Tyr^{385}$and Met^{522}.

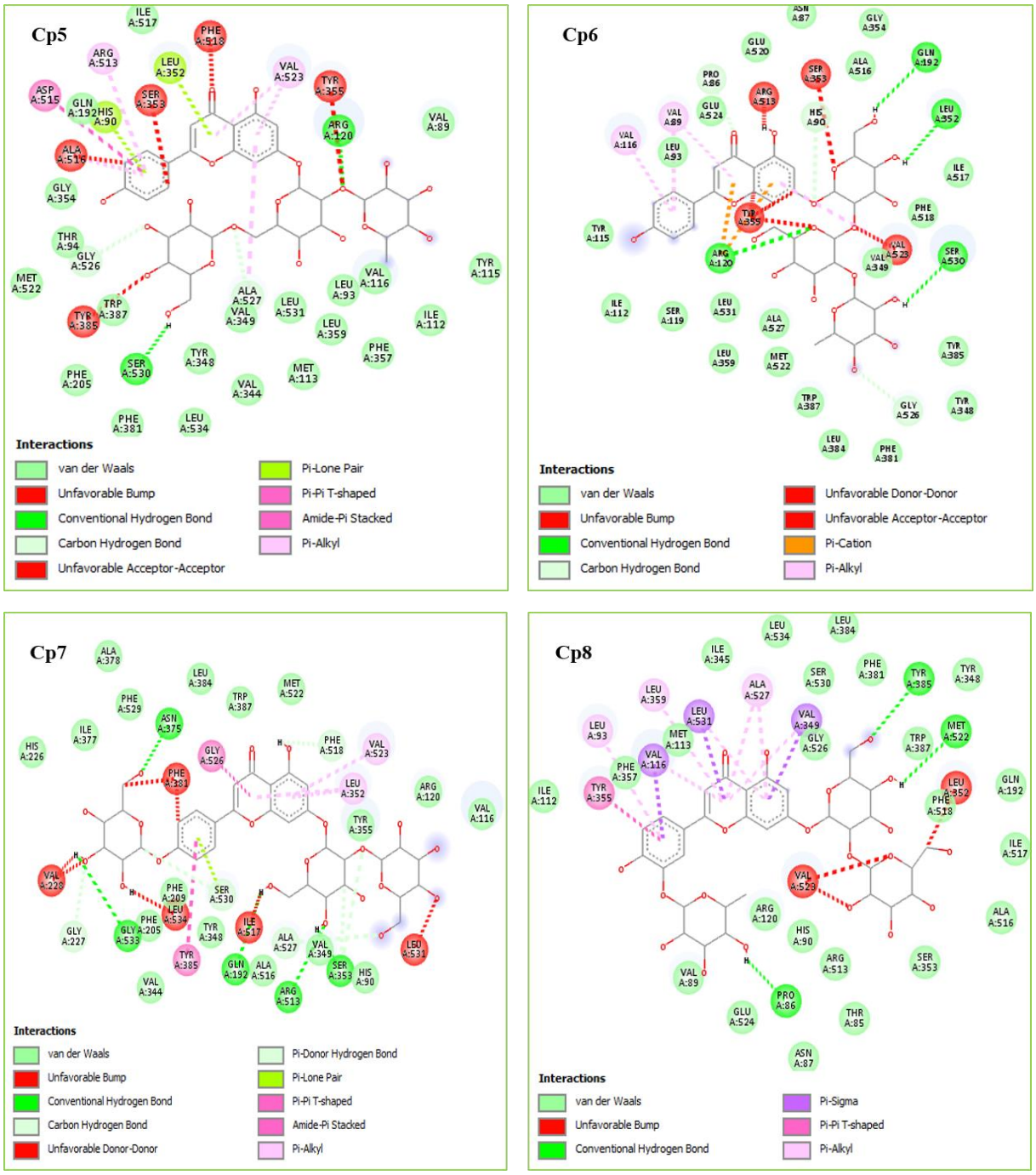

Figure III.52. Intra-molecular interactions of compounds Cp5–Cp8 with COX-2 enzyme in 2D.

Note 2: Similar to the previous results on Cp1–Cp4, the presence of numerous clashes like unfavorable bumping or Donor-Donor/Acceptor-Acceptor interactions makes the compounds Cp5–Cp8 unsuitable for inhibiting COX-2 enzyme. Even though the main interactions with the active site residues were associated with the studied compounds.

As shown in Figure III.53, both Cp9 and Cp10 share approximately the same hydrophobic interactions (VDW, π-δ, π- alkyl, π-π- T shaped (in Cp9) and amide- π stacked (in Cp10)) with the

following residues: Val[116, 349], Tyr[355], Ala[527], Arg[120], Leu[359, 531] and Gly[526] (only in Cp10). Furthermore, H-bonding was observed in Cp10 between Met[522] and 4′-OH and in Cp9 between the OH-groups of the disaccharide part and Ser[353], Leu[352] and Tyr[385].

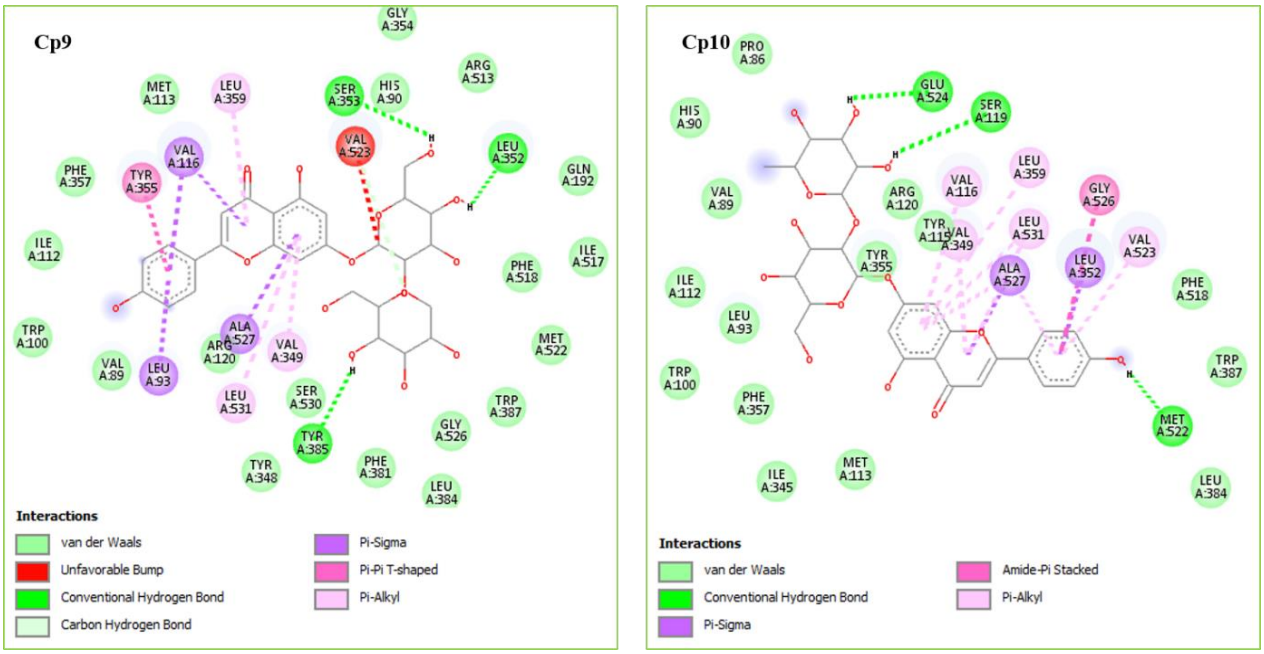

Figure III.53: Intra-molecular interactions of Cp9 and Cp10 with COX-2 enzyme in 2D.

Note 3: In comparison with the previous docked compounds (Cp1–Cp8), Cp9 and Cp10 showed satisfactory associations with the key amino acids in the target protein pocket. As a result, the both compounds may exhibit an inhibitory effect against the COX-2 enzyme. Deep analysis in Cp9 revealed that the unfavorable bumping interaction can make this compound less active than the Cp10 (reinforced by the binding energy values, $E_{Cp10} < E_{Cp9}$).

Deductive remarks

By ignoring all tested compounds from Cp1 to Cp9 and basing on the re-docking result obtained for the standard inhibitor NPX into the COX-2 enzyme and as reported earlier for some docked flavonoids **[25]**, compound **Cp10** arranged similarly and successfully inside the active site pocket by introducing its flavonoid part, mainly the B ring **[26]**. This result is in agreement with literature data **[27]** which revealed that the presence of H-bond and π-π hydrophobic interaction between the active site of the receptor and the compound are responsible for the potent anti-inflammatory activity. Although this compound has high binding energy in negative value (-3.4 kcal/mol) than the native ligand (-9.0 kcal/mol), it displays an acceptable alignment inside the protein pocket by forming several interactions.

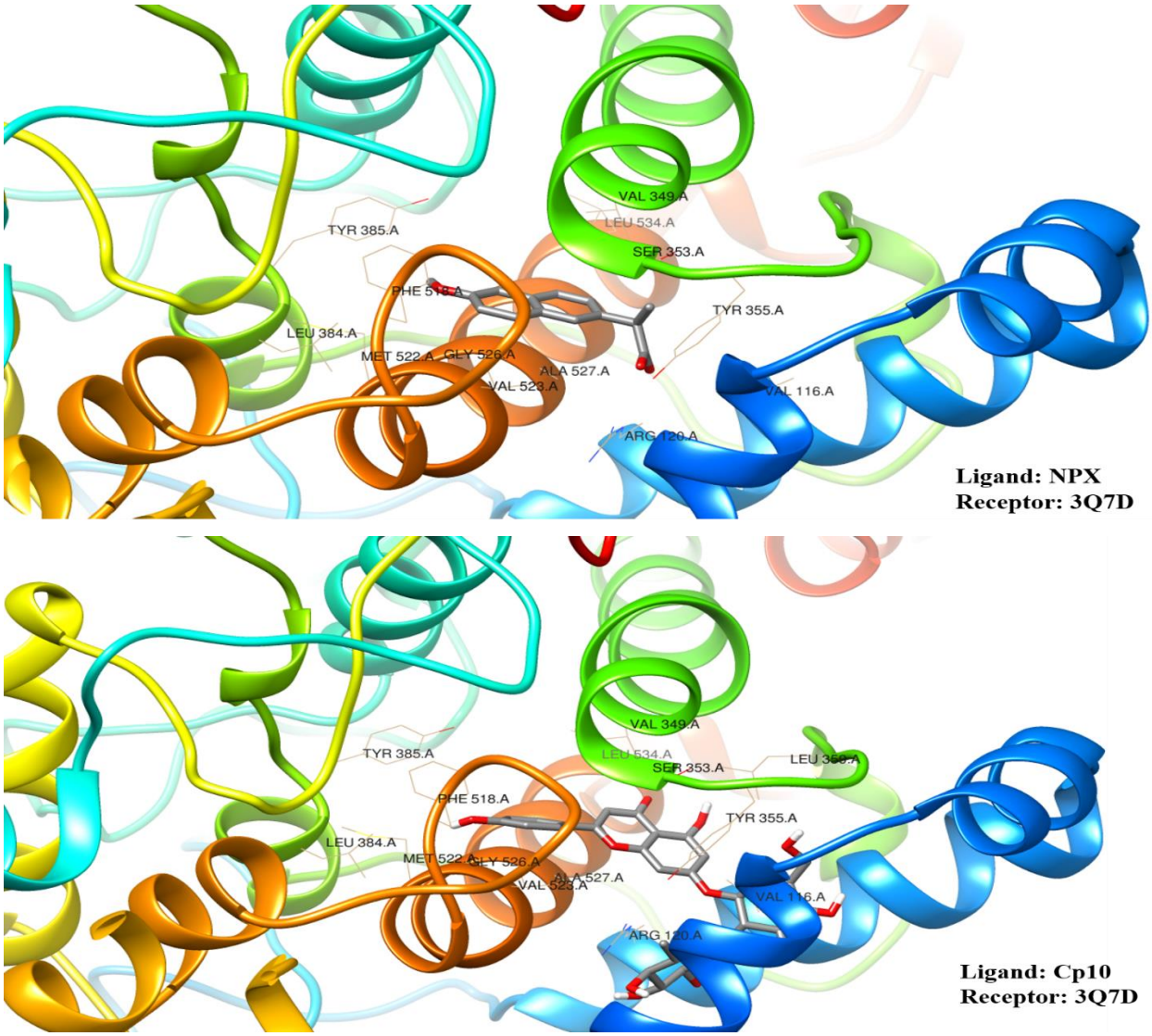

Figure III.54. 3D alignment of Cp10 inside the COX-2 (3Q7D) pocket.

The molecular docking studies on the glycosylated flavonoid compounds (Cp1–Cp10), which are identified from the *n*-butanolic extract of *Scilla lingulata*, delivered an approach to understand the affinity of this class of compounds to the hydrolytic enzymes (AChE and BChE). Both enzymes are present in the brain and they play an essential role as target receptors for treating the AD. For that reason, our study revealed that some of the investigated compounds present suitableness to the active site pocket of the studied proteins, by forming the main interactions with the key amino acids that are focused strongly on both flavonoid and glycosidic moieties. As a conclusion, the novel inhibitors were chosen by considering their pose inside the active site, vital interactions, and their lowest binding energy compared to the native inhibitors.

Furthermore, the same simulations were studied on the cyclooxygenase isozymes (COX-1 and 2) to perform the anti-inflammatory activity of those identified compounds. The results showed that only one compound was docked successfully into the active site of COX-2, while no interactions were observed into COX-1.

In addition, we may say that the observed unfavorable interactions inside the target receptors do not mean definitely that the tested compounds are non-active as inhibitors, but they can be related to the following suggested reasons:

- *The subtle details of the experimental setup*

Here, we may say that the 3D modeling of ligands has not been edited properly by the chosen software, or even their energies have not been minimized enough to be ready for docking.

Another proposition might be on the docking protocol that followed to create PDBQT files of the receptors, or on their Gid Box size parameter.

In conclusion, our molecular docking studies need further ameliorations on the tested parameter to get more results that are satisfactory. So, these deductive results must be enhanced by further *in vitro* studies to improve the biological activities of those compounds.

References

[1]. Diana NK, Florian CS, Dietmar RK. Simultaneous determination of bufadienolides and phenolic compounds in sea squill (*Drimia maritima* (L.) Stearn) by HPLC-DAD-MS^n as a means to differentiate individual plant parts and developmental stages. *Anal. Bioanal.Chem.* **2014**, 406: 6035–6050

[2]. Abad-García B, Garmon-Lobato S., Berrueta L.A., Gallo B, Vicente F. Practical guidelines for characterization of O-diglycosyl flavonoid isomers by triple quadrupole MS and their applications for identification of some fruit juices flavonoids. *J. Mass. Spectrom*. **2009**, 44(7): 1017–1025

[3]. Ma YL, Vedernikova I, Heuvel H, Claeys M. Internal glucose residue loss in protonated O-diglycosyl flavonoids upon low-energy collision-induced dissociation. *J. Am. Soc. Mass. Spectr.* **2000**, 11(2): 136–144

[4]. Dias C, Dias M, Borges C, Almoster Ferreira MA, Paulo A, Nascimento J. Structural elucidation of natural 2-hydroxy di- and tricarboxylic acids and esters, phenylpropanoid esters and a flavonoid from *Autonoë madeirensis* using gas chromatographic/electron ionization, electrospray ionization and tandem mass spectrometric techniques. *J. Mass Spectrom.* **2003**, 38: 1240–1244

[5]. Sadik K, Wilcock G. The increasing burden of Alzheimer disease. *Alzheimer Dis. Assoc. Disord*. **2003**, 17(3): S75–S79

[6]. Lane RM, Potkin SG, Enz A. Targeting acetylcholinesterase and butyrylcholinesterase in dementia. *Int. J. Neuropsychoph*. **2006**, 9:101–124

[7]. Bajda M, Więckowska A, Hebda M, Guzior N, Sotriffer C, Malawska B. Structure-Based search for new nnhibitors of cholinesterases. *Int. J. Mol. Sci*. **2013**, 14(3): 5608–5632

[8]. Bartolucci C, Perola E, Pilger C, Fels G, Lamba D. Three-dimensional structure of a complex of galanthamine (Nivalin®) with acetylcholinesterase from *Torpedo californica*: Implications for the design of new anti-Alzheimer drugs. *Proteins: Struct. Funct. Genet*. **2000**, 42(2): 182–191

[9]. Nachon F, Carletti E, Ronco C, Trovaslet M, Nicolet Y, Jean L, Renard PY. Crystal structures of human cholinesterases in complex with huprine W and tacrine: elements of specificity for anti-Alzheimer's drugs targeting acetyl- and butyryl-cholinesterase. *Biochem. J*. **2013**, 453(3): 393–399

[10]. Mahdavi M, et al. Design, synthesis, molecular docking, and cholinesterase inhibitory potential of phthalimide-dithiocarbamate hybrids as new agents for treatment of Alzheimer's disease. *Chem. Biodiversity* **2019**, 16: e1900370

[11]. Zhang L, Li D, Cao F, Xiao W, Zhao L, Ding G, Wang Z. Identification of human acetylcholinoesterase inhibitors from the constituent of EGb761 by modeling docking and molecular dynamics simulations. *Comb. Chem. High Throughput Screen*. **2018**, 21(1):41–49

[12]. Yerlikaya S, Zengin G, Mollica A, Baloglu MC, Celik Altunoglu Y, Aktumsek A. A multidirectional perspective for novel functional products: *In vitro* pharmacological activities and *in silico* studies on *ononis natrix* subsp. *hispanica*. *Front. Pharmacol*. **2017**, 8:600

[13]. Fan P, Hay A-E, Marston A, Hostettmann K. Acetylcholinesterase-Inhibitory activity of linarin from *Buddleja davidii*, structure-activity relationships of related flavonoids, and chemical investigation of *Buddleja nitida*. *Pharma. Bio.* **2008**, 46(9): 596–601

[14]. Mughal EU et al. Synthesis, structure-activity relationship and molecular docking studies of 3-*O*-flavonol glycosides as cholinesterase inhibitors. *Bioorg. Med. Chem*. **2018**, 26: 3696–3706

[15]. Katalinic´ M et al. Structural aspects of flavonoids as inhibitors of human butyrylcholinoesterase. *Eur. J. Med. Chem*. **2010**, 45: 186–192

[16]. Emery P. Early referral recommendation for newly diagnosed rheumatoid arthritis: evidence based development of a clinical guide. *Ann. Rheum. Dis*. **2002**, 61(4): 290–297

[17]. Dannhardt G, Kiefer W, Krämer G, Maehrlein S, Nowe U, Fiebich B. The pyrrole moiety as a template for COX-1/COX-2 inhibitors. *Eur. J. Med. Chem*. **2000**, 35(5):499–510

[18]. RCSB.org. (2020). *RCSB PBD-1Q4G | 2.0 Angstrom Crystal Structure of Ovine Prostaglandin H2 Synthase-1, in complex with alpha-meth-4-biphenylacetic acid.* [Online] Available at: https://www.rcsb.org/3d-view/1Q4G?preset=ligandInteraction&sele=BFL [Accessed 27 jun. 2020]

[19]. RCSB.org. (2020). *RCSB PBD-3Q7D | Structure of (R)-naproxen bound to mCOX-2.* [Online] Available at: https://www.rcsb.org/3d-view/3Q7D?preset=ligandInteraction&sele=NPX [Accessed 27 jun. 2020]

[20]. Gupta K, Selinsky BS, Kaub CJ, Katz AK, Loll PJ. The 2.0Å Resolution Crystal Structure of Prostaglandin H2 Synthase-1: Structural Insights into an Unusual Peroxidase. *J. Mol. Biol*. **2004**, 335(2):503–518

[21]. Duggan KC, Hermanson DJ, Musee J, Prusakiewicz JJ, Scheib JL, Carter BD, Banerjee S, Oates JA, Marnett LJ.(R)-Profens are substrate-selective inhibitors of endocannabinoid oxygenation by COX-2. *Nat. Chem. Biol*. **2011**, 7(11):803–809

[22]. Garavito RM, DeWitt DL. The cyclooxygenase isoforms: structural insights into the conversion of arachidonic acid to prostaglandins. *Biochim. Biophys. Acta*. **1999**, 1441(2-3):278–287

[23]. Proteopedia.org. *Cycloxygenase – Protopedia, life in 3D*. [Online] Available at: http://proteopedia.org/wiki/index.php/Cyclooxygenase [Accessed 27 jun. 2020]

[24]. Wu C-M et al. Antiplatelet effect and selective binding to cyclooxygenase (COX) by molecular docking analysis of flavonoids and lignans. *Int. J. Mol. Sci.* **2007**, 8 : 830 – 841

[25]. Dash R, NasirUddin MM, ZahidHosen SM, BinRahim Z,Dinar AM, Hafez Kabir MS, Sultan RA, Islam A, Hossain MK. Molecular docking analysis of known flavonoids as duel COX-2 inhibitors in the context of cancer. *Bioinformation* **2015**, 11(12): 543–549

[26]. Ribeiro D, Freitas M, Tomé SM, Silva AMS, Laufer S, Lima JLFC, Fernandes E. Flavonoids inhibit COX-1 and COX-2 enzymes and cytokine/chemokine production in human whole blood. *Inflammation*, **2014**, 38(2): 858–870

[27]. Madeswaran A, Umamaheswari M, Asokkumar K, Sivashanmugam T, Subhadradevi V, Jagannath P. *In silico* docking studies of cyclooxygenase inhibitory activity of commercially available flavonoids. *Asian J. Pharmacy life Sci*. **2012**, 2(2): 2231–4423

General

Conclusion

We have been reported in the bibliographic synthesis, that the *Scilla* species were well-known from the ancient time with their medicinal uses in folk healing. For that, several recent studies regarding the chemical compositions and the biological activities of the *Scilla* plant extract, have focused on the isolation, structural identifications and the biological behaviors of the phytochemicals that present in the plant. In that perspective, the current research work aims at casting light on the Algerian endemic species *S. lingulata* Poir. (Asparagaceae), which presents a lack of phytochemical and biological studies.

The use of the analytical technique LC-ESI/MS in the purpose of investigating phytochemically the *n*-BuOH extract of *S. lingulata*, allowed us to identify the chemical structure of ten compounds present in the polar solvent. They was classified as glycosylated flavonoids (flavone-type):

- **Glycosylated apigenin**

Apigenin 7-*O*-(glucosyl-(1‴→2″)-glucosyl-(1⁗→6‴)-glucosyl-(1⁗′→2⁗)-glucoside)
Apigenin 7-*O*-glucosyl-(1‴→2″)-glucosyl-(1⁗→6‴)-glucoside
Apigenin 7-*O*-glucosyl-(1‴→2″)-rhamnoside-(1⁗→6″)-glucoside
Apigenin 7-*O*-glucosyl-(1‴→2″)-glucosyl-(1⁗→2‴)-rhamnoside
Apigenin 7-*O*-(glucosyl-(1‴→2″)-glucoside)-4′-*O*-glucoside
Apigenin 7-*O*-(glucosyl-(1‴→2″)-glucoside)
Apigenin 7-*O*-(glucosyl-(1‴→2″)-rhamnoside)

- **Glycosylated luteolin**

Luteolin 7-*O*- (rhamnosyl-(1‴→2″)-glucoside)-3′-*O*-(glucosyl-(1⁗′→2⁗′)-rhamnoside)
Luteolin 7-*O*-rhamnoside-3′-*O*-(glucosyl-(1⁗→6‴)-glucoside)
Luteolin 7-*O*-(glucosyl-(1‴→2″)-glucoside)-3′-*O*-rhamnoside

Owing to the outbreak COVID-19 pandemic, the presented study is lacked in the *in vitro* assays that evaluate the biological activity of the studied extract. As a result, the *in silico* enzymatic assays were performed, using molecular docking method, to the identified molecules in order to understand the binding mode of these class of compounds into the target proteins and to give also an approach insight to the structure-activity relationships by establishing interactions inside the protein – ligand complexes.

The *in silico* anti-Alzheimer's activity was observed for compound **10** and **8** by inhibiting AChE and BChE ezymes, respectively. The anti-inflammatory activity (*in silico*) was detected for compound **10** by inhibiting only COX-2 enzyme.

Abstract

In this work, we mainly focused on the phytochemical study of the Algerian endemic species, *Scilla lingulata* Poir. (Asparagaceae), in order to structurally identify its chemical composition. The use of the analytical LC-ESI / MS technique, allowed us to investigate the phytoconstituents, especially the polar compounds, present in the *n*-butanolic extract of this plant. Profound analysis in the UV-Vis and ESI / MS spectra (in positive and negative mode) allowed us to elucidate the structure of ten glycosylated flavonoids (flavone type). The *in silico* assays of those latter were carried out by means of molecular docking to evaluate the anti-Alzheimer and anti-inflammatory activities of these molecules.

Keywords: *n*-butanolic extract of *Scilla ligulata*, UV-Vis, LC-ESI/MS, glycosylated flavonoids, Molecular docking, Anti-Alzheimer activity, Anti-inflammatory activity.

Résumé

Dans ce travail, nous nous sommes essentiellement concentrés sur l'étude phytochimique d'une plante algérienne, l'espèce endémique *Scilla lingulata* Poir. (Asparagaceae), dans le but d'identifier structuralement sa composition chimique. L'utilisation d'une technique d'analyse LC-ESI/MS nous a permis d'investiguer les phytoconstituants, notamment les composés polaires, présentant dans l'extrait *n*-butanolique de cette plante. L'analyse approfondie des spectres UV-Vis et ESI/MS (en mode positif et négatif) nous a permis d'élucider la structure de dix flavonoïdes glycosylés (type flavone). Les essayes *in silico* de ces derniers ont été réalisés au moyen de l'amarrage (docking en anglais) moléculaire pour évaluer les activités anti-Alzheimer et anti-inflammatoire de ces molécules.

Mots clés : l'extrait *n*-butanolique du *Scilla lingulata*, UV-Vis, LC-ESI/MS, flavonoïde glycosylés, L'amarrage moleculare, *in silico*, activité anti-Alzheimer, activité anti-inflammatoire.

مـــلـــخص

في هذا العمل، ركزنا بشكل أساسي على الدراسة الفيتوكيميائية للنبات المستوطن في الجزائر، *Scilla lingulata* Poir. (Asparagaceae), وذلك بهدف تحديد تركيبيه الكيميائي بنيويا. سمح لنا استعمال تقنية التحليل LC-ESI/MS البحث على المواد الطبيعية وعلى الخصوص المركبات القطبية الموجودة في المستخلص البيوتانولي لهذه النبتة. سمح لنا أيضا التحليل العميق لأطياف ESI/MS و UV-Vis من التعرف على بنية عشر فلافونويدات من نوع فلافون تحتوي على أجزاء سكرية. تم إجراء تجارب *in silico* لهذه الأخيرة باستخدام الرس الجزيئي لتقييم الأنشطة المضادة للزهايمر والمضادة للالتهاب لهذه الجزيئات.

الكلمات المفتاحية: المستخلص البيوتانولي ل *Scilla lingulata*، UV-Vis, LC-ESI/MS، فلافونويدات سكرية، *in silico*، تأثير مضاد للزهايمر، تأثير مضاد للالتهاب.

Abstract: In this work, we mainly focused on the phytochemical study of the endemic Algerian species, *Scilla lingulata* Poir. (Asparagaceae), in order to structurally identify its chemical composition. The use of the analytical LC-ESI / MS technique, allowed us to investigate the phytoconstituents, especially the polar compounds, present in the *n*-butanolic extract of this plant. Profound analysis in the UV-Vis and ESI / MS spectra (in positive and negative mode) allowed us to elucidate the structure of ten glycosylated flavonoids (flavone type). The *in silico* assays of those latter were carried out by means of molecular docking to evaluate the anti-Alzheimer and anti-inflammatory activities of these molecules.

Keywords: *n*-butanolic extract of *Scilla ligulata*, UV-Vis, LC-ESI/MS, glycosylated flavonoids, Molecular docking, *in silico*, Anti-Alzheimer activity, Anti-inflammatory activity.

Résumé: Dans ce travail, nous nous sommes essentiellement concentrés sur l'étude phytochimique d'une plante algérienne, l'espèce endémique *Scilla lingulata* Poir. (Asparagaceae), dans le but d'identifier structuralement sa composition chimique. L'utilisation d'une technique d'analyse LC-ESI/MS nous a permis d'investiguer les phytoconstituants notamment les composés polaires présentant dans l'extrait *n*-butanolique de cette plante. L'analyse approfondie des spectres UV-Vis et ESI/MS (en mode positif et négatif) nous a permis d'élucider la structure de dix flavonoïdes glycosylés (type flavone). Les essayes *in silico* de ces derniers ont été réalisés au moyen de l'amarrage (docking en anglais) moléculaire pour évaluer les activités anti-Alzheimer et anti-inflammatoire de ces molécules.

Mots clés: l'extrait *n*-butanolique du *Scilla lingulata*, UV-Vis, LC-ESI/MS, flavonoïde glycosylés, L'amarrage moléculaire, *in silico*, activité anti-Alzheimer, activité anti-inflammatoire.

ملخص : في هذا العمل، ركزنا بشكل أساسي على الدراسة الفيتوكيميائية للنبات المستوطن في الجزائر، *Scilla lingulata* Poir. (Asparagaceae), وذلك بهدف تحديد تركيبه الكيميائي بنيويا. سمح لنا استعمال تقنية التحليل LC-ESI/MS البحث على المواد الطبيعية وعلى الخصوص المركبات القطبية الموجودة في المستخلص البيوتانولي لهذه النبتة. سمح لنا أيضا التحليل العميق لأطياف ESI/MS و UV-Vis من التعرف على بنية عشر فلافونويدات من نوع فلافون تحتوي على أجزاء سكرية. تم إجراء تجارب *in silico* لهذه الأخيرة باستخدام الرس الجزيئي لتقييم الأنشطة المضادة للزهايمر والمضادة للالتهاب لهذه الجزيئات.

الكلمات المفتاحية: المستخلص البيوتانولي ل *Scilla lingulata*، LC-ESI/MS، UV-Vis ، فلافونويدات سكرية، *in silico*، مضاد للزهايمر، مضاد للالتهاب.